Lysine methyltransferase 2D regulates pancreatic carcinogenesis through metabolic reprogramming

Marina Koutsioumpa,[1] Maria Hatziapostolou,[2,3] Christos Polytarchou,[4] Ezequiel J Tolosa,[5] Luciana L Almada,[5] Swapna Mahurkar-Joshi,[1] Jennifer Williams,[6] Ana Belen Tirado-Rodriguez,[7] Sara Huerta-Yepez,[7] Dimitrios Karavias,[8] Helen Kourea,[8] George A Poultsides,[9] Kevin Struhl,[10] David W Dawson,[11] Timothy R Donahue,[6] Martín E Fernández-Zapico,[5] Dimitrios Iliopoulos[1,*]

[1]Center for Systems Biomedicine, Vatche and Tamar Manoukian Division of Digestive Diseases, David Geffen School of Medicine, University of California at Los Angeles, Los Angeles, California, USA

[2]Biological Sciences, University of Southampton, Southampton, UK

[3]Biosciences, School of Science and Technology, Nottingham Trent University, Nottingham, UK

[4]Interdisciplinary Biomedical Research Centre, School of Science and Technology, Nottingham Trent University, Nottingham, UK

[5]Schulze Center for Novel Therapeutics, Division of Oncology Research, Mayo Clinic, Rochester, Minnesota, USA

[6]Department of Surgery, Division of General Surgery, David Geffen School of Medicine, University of California at Los Angeles, Los Angeles, California, USA

[7]Unidad de Investigacion en Enfermedades Oncologicas, Hospital Infantil de Mexico, Mexico City, Mexico

[8]Department of Pathology, School of Medicine, University of Patras, Patras, Greece

[9]Department of Surgery, Stanford University School of Medicine, Stanford, California, USA

10Department of Biological Chemistry and Molecular Pharmacology, Harvard Medical School, Boston, Massachusetts, USA

[11]Department of Pathology and Laboratory Medicine, David Geffen School of Medicine, University of California at Los Angeles, Los Angeles, California, USA

* To whom correspondence should be addressed: iliopoulospharma@ gmail. com

ABSTRACT

Objective Despite advances in the identification of epigenetic alterations in pancreatic cancer, their biological roles in the pathobiology of this dismal neoplasm remain elusive. Here, we aimed to characterize the functional significance of histone lysine methyltransferases (KMTs) and demethylases (KDMs) in pancreatic tumourigenesis.

Design DNA methylation sequencing and gene expression microarrays were employed to investigate CpG methylation and expression patterns of KMTs and KDMs in pancreatic cancer tissues versus normal tissues. Gene expression was assessed in five cohorts of patients by reverse transcription quantitative-PCR. Molecular analysis and functional assays were conducted in genetically modified cell lines. Cellular metabolic rates were measured using an XF24-3 Analyzer, while quantitative evaluation of lipids was performed by liquid chromatography-mass spectrometry (LC-MS) analysis. Subcutaneous xenograft mouse models were used to evaluate pancreatic tumour growth in vivo.

Results We define a new anticancer function of histone lysine (K)-specific methyltransferase 2D (KMT2D) in pancreatic cancer. KMT2D is transcriptionally repressed in human pancreatic tumors through DNA methylation. Clinically, lower levels of this methyltransferase associate with poor prognosis and significant weight alterations. RNAi-based genetic inactivation of KMT2D promotes tumor growth and results in loss of H3K4me3 mark. In addition, KMT2D inhibition increases aerobic glycolysis and alters the lipidomic profiles of pancreatic cancer cells. Further analysis of this phenomenon identified the glucose transporter SLC2A3 as a mediator of KMT2Dinduced changes in cellular, metabolic and proliferative rates.

Conclusion Together our findings define a new tumor suppressor function of KMT2D through the regulation of glucose/fatty acid metabolism in pancreatic cancer.

WHAT IS ALREADY KNOWN ON THIS SUBJECT?

- Pharmacological targeting of epigenetic modifications contributes to uncovering therapeutic opportunities in pancreatic cancer.
- Several groups describe the deregulation and functional diversity of some histone methylation pathways in pancreatic adenocarcinomas.
- To date, the biological and translational significance of the aberrant function of the epigenetic regulators remains poorly understood, in particular for proteins controlling histone methylation.

WHAT ARE THE NEW FINDINGS?

- Transcriptional repression of histone lysine (K)-specific methyltransferase 2D (KMT2D) is double site, CG methylation-dependent.
- Pancreatic cancer growth is promoted by KMT2D downregulation.
- KMT2D suppression mediates loss of H3K4me3 signals in metabolic pathways and accounts for an induction of aerobic glycolysis and lipid levels.
- SLC2A3 (also known as GLUT3) is a mediator of KMT2D-induced effects in cellular metabolic and proliferative rates.
- Patients with pancreatic cancer harbouring low KMT2D levels have worse prognosis and significant weight/body mass index (BMI) alterations.

HOW MIGHT IT IMPACT ON CLINICAL PRACTICE IN THE FORESEEABLE FUTURE?

- Characterization of KMT2D-associated metabolic signatures provides a new molecular rationale to identify and develop a new generation of therapeutic agents.
- Future studies exploring the causal molecular link between KMT2D expression and clinical outcomes may offer prognostic information and insights into pancreatic tumourigenesis and progression.

INTRODUCTION

Emerging studies demonstrate that epigenetic rather than genetic changes modulate the phenotype of different cancer types, specifically the ones controlling chromatin modifications such as histone methylation. In fact, there is evidence showing that changes in histone lysine methyltransferases (KMTs) and demethylases (KDMs), including KDM2B[1] and EZH2,[2] could affect pancreatic tumour growth. This is particularly important as it has been recently indicated that KMTs and KDMs could alter gene expression in a selective manner, while other chromatin modifiers, such as histone deacetylases and DNA methyltransferases, globally regulate gene expression.[3] Thus, understanding the function of histone methylation pathways could lead to a high degree of specificity in targeting specific epigenetic factors that control pancreatic malignant transformation.

In the present study, we provide evidence for a novel role of histone lysine (K)-specific methyltransferase 2D (KMT2D) in pancreatic carcinogenesis. Our chromatin immunoprecipitation- sequencing (ChIP-seq) and genome-wide gene expression analysis, as well as tumour growth studies, strongly support its role as a pancreatic tumor suppressor. Specifically, KMT2D inhibition results in alterations of pancreatic cancer cells' bioenergetic and lipidomic profiles, by increasing aerobic glycolysis and lipid levels. Clinical outcomes

across the range of body weight and body mass index (BMI) were found to significantly correlate with KMT2D expression levels. Taken together, we have defined a previously uncharacterized function of KMT2D as growth-limiting factor in pancreatic cancer, and by mechanistic studies we demonstrate that the metabolic reprogramming underlies this anticancer function of KMT2D.

MATERIALS AND METHODS

Cell treatments.

Cells were transfected with small interfering RNAs (siRNAs) for KMT2D, #1 (s15605) and #2 (s15604), SLC2A3 (s12933), LDLR (s224008), SLC2A1 (s12926), mTOR (s604), RICTOR (s226000) and control (4390846) using Lipofectamine RNAiMax Transfection Reagent (13778150, Life Technologies). Lentiviruses were produced in HEK293T cells (ATCC) transfected with the packaging and expression constructs using Fugene 6 (E2691, Promega). Cells were infected with the viruses using DEAE-Dextran and selected with puromycin.

Mouse experiments.

Cells were transduced with short hairpin RNAs (shRNAs) for KMT2D or scramble (1864, Addgene) lentiviral expressing constructs. Sequences containing the shRNAs for KMT2D were annealed and cloned into the pLKO.1 puro (8453, Addgene) vector according to the Janes Lab protocol (http:// bme. virginia. edu/ janes/ protocols/ pdf/ Janes_ shRNAcloning. pdf):

#1–19: (sense: CCGG GAGT CGAA CTTT ACTG TCTC TGCA GAGA CAGT AAAG TTCG ACTC TTTTTG; antisense: AATT CAAA AAGA GTCG AACT TTAC TGTC TCTG CAGA GACA GTAA AGTT CGACTC).

#2–19: (sense: CCGG CCAC TCTC ATCA AATC CGAC TGCA GTCG GATT TGAT GAGA GTGG TTTTTG; antisense: AATT CAAA AACC ACTC TCAT CAAA TCCG ACTG CAGT CGGA TTTG ATGA GAGTGG).

#1–21: (sense: CCGG GAGT CGAA CTTT ACTG TCTC CCTG CAGG GAGA CAGT AAAG TTCG ACTC TTTTTG; antisense: AATT CAAA AAGA GTCG AACT TTAC TGTC TCCC TGCA GGGA GACA GTAA AGTT CGACTC).

#2–21: (sense: CCGG CCAC TCTC ATCA AATC CGAC ACTG CAGT GTCG GATT TGAT GAGA GTGG TTTTTG; antisense: AATT CAAA AACC ACTC TCAT CAAA TCCG ACAC TGCA GTGT CGGA TTTG ATGA GAGGG).

$3.5*10^6$ or $4.5*10^6$ MIA PaCa-2 or CAPAN-2 cells were injected subcutaneously at the right flank of NOD-SCID mice (five mice/group). Tumor volume was monitored every week for up to 42 and 84 days, respectively. Tumour volumes were calculated through the formula V (mm^3)

= $axb^2/2$, where a is the largest diameter and b is the perpendicular diameter. Bars represent mean ± SD.

Data availability section.

Array and sequencing data have been deposited in the Gene Expression Omnibus database (http://www. ncbi. nlm. nih. gov/geo/). Gene expression array, targeted bisulfite sequencing and ChIP-seq data are available under the following accession numbers: GSE85991, GSE85961 and GSE85886. Additional materials and methods are included as part of the online supplementary materials and methods section.

RESULTS

KMT2D exerts tumor suppressive activities in pancreatic cancer.

To define the role of KMTs and KDMs in pancreatic carcinogenesis, we initially determined the levels of these enzymes in tumours (n=14) and adjacent controls (n=8) and found different members of the KDM family (KDM2A, KDM4C, KDM5B, KDM8), SETD family (SETDB2, SETD6), and the SUV420H1 and KMT2D to be differentially expressed (online supplementary table S1). As shown in Figure 1A and supplementary figure S1A, statistically significant and consistent deregulation of gene expression was observed only for KMT2D in three independent patient cohorts. We further investigated the differential KMT2D expression based on previously published gene expression array data listed in the Oncomine database. Notably, KMT2D mRNA expression displays significantly decreased levels based on two independent studies [4 5] (supplementary figure S1B, C). The expression of other H3K4 methyltransferase genes sharing similar structural domains with KMT2D was also measured. As shown in online supplementary figure S1D, E, no significant changes were observed in the mRNA levels of neither KMT2B nor KMT2C in the human pancreatic cancer samples used in the current study.

Based on the above findings, we postulated the hypothesis that KMT2D might display tumor suppressive properties in pancreatic cancer. To address this hypothesis, we performed a series of *in vitro* and *in vivo* experiments where KMT2D was genetically inactivated, as evidenced in figure 1B. Transient downregulation of KMT2D by using two different siRNAs promoted cellular proliferative capacity (figure 1C, online supplementary figure S1F, G and supplementary tables S2–S3). To confirm the biological significance of KMT2D, pancreatic cancer cells stably suppressed of KMT2D expression were established (online supplementary figure S1H) and tested for their proliferative capacity (online supplementary figures S1I–L). The most efficient shRNA transfected cell population (#2–21) was subjected to clonal selection and used for further studies. Reverse transcription quantitative-PCR (RT-qPCR) and immunoblot (IB) analysis were used to verify the lower levels of KMT2D mRNA and protein in the clonal cell lines (figure 1D). Similar to transient knockdowns, stably decreased KMT2D

expression led to increased MIA PaCa-2 proliferation (figure 1E, online supplementary figure S1M, N and supplementary tables S4–S5) and cell anchorage-independent growth (figure 1F and online supplementary figure S10).

To further validate our hypothesis, the effects of KMT2D inhibition of expression were investigated in nude mice bearing human pancreatic cancer xenografts. Significant induction of tumor growth rate and weight was observed (figure 1G, H and online supplementary figure S1P, Q), and lower KMT2D mRNA levels were confirmed by RT-qPCR and immunohistochemical (IHC) analysis (supplementary figure S1R, S) in the excised tumours. Consistent with these observations, histopathological analysis of tumours from different mice at the endpoint revealed high proliferation rates, as evidenced by Ki-67 immunostaining (figure 1i). Taken together, these *in vitro* and *in vivo* results point towards a tumour suppressive role of KMT2D in pancreatic cancer.

Site specific DNA methylation associates with KMT2D transcriptional repression.

We then sought to determine the mechanism underlying KMT2D decreased expression in pancreatic cancer. To this end, we designed a complementary tissue-based and cell-based experimental approach for the evaluation of KMT2D transcriptional repression dependency on DNA methylation, as depicted in Figure 2A. We have investigated DNA methylation patterns of KMTs and KDMs in 20 pancreatic cancer tissues compared with 13 adjacent control tissues by using the Infinium Human Methylation 450 Bead ChIP Array. KMT2D, together with other four of these enzymes, was found to be significantly differentially methylated (at least over 25%) in pancreatic tumours compared with normal tissues (figure 2B and supplementary Table S6). Specifically, methylation of two individual CpG motifs was observed at nucleotides (nt) −29 and +45, relatively to the KMT2D transcription start site (TSS). By integrating the data originating from CpG methylation genome-wide analysis with gene expression profiling in cancerous versus normal pancreas, KMT2D was simultaneously identified to be hypermethylated and downregulated. Whole exome sequencing in the pancreatic cancer cell lines used in the current study (online supplemetary table S7), as well as published data from other groups, show that KMT2D harbours deletions and mutations in pancreatic ductal adenocarcinoma (PDAC); however, the actual frequencies of such mutations in PDAC are still debatable. [6, 7] Given the above, we cannot rule out the possibility that genetic inactivation of KMT2D relies partly on both its mutational and/or CpG methylation status.

Next, targeted bisulfite sequencing was performed for the specified region comprising nt −179 to +122, in a panel of five pancreatic cancer cell lines treated with the DNA methyltransferase inhibitor 5-AZA-2'-deoxycytidine (5-AZA-CdR, Decitabine). Boxplots of DNA methylation levels indicate that drug-treated cells have an extensive hypomethylated pattern (figure 2C and online supplementary figure S2A). Further evidence on the impact of CpG methylation to

repress KMT2D transcriptional activity was obtained from analysis of KMT2D mRNA levels on different exposure times and drug concentrations (figure 2D and online supplementary figure S2B). The most robust time-dependent and dose-dependent changes occurred in MIA PaCa-2 and AsPC-1 cell lines, an observation that was further validated by IB analysis (figure 2E). However, since this agent induces genome-wide demethylation, the observed increase in expression after treatment could be indirect. To eliminate this possibility, we designed a luciferase reporter assay for in vitro methylated KMT2D genomic region of interest (ROI) in wild-type or mutated state (figure 2F). Linearized constructs were *in vitro* methylated with high efficiency, as evidenced by resistance to digestion with HpaII methylation-specific endonuclease (figure 2G). As proof of concept, no significant differences were found among the promoter activity of unmethylated inserts (serving as positive controls), while in the totally unmodified methylated insert *Renilla luciferase reporter* (*hRluc*) gene activity was almost absent, thus confirming that CpG methylation controls transcriptional repression of KMT2D. Remarkably, both mutations applied in the ROI seem to derepress the *hRluc* activity of the *in vitro* methylated constructs by approximately 22-fold or 12-fold for Mut 1 and Mut 2, respectively (figure 2H, I). Taken together, our results identified that single-site CpGs methylation is critical for the suppression of KMT2D expression levels in pancreatic cancer.

KMT2D suppression promotes a metabolic shift to aerobic glycolysis through regulation of *SLC2A3*.

Next, we investigated the mechanisms downstream of KMT2D underlying its tumor suppressor functions. KMT2D belongs to the complex of proteins associated with Set1 (COMPASS) family of H3K4 methyltransferases[8]; thus, we first examined the effects of KMT2D on global H3K4 methylation marks in pancreatic cancer cells. Using IB we showed that H3K4 mono-methylated and di-methylated were slightly downregulated in the siKMT2D treated cells, while the tri-methylated form of H3K4 (H3K4me3) was significantly reduced (figure 3A). Furthermore, we tested the effect of 5-AZA-CdR treatment, as a mean to overexpress KMT2D, on the H3K4me3 levels of pancreatic cancer cells. Consistent with the notion that H3K4 methylation is enriched on 5-Aza-dCdR treatment, potentially as a secondary event following the promoter demethylation and gene re-expression,[9 10] we observed a remarkable enrichment of H3K4me3 methylation upon agent treatment. Interestingly, silencing of KMT2D in 5-Aza-dCdR-treated cells did not decrease H3K4me3 methylation levels as efficiently as in untreated cells, most possibly due to higher KMT2D levels (online supplementary figure S3A, B), while non-significant alterations in H3K4me1/2 levels were observed (online supplementary figure S3C). To complement these initial findings, ChIP-seq analysis for H3K4me3 and microarray gene expression profiling were performed in MIA PaCa-2 cells. ChIP-seq analysis showed significant decrease in H3K4me3 signals in KMT2D-

silenced versus non-targeting control cells (Figure 3B). The H3K4me3 peaks significantly overlap between the two different siRNAs used, as shown by the Venn diagram (figure 3C). H3K4me3 peaks were associated mostly with intergenic and intronic regions and were located around the TSS site (figure 3D, E). Marked loss of H3K4me3 peaks also occurs in *loci* essential for gene transcription as in the case of the *general transcription factor IIA subunit 1* (*GTF2A1*), a component of the transcription machinery of RNA polymerase II that plays an important role in transcriptional activation (online supplementary figure S4). Gene ontology (GO) analysis of the H3K4me3 peaks found to be diminished on KMT2D silencing identified association with transcription-related pathways, with the highest enrichment score being observed for 'transcription from RNA polymerase II promoter' and 'metabolic processes' (figure 3F). *Serine/Threonine kinase 11* (*STK11*) represents an example of KMT2D-mediated regulation of metabolic gene through reduction of H3K4me3 occupancy that was further experimentally validated as a direct regulatory target of KMT2D (online supplementary figure S5). Gene expression studies demonstrated 1035 genes to be downregulated, while a smaller subset of genes was upregulated on KMT2D suppression (figure 3G). We mapped the differentially regulated genes to well-established (canonical) pathways by using the Ingenuity Pathway Analysis (IPA) software (Ingenuity Systems, http://www. ingenuity. com/). Energy-converting biochemical processes, primarily related to glucose and fatty acid (FA) metabolism, were distinguished as KMT2D-mediated cellular functions (figure 3H). Collectively, both the ChIP-seq and microarray studies point to the association of KMT2D expression with metabolism-related pathways.

To further explore the functional consequences of the metabolism-associated KMT2D target(s), we measured changes of nicotinamide adenine dinucleotide phosphate (NADPH), which represents a fundamental common mediator of various biological processes including energy metabolism.[11] We found that cells harbouring low KMT2D levels accumulate higher NADPH levels in comparison with control cells (supplementary figure S6A). Given this observation, we reasoned to assay cultured cells in real time using an XF24-3 Analyzer to query changes in the bioenergetic status of KMT2D-suppressed versus control pancreatic cancer cells. Simultaneous assessment of both oxygen consumption rate (OCR) and extracellular acidification rate (ECAR) in basal state showed enhanced relative contribution of glycolysis on KMT2D suppression (figure 3I and online supplementary figure S6B, C). In particular, significant increase in ECAR values was observed, while OCR seems to remain unaffected, thus augmenting cellular preference for aerobic glycolysis. By quantifying the activity of the two major energy-yielding pathways in the cell, mitochondrial respiration and glycolysis, we provide evidence of a clear discrimination in the metabolic profiles driven by

loss of KMT2D expression. Furthermore, lactate production as well as glucose uptake were found to be significantly elevated on KMT2D silencing (online supplementary figure S6D–G).

In light of the above results, we hypothesised that KMT2D could influence glucose metabolism by controlling key glycolytic genes. Expression of the SLC2A1 (glucose transporter-1 (GLUT-1) that typically correlates with the rate of cellular glucose metabolism was found to be merely upregulated (+1.25-fold change) in *KMT2D*-silenced cells (figure 4A) and was not significantly affected in the tumors originating from xenografts bearing KMT2D stably suppressed pancreatic cancer cells (supplementary figure S7). Of note, *solute carrier family 2 member 3* (*SLC2A3*) (also known as *GLUT3*) was distinguished as the top differentially expressed glycolysis-related gene on KMT2D downregulation (figure 4A–C and online supplementary figure S8). To rule out secondary effects related to the genetic status of *SLC2A3* in the two different pancreatic cancer cell lines, we demonstrate that mostly common single nucleotide changes of SLC2A3 gene are observed, all of them ensuing synonymous substitutions (online supplementary table S8). Mapped DNA sequence reads from the ChIP-seq experiments mentioned above do not support the role of *SLC2A3* as a direct KMT2D transcriptional target. Hence, we assessed whether KMT2D transcriptionally regulates SLC2A3 through an indirect effect.

Tuberous sclerosis 1 (TSC 1), which acts as upstream negative regulator of mechanistic target of rapamycin (mTOR) activation, [12] was found to be significantly downregulated based on the gene expression array employed in KMT2D-supressed cells (figure 3G). In addition, by pharmacological or genetic strategies, it has been demonstrated that rapamycin-sensitive mTOR complex 1, consisting of mTOR itself and the regulatory-associated protein of mTOR (Raptor), is involved in the regulation of SLC2A3 expression. Specifically, loss of the TSC1 induced mTOR hyperactivation and SLC2A3 overexpression through the activation of the IκB kinase/nuclear factor kappa-light chain- enhancer of activated B cells (IKK/NF-κB) pathway.[13] In another report, stimulation of NF-κB activity has also been shown to directly upregulate *SLC2A3* gene transcription in mouse and human cells.[14] Indeed, IB analysis shows that reduction of KMT2D expression leads to increased phosphorylation and thus activation of mTOR (figure 4D) and increased phosphorylation of NF-κB p65 in Ser 536 (figure 4E). On the other hand, the expression of REL-associated protein (p65) involved in NF-κB heterodimer formation, nuclear translocation and activation is not influenced on KMT2D genetic manipulation (supplementary figure S9). Silencing of mTOR, but not Rictor (a specific component of mTORC2), as well as rapamycin treatment, reverse the SLC2A3 upregulation that is induced by low KMT2D levels (figure 4F and online supplementary figure S10). Furthermore, the use of inhibitors of NF-κB activation resulted in the partial reversal of SLC2A3 mRNA levels induction caused by KMT2D silencing (figure 4G). These data suggest that

KMT2D suppression promotes SLC2A3 expression via activation of the mTOR/NF-kB axis. The immunostaining patterns of activated NF-κB p65 and SLC2A3 in tumors from xenografts bearing KMT2D stably suppressed or mock-transfected MIA PaCa-2 cells (online supplementary figure S11) validated our *in vitro* findings. Most importantly, treatment of pancreatic cancer cells with siRNA for SLC2A3 rescues the metabolic (figure 4H), proliferative (figure 4I and online supplementary tables S9–S10) and anchorage-independent growth phenotypes (figure 4J) that are associated with KMT2D suppression. Collectively, the functional features displayed by SLC2A3 reduction in KMT2D low-expressing cells highlight its role as a mediator of KMT2D-induced effects.

Polyunsaturated fatty acids are increased in KMT2Dsuppressed cells and promote cell growth time-dependently.

It is now considered that cancer cells support their increased growth rate by increasing either the uptake of exogenous lipids or their endogenous synthesis.15 Functional enrichment analysis (figure 5A), as well as bioinformatics prediction of the top-rated pathways and networks (figure 3G and supplementary table S11) of differentially expressed genes in KMT2D-silenced cells, suggest that KMT2D expression has an impact on lipid metabolic processes. Genes found in the functional cluster are illustrated in figure 5B, and among those, *fatty acid synthase* (*FASN*), which encodes a multienzyme protein catalysing FA synthesis, is one of the top differentially regulated genes on *KMT2D* downregulation (supplementary figure S12). Interestingly, we noticed that MIA PaCa-2 and CAPAN-2 bearing xenografts exhibit a clear trend of increased body weight, mainly at prolonged stages of tumour growth (figure 5C and online supplementary figure S13), even though these mice were possibly expected to be of poorer health given their increased tumor burden. However, the increase in the overall body weight of the mice most possibly relates to the increased weight of the tumours.

As a next step, we used mass spectrometry-based technology to assess quantitative changes in FA composition and cholesterol content as a response to KMT2D silencing. Specifically, the total number of lipid species identified accounts for 28 FAs, all of which displayed increased levels relative to control cells (Table 1), with the most prominent differences being observed for the polyunsaturated fatty acids (PUFAs) docosadienoic, docosatrienoic and docosatetraenoic (Table 1 and figure 5D).

Interestingly, addition of the aforementioned lipids in serum free conditions resulted in increased MIA PaCa-2 cell growth in a time-dependent and dose-dependent manner (figure 5E) but did not affect pancreatic cancer cell's invasive capacity (supplementary figure S14). Furthermore, elevated cholesterol uptake was detected in MIA PaCa-2 cultured cells transiently transfected with an siRNA against KMT2D, as assessed by fluorescence microscopy (figure 5F). Subsequently, we explored whether cells harbouring low or high

KMT2D levels differentially respond to perturbations in lipid homeostasis by (1) silencing the low-density lipoprotein receptor (LDLR), the main selective route of cholesterol-rich lipoprotein entrance into cancer cells; (2) blocking the ATP citrate lyase, a critical enzyme for *de novo* synthesis of a wide range of complex cellular lipids such as cholesterol and long-chain FAs using the SB 204990 inhibitor; and (c) blocking the Δ6 desaturase, the rate-limiting enzyme that initiates the metabolism of the n-6 and n-3 PUFAs, linoleic acid and α-linolenic acid, respectively, into their downstream long-chain FA conversion products using the selective SC 26196 inhibitor. We found that reduction in MIA PaCa-2 cell proliferation rate caused by lipid synthesis/ uptake blockage is more pronounced in cells lacking KMT2D expression, with the maximum effect among the compounds used being observed in the case of the selective Δ6 desaturase inhibitor SC 26196 (figure 5G). The latter result substantiates the functional importance of the top KMT2D-regulated lipids in pancreatic cancer, since the SC26196 compound inhibits the rate-limiting step in arachidonic acid synthesis pathway, in which both docosadienoic and docosatetraenoic acids are implicated. Overall, these results revealed that the cellular lipid profiles depend on KMT2D expression. Furthermore, we are the first ones to show the potential of docosadienoic, docosatrienoic and docosatetraenoic acids to promote growth of pancreatic cancer cells, as evidenced by time-dependent studies.

Synergistic role of glycolytic and lipidomic effectors in KMT2D-related phenotype.

Lipogenic phenotype (characterised by increased FA synthesis, lipids' uptake and metabolism) has been functionally and temporally linked to the glycolytic metabolism in primary and metastatic cancers as essential interaction regulating the malignant phenotype.[16] Thus, we explored whether KMT2D-mediated impact on cancer cell proliferation is interdependent on both glucose/lipid metabolism-related downstream effectors. Notably, combined treatment of cells with an siRNA for SLC2A3 and the SC26196 inhibitor completely reversed the effect of *KMT2D* depletion in MIA PaCa-2 cell proliferation (figure 5H), thus indicating the synergistic role of both SLC2A3 expression and maintenance of proper lipid composition as mediators of KMT2D-induced proliferative phenotype.

Clinical relevance of the KMT2D expression in pancreatic cancer.

To define the clinical relevance of our findings, KMT2D expression was examined by IHC and quantitative automated image analysis in matched adjacent control-cancerous tissues from 26 patients with pancreatic cancer (cohort IV). KMT2D staining patterns showed that its nuclear localisation is almost absent in tumour samples, while highly expressed in normal tissues (Figure 6A and supplementary figure S15A). Further analysis of KMT2D expression in subgroups reflecting stage I or II of patients with pancreatic cancer (cohort IV), shows that the decrease in KMT2D levels may be significant in advanced stages of the disease (supplementary figure S15B). However, whether KMT2D levels relate to disease progression

needs to be further explored in extended numbers of human biopsies and genetically engineered mouse models of pancreatic cancer. Kaplan-Meier analysis performed in 158 cases (cohort V) and in 22 cases (cohort III) revealed that patients with pancreatic cancer harbouring low KMT2D expression levels had worse prognosis in comparison with patients harbouring high KMT2D levels (figure 6B and online supplementary figure S16). Sample power calculations conducted for the larger cohort V suggest that an extended sample size (over 2800 cases) is needed to reach statistical significance supplementary table S12). It should be highlighted that the samples derived from cohort V reflect mostly (90%) stage II cases, thus rendering it very difficult to detect survival differences with statistical significance. On the other hand, 86% of the tumours derived from cohort III reflect patients with stage III pancreatic cancer. Subsequently, we conducted correlation analysis for the levels of KMT2D with its downstream effectors. Expectedly, the Pearson coefficients computed reflect a negative correlation between KMT2D and SLC2A3 mRNA levels (figure 6C, D), based on publicly available gene expression array data and our experimental RT-qPCR validation studies. Significantly, IHC analysis of activated NF-κB p65 and SLC2A3 in matched adjacent control-cancerous tissues shows increased immunostaining of both in the tumor-derived samples where KMT2D protein levels were found to be very low compared with normal samples. These results further validate our in vitro mechanistic findings that suggest KMT2D-dependent NF-kB activation and thus SLC2A3 upregulation in pancreatic cancer.

Correlation of KMT2D expression with various clinical parameters is illustrated in table 2 and supplementary table S13. No significant association was observed between KMT2D expression and age (p=0.4976), sex (p=0.2999) or race (p=0.3702). Interestingly, patients with high KMT2D levels display dramatic weight loss and higher BMI values with high statistical significance. Out of 106 cases with above median (>3.917) KMT2D expression, 84 (79.2%) cases lost an average of 9.366 kg (20.65 pounds). On the other hand, a significant correlation of KMT2D expression was further observed in 95 cases with increased body fat, as assessed by BMI measurements. In our attempt to address whether biopsies derived from patients harbouring low KMT2D levels exert quantitative changes in FA composition and cholesterol content relatively to control tissues, we performed lipidomics analysis in samples derived from cohort II. Remarkably, we found that among the top lipids being robustly upregulated with statistical significance in human biopsies are docosadienoic, docosatrienoic and docosatetraenoic acids, thus validating our in vitro results showing dramatic increase of these PUFAs on genetic inactivation of KMT2D in pancreatic cancer cells (Table 3). Overall, these findings support the relevance of KMT2D for human pancreatic carcinogenesis. Figure 7 shows a diagram illustrating the upstream and downstream effectors of KMT2D expression and activity in pancreatic cancer.

DISCUSSION

Novel role for the KMT2D-H3K4me axis in pancreatic cancer.

Studies illustrating the role of KMT2D in histone H3K4 methylation at enhancers[17] or in the maintenance of genome stability in genes[18] help rationalize its widespread role in tumorigenesis. Based on a somatic knockout of KMT2D in human cells, microarray analysis revealed that a subset of genes that were associated with KMT2D-enriched loci displayed reduced expression in KMT2D-depleted cell lines that was accompanied by reduced H3K4me3.[19] Recent research focus indicates the direct connections between metabolism and chromatin dynamics, underlying many aspects of metabolic dysfunction. Interestingly, KMT2D-activating signal cointegrator-2 complex has been shown to play redundant but essential roles in ligand-dependent H3K4me3 and expression of liver X receptor target genes[20] and peroxisome proliferator-activated receptor gamma-dependent adipogenesis[21] and hepatic steatosis.[22]

Here, by analysing pathways derived from H3K4me3 regions, we identified an association of KMT2D expression with metabolic processes. Our ChIP-seq data and mechanistic experiments support that STK11 represents a direct regulatory target of KMT2D. Noteworthy, several groups suggest that STK11 role as a master regulator of polarity and metabolism contributes to its tumor suppressor function.[23 24] Beyond that, our ChIP-Seq data show that several transcription factors' loci exhibit significantly reduced H3K4me3 occupancy in KMT2D-silenced cells. Interestingly, it has been reported that focal rather than global loss of the H3K4me1/me2 marks has been observed at putative enhancers in mouse KMT2D-depleted lymphomas, and among the genes with concurrent expression changes were tumor suppressor genes.[25] In the present study, we did not explore H3K4me1 and H3K4me2 abundance on KMT2D silencing, since global loss of the marks genome-wide was not observed in pancreatic cancer cells. However, the possibility of H3K4me1/ me2 enrichment loss on KMT2D silencing in a focal manner could not be excluded. These data point to the complexity of a gene network contributing to the KMT2D-related metabolic phenotype of pancreatic cancer cells, either by the direct action of metabolic genes and/or by the secondary effects induced by transcription factors.

Importance of *SLC2A3* glucose transporter in pancreatic cancer.

Many studies have reported oncogenic aberrations of key glycolytic enzymes that mechanistically stimulate activation of glucose uptake.[26] SLC2A1 (GLUT-1) is a member of the GLUT family of facilitative glucose transporters that accounts for the uptake of glucose by malignant cells to a high extent. It is overexpressed in a wide range of human cancers, including pancreas,[27] and forced overexpression of SLC2A1 has been shown to induce pancreatic cancer cellular invasiveness.[28] However, in pancreatic cancer cells and xenografts

harbouring low KMT2D levels, minor changes in *SLC2A1* levels were observed, while very significant alterations were found in SLC2A3 expression. We found induction of the SLC2A3 glucose transporter triggered by KMT2D suppression, the former mediating the effect of KMT2D on cellular metabolism and proliferation. SLC2A3 displays a high affinity for glucose, thus ensuring efficient glucose uptake[29]; however, its expression is very low or undetectable in most organs of healthy adults. Of note, the impact of *SLC2A3* levels on the stimulation of brain tumour initiating cells' growth has been recently demonstrated,[30] and pathological SLC2A3 overexpression has been reported in pancreatic cancer.[31] In this realm, we now unveil a novel mechanism where the epigenome regulates the glycolytic profile of pancreatic cancer cells via SLC2A3 regulation.

Disease relevance for KMT2D-regulated pathways.

The biological findings reported in the literature suggest a cell type or context-dependent functional role of KMT2D in cancer. Impairment of cellular growth and invasion in breast cancer mouse xenografts, as well as in human colorectal and medulloblastoma cell lines, has been attributed to KMT2D knockdown. [32 33] On the other hand, Lee and colleagues[34] showed that KMT2D interacts directly with p53 to promote expression of p53 target genes. Remarkably, its early loss has been shown to facilitate lymphomagenesis by remodelling the epigenetic landscape of the cancer precursor cells.35 Our study supports that KMT2D restrains pancreatic cancer growth through the regulation of metabolic pathways. However, the study of Dawkins et al[36] focusing on the impact of H3K4 methyltransferases KMT2C and KMT2D in pancreatic adenocarcinoma biology points towards an oncogenic role for KMT2D. Specifically, transient knockdown of KMT2D in a panel of pancreatic cancer cell lines resulted in growth inhibition.[36] In our study KMT2D expression was stably blocked by four different shRNA sequences, thus evaluating the long-term effects of KMT2D inhibition of expression. The latter provides confidence for the specificity of the KMT2D-induced functional effects. Moreover, we performed real-time cell proliferation analysis based on the application of electrical cell substrate impedance changes method, which exhibits many advantages over the conventional endpoint assays for monitoring cell proliferation. Beyond the differences in the technical set-up, acquisition or loss of mutations by cancer cell lines could not be excluded. Nonetheless, the functional effects of KMT2D are supported by our mechanistic studies, showing that the genomic, glycolytic and lipidomic changes caused by KMT2D suppression refer and relate to a status of increased bioenergetic needs of proliferating cells. Furthermore, silencing of KMT2D causes significant alterations on the expression levels of genes with well-established roles in the biosynthesis, beta-oxidation, degradation or uptake facilitation of lipids, such as FASN, ACACA, LIPA and HMGCR. FASN, which was distinguished among the top differentially regulated genes on KMT2D downregulation, is essential for catalyzing the

formation of palmitate from acetyl-coenzyme A and malonyl-coenzyme A in the presence of NADPH, thus controlling the FAs biosynthesis.[37] It is considered a viable candidate as indicator of pathological state, marker of neoplasia, as well as pharmacological treatment target in pancreatic cancer.[38 39] In our *in vitro* experimental setting, FASN upregulation triggering increased FA synthesis possibly accounts for the moderate increase in palmitic acid levels, which is the first FA produced during FA synthesis and is the precursor to longer FAs. However, this finding was not validated in patients with pancreatic cancer (cohort III), as assessed by correlation analysis or KMT2D/FASN mRNA levels. This discrepancy could possibly be attributed to the small sample size used, which may not be adequate to detect significant correlations and/or the diversity of the genetic/ epigenetic patterns and other features of human pancreatic tumours. Nonetheless since a broader network of lipid-related genes are affected in KMT2D-suppressed pancreatic cancer cells, the extent to which distinct pathways such as lipid synthesis/ degradation/metabolism or efflux contribute to the phenotype of altered lipid profiles is currently under further investigation.

Interestingly, by using adipogenesis as a synchronised model of cell differentiation, it has been previously indicated that KMT2D exhibits cell type-specific and differentiation stage-specific genomic binding and is predominantly localised on enhancers. These data suggest a stepwise model of enhancer activation during adipogenesis that includes cooperative recruitment of KMT2D to perform H3K4me1/2 on enhancer-like regions by lineage-determining transcription factors, such as C/EBPβ, PPARγ and C/ EBPα.[17] In accordance to the concept of KMT2D as a component of genetic regulation that affects adipose/lipid homeostasis, our human data point out that patients harbouring high KMT2D expression experience greater weight loss and higher BMI than patients whose KMT2D levels are below the median value. The sample size of cohort V did not have enough power to define survival differences; however, there was a trend of increased survival in patients with higher levels of KMT2D. Discordance with the study of Dawkins *et al*,[36] showing that reduced expression of KMT2D correlates with improved outcome in PDAC, most possibly arises due to sample type differences, especially given that cohort V consists of samples from resected (stage II) cases. It has been documented that not only the degree of weight loss impacts survival of patients with pancreatic cancer, but also the proportion of muscle and fat loss in the different compartments.[40] Fat oxidation, decreased lipogenesis, impaired lipid deposition/adipogenesis and mainly elevated lipolysis have been linked to fat loss; however, the underlying mechanisms have not been clearly defined.[41] It is tempting to speculate that KMT2D expression may account for body weight and composition changes during illness progression, as a factor causing alterations in glucose/lipid/metabolism.

Taken together, our experimental strategy has revealed the mechanisms that regulate KMT2D expression and its downstream effectors in pancreatic oncogenesis. The present study offers

significant mechanistic value for potential treatment of pancreatic cancer as a metabolic disease regulated by the epigenome.

ACKNOWLEDGEMENTS

We thank Dr Emmanuelle Faure in the UCLA Integrated Molecular Technologies Core for her help and services.

CONTRIBUTORS

MK and DI conceived the project and designed the experiments. MK designed and executed most of the experiments. KS designed the chromatin related experiments. MH and CP assisted in mouse experiments, design/ development of the shRNAs, production of lentiviral expressing constructs and cell infections. ABT-R and SH-Y performed the immunohistochemical and digital pathology analysis (cohort IV). Clinical specimens were ascertained and provided by DK, HK, GAP, DWD, and TRD and JW processed all clinical information related to human patients' cohort III and cohort V, respectively. SM-J performed bioinformatics analysis and generated heatmaps, GO enrichment plots and Venn diagrams. EJT and LLA performed expression and statistical analyses. MK wrote the manuscript, prepared the figures and performed the statistical analyses, and revised by KS, MEF-Z and DI.

FUNDING

This study was supported in part by S10RR026744 from the National Center for Research Resources, S10RR027926 from the National Center for Research Resources, CA136526 from the National Institutes of Health, and P30 DK041301/ UL1TR000124 from the Center for Ulcer Research and Education Digestive Diseases Research Center and the National Center for Advancing Translational Sciences.

REFERENCES

1 Tzatsos A, Paskaleva P, Ferrari F, *et al*. KDM2B promotes pancreatic cancer via Polycomb-dependent and -independent transcriptional programs. *J Clin Invest* 2013;123:727–39.

2 Mallen-St Clair J, Soydaner-Azeloglu R, Lee KE, *et al*. EZH2 couples pancreatic regeneration to neoplastic progression. *Genes Dev* 2012;26:439–44.

3 Kubicek S, Gilbert JC, Fomina-Yadlin D, *et al*. Chromatin-targeting small molecules cause class-specific transcriptional changes in pancreatic endocrine cells. *Proc Natl Acad Sci U S A* 2012;109:5364–9.

4 Badea L, Herlea V, Dima SO, *et al*. Combined gene expression analysis of whole-tissue and microdissected pancreatic ductal adenocarcinoma identifies genes specifically overexpressed in tumor epithelia. *Hepatogastroenterology* 2008;55:2016–27.

5 Segara D, Biankin AV, Kench JG, *et al*. Expression of HOXB2, a retinoic acid signalling target in pancreatic cancer and pancreatic intraepithelial neoplasia. *Clin Cancer Res* 2005;11:3587–96.

6 Sausen M, Phallen J, Adleff V, *et al*. Clinical implications of genomic alterations in the tumour and circulation of pancreatic cancer patients. *Nat Commun* 2015;6:7686.

7 Bailey P, Chang DK, Nones K, *et al*. Genomic analyses identify molecular subtypes of pancreatic cancer. *Nature* 2016;531:47–52.

8 R uthenburg AJ, Allis CD, Wysocka J. Methylation of lysine 4 on histone H3: intricacy of writing and reading a single epigenetic mark. *Mol Cell* 2007;25:15–30.

9 Fahrner JA, Eguchi S, Herman JG, *et al*. Dependence of histone modifications and gene expression on DNA hypermethylation in cancer. *Cancer Res* 2002;62:7213–8.

10 Si J, Boumber YA, Shu J, *et al*. Chromatin remodeling is required for gene reactivation after decitabine-mediated DNA hypomethylation. *Cancer Res* 2010;70:6968–77.

11 Ying W. NAD+/NADH and NADP+/NADPH in cellular functions and cell death regulation and biological consequences. *Antioxid Redox Signal* 2008;10:179–206.

12 Zhang H, Bajraszewski N, Wu E, *et al*. PDGFRs are critical for PI3K/Akt activation and negatively regulated by mTOR. *J Clin Invest* 2007;117:730–8.

13 Zha X, Hu Z, Ji S, *et al*. NFκB up-regulation of glucose transporter 3 is essential for hyperactive mammalian target of rapamycin-induced aerobic glycolysis and tumor growth. *Cancer Lett* 2015;359:97–106.

14 Kawauchi K, Araki K, Tobiume K, *et al*. p53 regulates glucose metabolism through an IKK-NF-kappaB pathway and inhibits cell transformation. *Nat Cell Biol* 2008;10:611–8.

15 Beloribi-Djefaflia S, Vasseur S, Guillaumond F. Lipid metabolic reprogramming in cancer cells. *Oncogenesis* 2016;5:e189.

16 Zaidi N, Lupien L, Kuemmerle NB, *et al*. Lipogenesis and lipolysis: the pathways exploited by the cancer cells to acquire fatty acids. *Prog Lipid Res* 2013;52:585–9.

17 L ee JE, Wang C, Xu S, *et al*. H3K4 mono- and di-methyltransferase MLL4 is required for enhancer activation during cell differentiation. *Elife* 2013;2:e01503.

18 Kantidakis T, Saponaro M, Mitter R, *et al*. Mutation of cancer driver MLL2 results in transcription stress and genome instability. *Genes Dev* 2016;30:408–20.

19 G uo C, Chang CC, Wortham M, *et al*. Global identification of MLL2-targeted loci reveals MLL2's role in diverse signaling pathways. *Proc Natl Acad Sci U S A* 2012;109:17603–8.

20 Lee S, Lee J, Lee SK, *et al*. Activating signal cointegrator-2 is an essential adaptor to recruit histone H3 lysine 4 methyltransferases MLL3 and MLL4 to the liver X receptors. Molecular endocrinology (Baltimore, Md. 2008;22:1312–9.

21 Lee J, Saha PK, Yang QH, *et al*. Targeted inactivation of MLL3 histone H3-Lys-4 methyltransferase activity in the mouse reveals vital roles for MLL3 in adipogenesis. *Proc Natl Acad Sci U S A* 2008;105:19229–34.

22 Kim DH, Kim J, Kwon JS, *et al*. Critical Roles of the Histone Methyltransferase MLL4/KMT2D in Murine Hepatic Steatosis Directed by ABL1 and PPARγ2. *Cell Rep* 2016;17:1671–82.

23 Hezel AF, Bardeesy N. LKB1; linking cell structure and tumor suppression. *Oncogene* 2008;27:6908–19.

24 Spicer J, Ashworth A. LKB1 kinase: master and commander of metabolism and polarity. *Curr Biol* 2004;14:R383–R385.

25 Ortega-Molina A, Boss IW, Canela A, *et al*. The histone lysine methyltransferase KMT2D sustains a gene expression program that represses B cell lymphoma development. *Nat Med* 2015;21:1199–208.

26 Kroemer G, Pouyssegur J. Tumor cell metabolism: cancer's Achilles' heel. *Cancer Cell* 2008;13:472–82.

27 Reske SN, Grillenberger KG, Glatting G, *et al*. Overexpression of glucose transporter 1 and increased FDG uptake in pancreatic carcinoma. *J Nucl Med* 1997;38:1344–8.

28 Ito H, Duxbury M, Zinner MJ, *et al*. Glucose transporter-1 gene expression is associated with pancreatic cancer invasiveness and MMP-2 activity. *Surgery* 2004;136:548–56.

29 Simpson IA, Dwyer D, Malide D, *et al*. The facilitative glucose transporter GLUT3: 20 years of distinction. *Am J Physiol Endocrinol Metab* 2008;295:E242–E253.

30 Flavahan WA, Wu Q, Hitomi M, *et al*. Brain tumor initiating cells adapt to restricted nutrition through preferential glucose uptake. *Nat Neurosci* 2013;16:1373–82.

31 Yamamoto T, Seino Y, Fukumoto H, *et al*. Over-expression of facilitative glucose transporter genes in human cancer. *Biochem Biophys Res Commun* 1990;170:223–30.

32 Kim JH, Sharma A, Dhar SS, *et al*. UTX and MLL4 coordinately regulate transcriptional programs for cell proliferation and invasiveness in breast cancer cells. *Cancer Res* 2014;74:1705–17.

33 Guo C, Chen LH, Huang Y, *et al*. KMT2D maintains neoplastic cell proliferation and global histone H3 lysine 4 monomethylation. *Oncotarget* 2013;4:2144–53.

34 Lee J, Kim DH, Lee S, *et al*. A tumor suppressive coactivator complex of p53 containing ASC-2 and histone H3-lysine-4 methyltransferase MLL3 or its paralogue MLL4. *Proc Natl Acad Sci U S A* 2009;106:8513–8.

35 Zhang J, Dominguez-Sola D, Hussein S, *et al*. Disruption of KMT2D perturbs germinal center B cell development and promotes lymphomagenesis. *Nat Med* 2015;21:1190–8.

36 Dawkins JB, Wang J, Maniati E, *et al*. Reduced Expression of Histone Methyltransferases KMT2C and KMT2D Correlates with Improved Outcome in Pancreatic Ductal Adenocarcinoma. *Cancer Res* 2016;76:4861–71.

37 Baenke F, Peck B, Miess H, *et al*. Hooked on fat: the role of lipid synthesis in cancer metabolism and tumour development. *Dis Model Mech* 2013;6:1353–63.

38 Swierczynski J, Hebanowska A, Sledzinski T. Role of abnormal lipid metabolism in development, progression, diagnosis and therapy of pancreatic cancer. *World J Gastroenterol* 2014;20:2279–303.

39 Tadros S, Shukla SK, King RJ, *et al*. De Novo Lipid Synthesis Facilitates Gemcitabine Resistance through Endoplasmic Reticulum Stress in Pancreatic Cancer. *Cancer Res* 2017;77:5503–17.

40 Di Sebastiano KM, Yang L, Zbuk K, *et al*. Accelerated muscle and adipose tissue loss may predict survival in pancreatic cancer patients: the relationship with diabetes and anaemia. *Br J Nutr* 2013;109:302–12.

41 Ebadi M, Mazurak VC. Evidence and mechanisms of fat depletion in cancer. *Nutrients* 2014;6:5280–97.

FIGURE LEGENDS

Figure 1: **Histone methyltransferase KMT2D acts as a tumour suppressor in pancreatic cancer. (A)** KMT2D mRNA expression levels in three cohorts of pancreatic cancer and normal tissues, as assessed by RT-qPCR. **(B)** Transient suppression of KMT2D expression by two different siRNAs in pancreatic cancer cells. Efficiency of KMT2D downregulation, as assessed by RT-qPCR (left panel) and by IB analysis (right panel). Whole cell protein extracts were analysed by IB analysis for total KMT2D or CREB (used as a loading control). Numbers in parentheses denote the average fold change of the KMT2D:CREB total protein ratio of

siKMT2D transiently transfected cells compared with siC#1-treated cells (set as default 1) of at least two independent experiments, as assessed by densitometric analysis of the immunoreactive bands. **(C)** Dynamic monitoring of cellular proliferation on KMT2D transient suppression by using siKMT2D#2, using the xCELLigence RTCA SP system. **(D)** Assessment of KMT2D expression levels in MIA PaCa-2 cells transfected with #2–21 shRNA against KMT2D that underwent clonal selection resulting in clones a, b and c, by RT-qPCR (left panel) and IB analysis (right panel). Numbers in parentheses denote the average fold change of the KMT2D:CREB total protein ratio of shKMT2D stably transfected cells compared with mock-treated cells (set as default 1), as assessed by densitometric analysis of the immunoreactive bands. **(E)** Dynamic monitoring of the proliferation of the shKMT2D#2-21a clonal pancreatic cancer cell lines versus mock-transfected cells. **(F)** Effect of KMT2D stable suppression on soft agar colony formation. **(G)** Representative images of the excised tumours and **(H)** tumour volume (mm3) graphs of xenografts bearing KMT2D stably suppressed MIA PaCa-2 and CAPAN-2 cells (n=5 mice per group). For establishing shKMT2D#2-21a xenografts, MIA PaCa-2 or CAPAN-2 cells were injected subcutaneously in the right flank of NOD-SCID mice (five mice/group). **(I)** Representative IHC images for the proliferation marker Ki-67, corresponding to MIA PaCa-2 (upper two rows) and CAPAN-2 (bottom two rows) xenografts from mice injected with mock or shKMT2D#2-21a cells. Scale bars represent 50 μm. siC#1, cells transfected with a negative control scramble siRNA; siKMT2D#1, cells transfected with siRNA#1 for KMT2D; siKMT2D#2, cells transfected with siRNA#2 for KMT2D; mock, cells transfected with shRNA empty vector; shKMT2D#2–21, cells transfected with #2–21 shRNA for KMT2D; shKMT2D#2-21a, b or c, cells transfected with #2–21 shRNA for KMT2D that underwent clonal selection resulting in clones a, b and c; MX, mouse xenograft. OD, optical density. Statistical analyses were performed using one-way analysis of variance. Asterisks denote statistically significant differences, *p<0.05, **p<0.01, ***p<0.001. IB, immunoblot; IHC, immunohistochemical; KMT2D, histone lysine (K)-specific methyltransferase 2D; RT-qPCR, reverse transcription quantitative PCR; shRNA, short hairpin RNA; siRNA, small interfering RNA.

Figure 2: Epigenetic regulation of KMT2D levels through DNA methylation of two CpG sites. (A) Experimental design for the evaluation of KMT2D transcriptional repression-dependency on CpG methylation in pancreatic cancer. **(B)** Heatmap of methylation beta values for the selected probes (p<0.05, mean difference ≥0.25). Wilcoxon rank-sum tests were conducted to compare methylation array data between patients with pancreatic cancer and healthy controls. **(C)** Validation of CpG methylation levels via targeted bisulfite sequencing for the selected ROI (chr12: 49448986–49449286). Quantitative methylation measurements at the single CpG site level for untreated or 5-AZA-CdR-treated cells are box plotted (left panel)

or depicted as heatmaps of the methylation ratio (right panel). The colour indicates the level of methylation from higher to lower in yellow > orange> red order. **(D)** Dose response evaluation of 5-AZA-CdR treatment for 48 hours in KMT2D mRNA levels, as assessed by RT-qPCR. **(E)** Effect of 5-AZACdR treatment for 48 hours on KMT2D protein levels, as assessed by IB analysis. Numbers in parentheses denote the average fold change of the KMT2D:CREB total protein ratio in 5-AZA-CdR-treated cells compared with 0.005% DMSO-treated cells (set as default 1). **(F)** Schematic depiction of the distinct *KMT2D/hRluc* constructs used; the engineered *hRluc* was coupled to the genomic region (positions −179 to +121) of the human *KMT2D* gene. Tick marks represent the number and location of CpG dinucleotides. **(G)** The efficiency of CpG methylation was assessed in unmethylated and methylated, linearized and gel-purified constructs by resistance to digestion with HpaII endonuclease and subsequently agarose gel analysis. **(H, I)** Relative *hRluc* activity after *in vitro* methylation of *KMT2D* constructs using the promoterless pGL4.82 (*hRluc/Puro*) vector gene system. *HRluc* mean fluorescence intensity was measured in MIA PaCa-2 cells transfected with either (H) untreated or (I) CpG methyltransferase (MSssl)-treated *KMT2D/hRluc* constructs. To control for transfection efficiency, cells were co-transfected with a plasmid containing firefly luciferase (Luc) reporter gene and the levels of *hRluc* fluorescence were averaged over all *Luc* expressing cells. Statistical analyses were performed using one-way analysis of variance. Asterisks denote statistically significant differences, *p<0.05, **p<0.01, ***p<0.001. 5-AZA-CdR, 5-AZA-2'-deoxycytidine; DMSO, dimethyl sulfoxide; IB, immunoblot; KMT2D, histone lysine (K)-specific methyltransferase 2D; ROI, region of interest; RT-qPCR, quantitative reverse transcription PCR.

Figure 3: KMT2D-regulated pancreatic cancer cells' transcriptome and epigenome. (A) Effects of KMT2D silencing on the global levels of histone H3K4 monomethylation, dimethylation and trimethylation using IB analysis. Numbers in parentheses denote the average fold change of the H3K4me1, H3K4me2 or H3K4me3:H3 total protein ratio in *KMT2D*-silenced cells versus siC#1-treated cells (set as default 1). **(B)** Enrichment scores comparing the read density conditions for each set of peak regions are shown in the jittered boxplots. The enrichment values were tested with the Mann-Whitney U test (p<0.001). **(C)** Overlap of H3K4me3 peaks on KMT2D suppression using two different siRNAs. (D) Effect of *KMT2D* silencing on the genomic distribution of H3K4me3 peaks in MIA PaCa-2 cells. Pie chart indicates the enriched H3K4me3 peaks in negative siRNA versus siKMT2D#2-treated cells. **(E)** Distribution of H3K4 trimethylation mark around TSS. **(F)** GO terms associated with H3K4me3 binding sites were determined as follows: ChIP-seq peaks found in siC#1-treated cells versus peaks found in cells treated with siKMT2D#2 were associated with the nearest ENSEMBL transcript and processed using the DAVID (V.6.7) tool. The data presented are

log-transformed p value of GO terms found to be enriched in the tested group of genes. **(G)** Heatmap showing the differentially expressed genes in MIA PaCa-2 cells on KMT2D suppression. Data were filtered using a p value cut-off of 0.05 and a fold change cut-off of 2.0. Clustering dendrograms show the relative expression values according to the following colouring scheme: red: high; black: moderate; green: low. **(H)** List of metabolism-associated canonical pathways derived from the IPA GO algorithms for the KMT2D-regulated genes (from figure 3G). −log (p value) is measured by the bar length, while R refers to the number of molecules from the data set that map to the pathway listed divided by the total number of molecules that map to the pathway from within the IPA knowledge base. **(I)** OCR/ECAR curves for KMT2D stably transfected pancreatic cancer cells (Seahorse Technology). R, ratio; oligo, oligomycin; FCCP, carbonyl cyanide-4-(trifluoromethoxy) phenylhydrazone; RM, rotenone/myxothiazol. ChIP-seq, chromatin immunoprecipitation-sequencing; ECAR, extracellular acidification rate; GO, Gene Ontology; IB, immunoblot; IPA, Ingenuity Pathway Analysis; KMT2D, histone lysine (K)-specific methyltransferase 2D; OCR, oxygen consumption rate; siC#1, cells transfected with a negative control scramble siRNA; siKMT2D#1, cells transfected with siRNA#1 for KMT2D; siKMT2D#2, cells transfected with siRNA#2 for KMT2D; siRNA, small interfering RNA; TSS, transcription start site.

Figure 4: KMT2D regulates pancreatic cancer cell growth and metabolism by affecting SLC2A3 glucose transporter. (A) Heatmap summarising the differentially expressed glycolysis-related genes in MIA PaCa-2 cells on KMT2D suppression. Data were filtered using a p value cut-off of 0.05 and a fold change cut-off of 1.25. **(B)** *SLC2A3* mRNA expression in pancreatic cancer cells on KMT2D silencing. **(C)** *SLC2A3* expression in MIA PaCa-2 xenografts from mice injected with mock or shKMT2D#2-21a cells, as assessed by RT-qPCR. **(D)** Representative IB images for the activated and total (D) mTOR and **(E)** NF-κB p65 on KMT2D silencing. Numbers in parentheses denote the average fold change of the phosphorylated:total protein ratio of KMT2D-silenced cells versus siC#1-treated cells (set as default 1) of at least two independent experiments. **(F)** Representative IB images for SLC2A3, mTOR, Rictor and CREB protein levels on treatment of MIA PacA-2 cells harbouring differential KMT2D levels with siRNAs against mTOR, Rictor or the respective scramble control. Numbers in parentheses denote the average fold change of the SLC2A3:CREB total protein ratio of siRNAtreated cells versus siC#1-treated cells (set as default 1). **(G)** Treatment of MIA PaCa-2 cells with inhibitors of NF-κB activation for 24 hours reverses the KMT2D-mediated increase in SLC2A3 mRNA levels. Effects of *SLC2A3* silencing on the **(H)** bioenergetic status, *(I)* proliferation and *(J)* colony formation ability of KMT2D-suppressed cells. Statistical analyses were performed using one-way analysis of variance. Asterisks denote statistically significant differences, *p<0.05, **p<0.01, ***p<0.001. DMSO, dimethyl

sulfoxide; ECAR, extracellular acidification rate; FCCP, carbonyl cyanide-4-(trifluoromethoxy) phenylhydrazone; IB, immunoblot; KMT2D, histone lysine (K)-specific methyltransferase 2D; mechanistic target of rapamycin (mTOR);NF-κB, nuclear factor kappa-light-chain-enhancer of activated B cells; OCR, oxygen consumption rate; OD, optical density; oligo, oligomycin; RM, rotenone/myxothiazol; RT-qPCR, reverse transcription quantitative PCR;siRNA; small interfering RNA; siC#1, cells transfected with a negative control scramble siRNA; siKMT2D#1, cells transfected with siRNA#1 for KMT2D; siKMT2D#2, cells transfected with siRNA#2 for KMT2D; siSLC2A3, cells transfected with siRNA for SLC2A3.

Figure 5: KMT2D inhibition alters the lipid composition and cholesterol content in pancreatic cancer. (A) GO-based annotation was used to perform functional enrichment analysis using the DAVID (V.6.7) tool. Fold enrichment of genes (associated with lipid metabolic processes) regulated by KMT2D levels is measured by the bar length while p value represents the significance of the enrichment. (B) Heatmap summarising the differentially expressed lipid metabolism-related genes in MIA PaCa-2 cells on KMT2D suppression. Data were filtered using a p value cut-off of 0.05 and a fold change cut-off of 1.5. (C) Body weight graphs of mouse xenografts bearing MIA PaCa-2 or CAPAN-2 shKMT2D#2-21a clonal cell lines and mock transfected cells (n=5 mice per group). (D) Column graph illustrating quantitative changes of the top 3 FAs regulated by KMT2D. (E) Time-dependent and dose-dependent effects of exogenously added FAs on cell proliferation, as assessed by CellTiter Glo Luminescence Cell Viability Assay. (F) Detection of cholesterol uptake within MIA PaCa-2 cultured cells, as assessed by fluorescence microscopy. Scale bars represent 50 μm. (G, H) Time-dependent effect of LDLR or SLC2A3 silencing, SC 26196 and SC 204990 inhibitors on cell proliferation in high and low KMT2D-expressing cells, as assessed by CellTiter Glo Luminescence Cell Viability Assay. Statistical analyses were performed using one-way analysis of variance. Asterisks denote statistically significant differences, *p<0.05, **p<0.01, ***p<0.001. FA, fatty acid; FBS, fetal bovine serum; GO, Gene Ontology; KMT2D, histone lysine (K)-specific methyltransferase 2D; LDLR, low-density lipoprotein receptor.

Figure 6: Correlation of KMT2D levels between its targets and disease aggressiveness. (A) (i) Representative images (10× magnification) of KMT2D expression, as assessed by IHC analysis, in matched cancer and normal tissues from patients with pancreatic cancer (cohort IV). (ii) Automated image analysis using the Spectrum Software V.11.1.2.752 (Aperio) was performed for nuclear staining quantification. (B) Correlation of KMT2D expression with overall patient survival. Kaplan-Meier survival curves of patients harbouring below median (<3.917) and above median (>3.917) KMT2D levels derived from cohort V. (C, D) Correlation of KMT2D levels with SLC2A3 expression in patients with pancreatic cancer based on the study by Badea *et al*[4] and as assessed by RT-qPCR (cohort III). (E) Representative images (10×

magnification) of phospho-NF-kB p65 (Ser 536) and *SLC2A3* expression, as assessed by IHC analysis, in matched cancer and normal tissues from patients with pancreatic cancer (cohort IV). Scale bars represent 50 μm. r, Pearson correlation coefficient; Kaplan-Meier test was used for univariate survival analysis. Cox proportional hazard model was used for multivariate analysis and for determining the 95% CI. Statistical analyses were performed using one-way analysis of variance or Pearson correlation. Asterisks denote statistically significant differences, **p<0.01. BMI, body mass index; IHC, immunohistochemical; KMT2D, histone lysine (K)-specific methyltransferase 2D; NF-kB, nuclear factor kappa-light-chain-enhancer of activated B cells; RT-qPCR, reverse transcription quantitative PCR.

Figure 7: Schematic depiction of KMT2D transcriptional regulation and downstream mechanistic targets and pathways in pancreatic cancer. Methylation of two single CpG sites transcriptionally represses KMT2D histone methyltransferase expression. Suppression of KMT2D induces aerobic glycolysis and lipid levels in pancreatic cancer. SLC2A3 consists a key mediator of the cellular growth and metabolic effects triggered by KMT2D downregulation. Docosadienoic, docosatrienoic and docosatetraenoic acid represent the top KMT2D-regulated fatty acids and harbour oncogenic properties in pancreatic cancer cells. KMT2D, histone lysine (K)-specific methyltransferase 2D.

TABLE LEGENDS

Table 1: Quantitative LC-MS data of fatty acids and total cholesterol in MIA PaCa-2 cells pretreated with siC#1 or siKMT2D#2. The top three lipids most significantly elevated by KMT2D reduction are shown in bold. Statistical analyses were performed using one-way analysis of variance. KMT2D, histone lysine (K)-specific methyltransferase 2D.

Table 2: Pancreatic carcinomas were subdivided into two groups: carcinomas with below median (<3.917) KMT2D expression and carcinomas with above median (>3.917) KMT2D expression. n is the number of patients with clinical information. Clinical correlations were examined using the SAS 9.4 for LINUX platform. BMI, body mass index; KMT2D, histone lysine (K)-specific methyltransferase 2D; LC-MS, Liquid Chromatography-Mass Spectrometry.

Table 3: Quantitative LC-MS data of fatty acids and total cholesterol in pancreatic cancer biopsies versus normal tissues. Pancreatic carcinomas from cohort II were subdivided into two groups: carcinomas with below median (<0.3) KMT2D expression and carcinomas with above median (>0.3) KMT2D expression. Four cancerous tissues displaying below median (<0.3) KMT2D levels underwent lipidomic profiling. The top three lipids most significantly elevated are shown in bold. Statistical analyses were performed using one-way analysis of variance. ∞ represents infinity as the denominator is so small that is virtually zero; KMT2D,

histone lysine (K)-specific methyltransferase 2D; LC-MS, liquid chromatography mass spectrometry.

TABLES

Table 1: Effect of KMT2D silencing on the lipidomic profile of pancreatic cancer cells

Lipid	siC#1 (ng) per 50000 cells	siKMT2D#2 (ng) per 50000 cells	Percentage change	P values
Docosatrienoic acid	0.6	1.5	+150	0.00482
Docosadienoic acid	0.35	1	+186	0.00971
Docosatetraenoic acid	1.425	3.5	+150	0.01084
Nervonic acid	4.1	10.1	+146.3	0.00217
Eicosadienoic acid	2.825	6.55	+131.8	0.00557
Dihomo-g-linolenic acid	1.3	2.925	+125	0.0075
Eicosapentaenoic acid	8	17.075	+113.4	0.19345
Eicosenoic acid	32.675	68.675	+110.2	0.00116
Docosapentaenoic acid (n=3)	4.55	9.1	+100	0. 0 00 229
Docosenoic acid	3.65	6.825	+87	0.00364
Docosahexaenoic acid	4.675	8.2	+75.4	0.02643
Arachidonic acid	8.933	13.825	+54.8	0.009
g-Linolenic acid	8.325	12.175	+46.2	0.16032
Oleic acid	715.6	1049.775	+46.7	0.01402
a-Linolenic acid	4.1	5.9	+43.9	0.16846
Stearic acid	2563.2	3667.875	+43.1	0.11082
Linoleic acid	23.7	33.575	+41.7	0.07341
Hexacosanoic acid	7.05	9.95	+41.1	0.13026
Cholesterol	359.25	474.75	+32.2	0.04811
Dodecanoic acid	82.25	108.1	+31.4	0.0013
Palmitoleic acid	118.775	148.575	+25.1	0.26513
Lignoceric acid	25.375	30.825	+21.5	0.21665
Palmitic acid	7676	8941.525	+16.5	0.05763
Docosanoic (Behenic acid)	9.575	10.475	+9.4	0.38668
Heptadecenoic acid	71.55	78.075	+9.1	0.10477
Pentadecanoic	486.375	524.125	+7.8	0.27158
Heptadecanoic acid	91.15	96.85	+6.3	0.35989
Arachidic acid	20.55	21.65	+5.4	0.5251
Myristic acid	459.625	480.375	+4.5	0.08533

Table 2: Correlation of KMT2D expression with demographic and clinical characteristics of patients with pancreatic cancer (cohort V)

KMT2D expression	below median (≤3.917) (n=109)	Above median (>3.917) (n=111)	P values
Age at diagnosis			0.4976
n	86	102	
Mean (SD)	64.65 (11.72)	64.01 (11.53)	
Median	66.50	63.50	
Q1, Q3	55.00, 75.00	57.00, 74.00	
Range	(37.00–88.00)	(41.00–92.00)	
Vital status			0.1274
Missing	10	5	
Alive	14 (14.1%)	8 (7.5%)	
Deceased	85 (85.9%)	98 (92.5%)	
Survival (days)			
n	69	89	
Events	60	81	
Median survival days	712.0 (552.0–1017.0)	608.0 (518.0–811.0)	
5-year survival rate	11.7% (3.5%–20.0%)	19.7% (11.3%–28.2%)	
Year 5, n at risk	6	15	
Sex			0.2999
Missing	10	5	
Female	52 (52.5%)	48 (45.3%)	
Male	47 (47.5%)	58 (54.7%)	
Race			0.3702
Missing	14	5	
1=American Indian/Alaskan Native	0 (0.0%)	1 (0.9%)	
2=Asian/Asian-American	2 (2.1%)	0 (0.0%)	
3=Black/African–American	1 (1.1%)	1 (0.9%)	
5=White	92 (96.8%)	104 (98.1%)	
Usual adult BMI			0.0040
n	74	95	
Mean (SD)	27.31 (5.40)	29.92 (5.64)	
Median	27.01	29.19	
Q1, Q3	24.24, 30.04	25.75, 32.96	
Range	(15.31–43.72)	(18.88–46.18)	
Usual adult BMI (<30, 30+)			0.0367
Missing	35	16	
<30	55 (74.3%)	56 (58.9%)	
30+	19 (25.7%)	39 (41.1%)	
Weight loss			0.0005
Missing	10	5	
No	43 (43.4%)	22 (20.8%)	
Yes	56 (56.6%)	84 (79.2%)	
Pounds lost			0.0001
n	99	106	
Mean (SD)	5.116 (6.191)	9.3664 (8.323)	
Median	2.698	7.937	
Q1, Q3	0.00, 9.071	4.499, 13.607	
Range	(0.00–27.215)	(0.00–38.555)	
Stage at surgery			0.3117
Missing	49	26	
IA	0 (0.0%)	1 (1.2%)	
IB	6 (10.0%)	6 (7.1%)	
IIA	12 (20.0%)	28 (32.9%)	
IIB	42 (70.0%)	49 (57.6%)	
IV	0 (0.0%)	1 (1.2%)	

Table 3: Lipidomic profiling of low KMT2D-expressing pancreatic cancer biopsies versus normal pancreata

Lipid	Adjacent normal	Cancerous tissue	Percentage change	P values
Docosatrienoic acid	–	0.0125	∞	0.04006
Docosadienoic acid	–	0.0225	∞	0.02401
Docosatetraenoic acid	0.0325	0.2125	+553.8	0.03181
Nervonic acid	0.05	0.275	+450	0.07178
Eicosadienoic acid	0.0475	0.6325	+1232	0.06733
Dihomo-g-linolenic acid	0.075	0.34	+353	0.03279
Eicosapentaenoic acid	0.085	0.1125	+32.35	0.64401
Eicosenoic acid	1.0775	13.371	+1426.2	0.06179
Docosapentaenoic acid (n=3)	0.045	0.2025	+350	0.08372
Docosenoic acid	0.2375	1.34	+464.21	0.03204
Docosahexaenoic acid	0.055	0.1625	+195.45	0.09208
Arachidonic acid	0.695	1.32	+89.93	0.07636
Oleic acid	36.4525	347.835	+854.2	0.13282
a-Linolenic acid and g-linolenic acid	0.0225	0.315	+1300	0.05199
Stearic acid	15.275	20.23	+32.94	0.59416
Linoleic acid	3.1525	15.5675	+393.8	0.09712
Hexacosanoic acid	0.0125	0.0225	+80.0	0.71105
Cholesterol	23.28843	53.64114	+130.33	0.00787
Dodecanoic acid	0.5075	1.87	+268	0.03587
Palmitoleic acid	3.515	29.14	+788	0.09423
Lignoceric acid	0.12	0.27	+125	0.29288
Palmitic acid	25.89	59.3875	+129.4	0.17425
Docosanoic (Behenic acid)	0.13	0.2725	+109.62	0.02932
Heptadecenoic acid	0.4525	3.64	+704	0.10735
Pentadecanoic	0.34	1.86	+447.1	0.06233
Heptadecanoic acid	0.33	1.72	+421.2	0.06334
Arachidic acid	0.14	0.5875	+319.64	0.02278
Myristic acid	1.5275	10.325	+675.9	0.05614

FIGURE 1

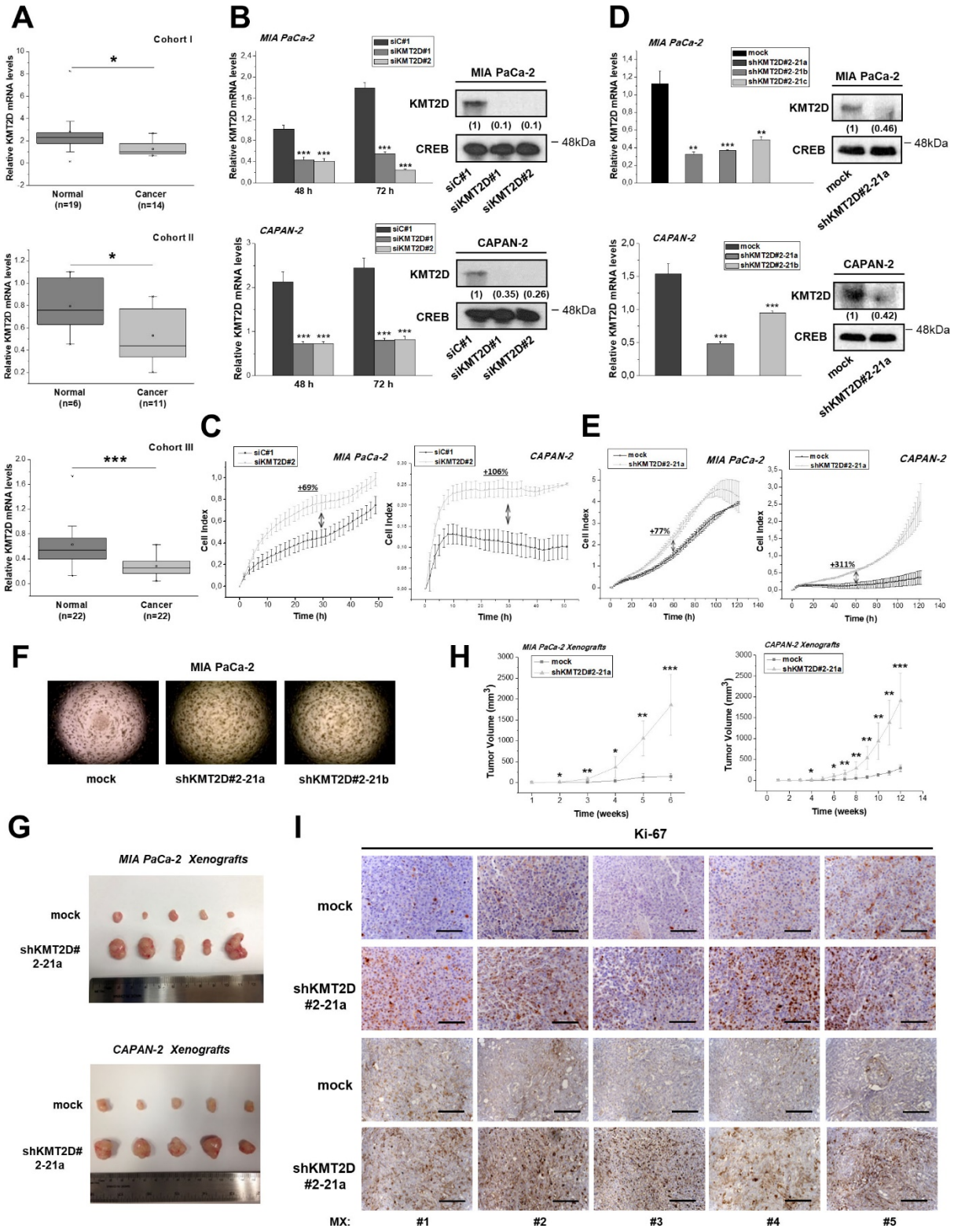
A
Cohort I
Relative KMT2D mRNA levels
Normal (n=19)
Cancer (n=14)
Cohort II
Normal (n=6)
Cancer (n=11)
Cohort III
Normal (n=22)
Cancer (n=22)
B
MIA PaCa-2
CAPAN-2
siC#1
siKMT2D#1
siKMT2D#2
48 h
72 h
KMT2D
CREB
48kDa
D
mock
shKMT2D#2-21a
shKMT2D#2-21b
shKMT2D#2-21c
C
Cell Index
Time (h)
+69%
+106%
E
+77%
+311%
F
mock
shKMT2D#2-21a
shKMT2D#2-21b
H
Tumor Volume (mm3)
Time (weeks)
G
MIA PaCa-2 Xenografts
CAPAN-2 Xenografts
I
Ki-67
MX:
#1
#2
#3
#4
#5

FIGURE 2

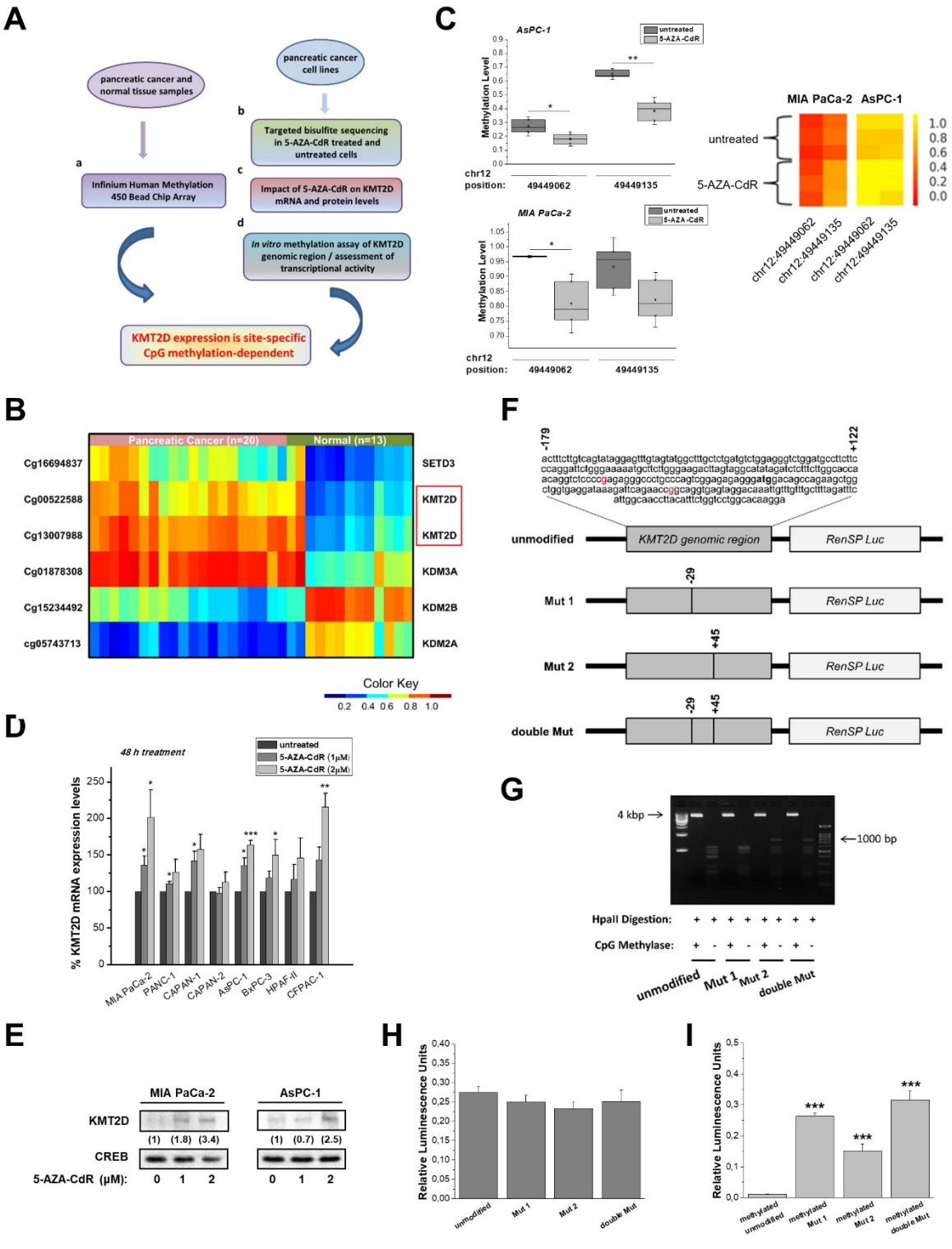
A
pancreatic cancer and normal tissue samples
pancreatic cancer cell lines
a
Infinium Human Methylation 450 Bead Chip Array
b
Targeted bisulfite sequencing in 5-AZA-CdR treated and untreated cells
c
Impact of 5-AZA-CdR on KMT2D mRNA and protein levels
d
In vitro methylation assay of KMT2D genomic region / assessment of transcriptional activity
KMT2D expression is site-specific CpG methylation-dependent
C
AsPC-1
untreated
5-AZA-CdR
Methylation Level
chr12 position:
49449062
49449135
MIA PaCa-2
MIA PaCa-2 AsPC-1
untreated
5-AZA-CdR
chr12:49449062
chr12:49449135
B
Pancreatic Cancer (n=20)
Normal (n=13)
Cg16694837
Cg00522588
Cg13007988
Cg01878308
Cg15234492
cg05743713
SETD3
KMT2D
KMT2D
KDM3A
KDM2B
KDM2A
Color Key
F
-179
+122
unmodified
KMT2D genomic region
RenSP Luc
Mut 1
-29
Mut 2
+45
double Mut
D
48 h treatment
untreated
5-AZA-CdR (1μM)
5-AZA-CdR (2μM)
% KMT2D mRNA expression levels
MIA PaCa-2
PANC-1
CAPAN-1
CAPAN-2
AsPC-1
BxPC-3
HPAF-II
CFPAC-1
G
4 kbp
1000 bp
HpaII Digestion:
CpG Methylase:
unmodified
Mut 1
Mut 2
double Mut
E
MIA PaCa-2
AsPC-1
KMT2D
CREB
(1) (1.8) (3.4)
(1) (0.7) (2.5)
5-AZA-CdR (μM):
0 1 2
0 1 2
H
Relative Luminescence Units
unmodified
Mut 1
Mut 2
double Mut
I
Relative Luminescence Units
methylated unmodified
methylated Mut 1
methylated Mut 2
methylated double Mut

FIGURE 3

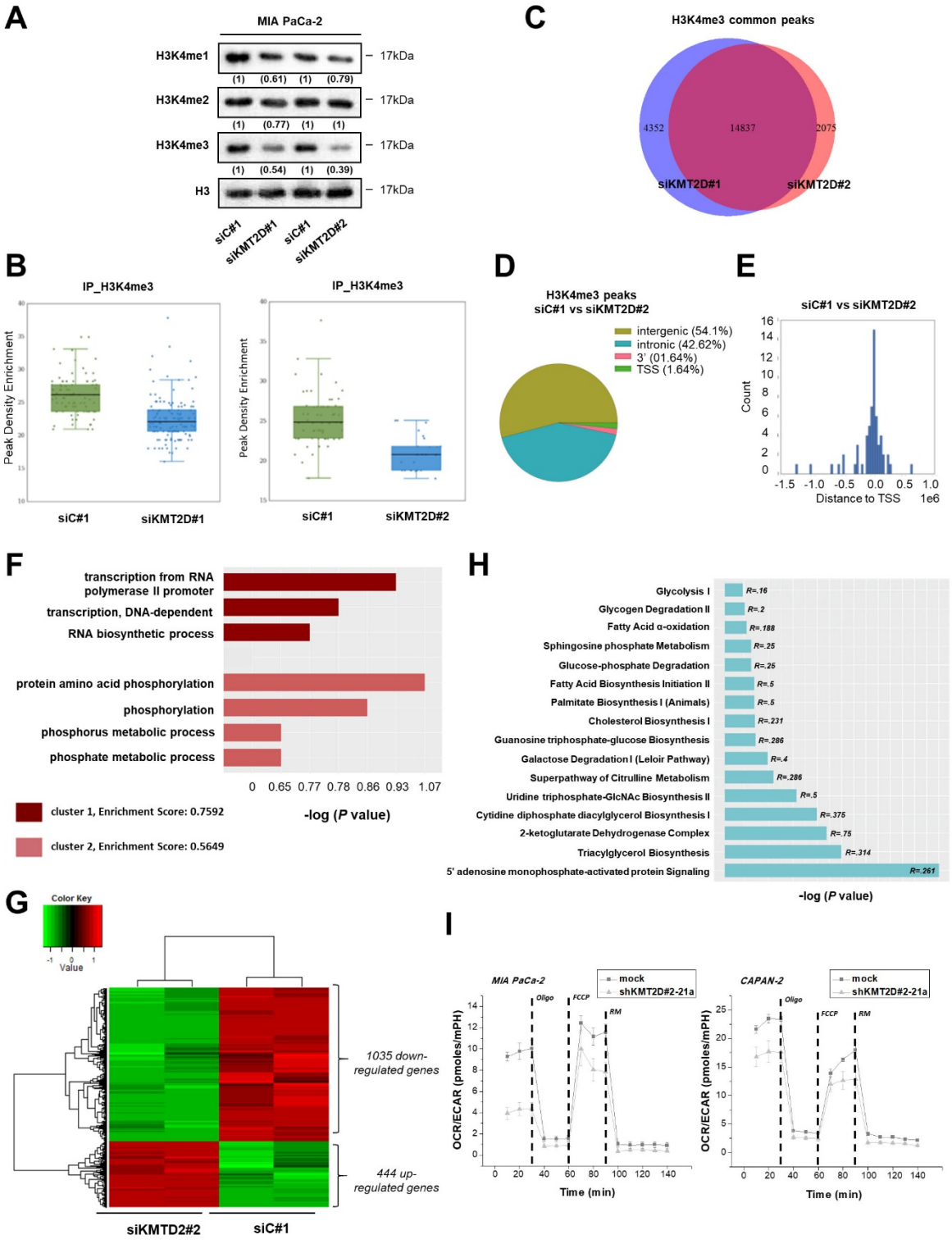
A
MIA PaCa-2
H3K4me1
H3K4me2
H3K4me3
H3
17kDa
(1) (0.61) (1) (0.79)
(1) (0.77) (1) (1)
(1) (0.54) (1) (0.39)
siC#1
siKMT2D#1
siC#1
siKMT2D#2
C
H3K4me3 common peaks
4352
14837
2075
siKMT2D#1
siKMT2D#2
B
IP_H3K4me3
Peak Density Enrichment
siC#1
siKMT2D#1
IP_H3K4me3
Peak Density Enrichment
siC#1
siKMT2D#2
D
H3K4me3 peaks
siC#1 vs siKMT2D#2
intergenic (54.1%)
intronic (42.62%)
3' (01.64%)
TSS (1.64%)
E
siC#1 vs siKMT2D#2
Count
Distance to TSS
1e6
F
transcription from RNA polymerase II promoter
transcription, DNA-dependent
RNA biosynthetic process
protein amino acid phosphorylation
phosphorylation
phosphorus metabolic process
phosphate metabolic process
0 0.65 0.77 0.78 0.86 0.93 1.07
-log (P value)
cluster 1, Enrichment Score: 0.7592
cluster 2, Enrichment Score: 0.5649
H
Glycolysis I
Glycogen Degradation II
Fatty Acid α-oxidation
Sphingosine phosphate Metabolism
Glucose-phosphate Degradation
Fatty Acid Biosynthesis Initiation II
Palmitate Biosynthesis I (Animals)
Cholesterol Biosynthesis I
Guanosine triphosphate-glucose Biosynthesis
Galactose Degradation I (Leloir Pathway)
Superpathway of Citrulline Metabolism
Uridine triphosphate-GlcNAc Biosynthesis II
Cytidine diphosphate diacylglycerol Biosynthesis I
2-ketoglutarate Dehydrogenase Complex
Triacylglycerol Biosynthesis
5' adenosine monophosphate-activated protein Signaling
R=.16
R=.2
R=.188
R=.25
R=.26
R=.5
R=.5
R=.231
R=.286
R=.4
R=.286
R=.5
R=.375
R=.75
R=.314
R=.261
-log (P value)
G
Color Key
Value
1035 down-regulated genes
444 up-regulated genes
siKMTD2#2
siC#1
I
MIA PaCa-2
mock
shKMT2D#2-21a
Oligo
FCCP
RM
OCR/ECAR (pmoles/mPH)
Time (min)
CAPAN-2
mock
shKMT2D#2-21a
Oligo
FCCP
RM
OCR/ECAR (pmoles/mPH)
Time (min)

FIGURE 4

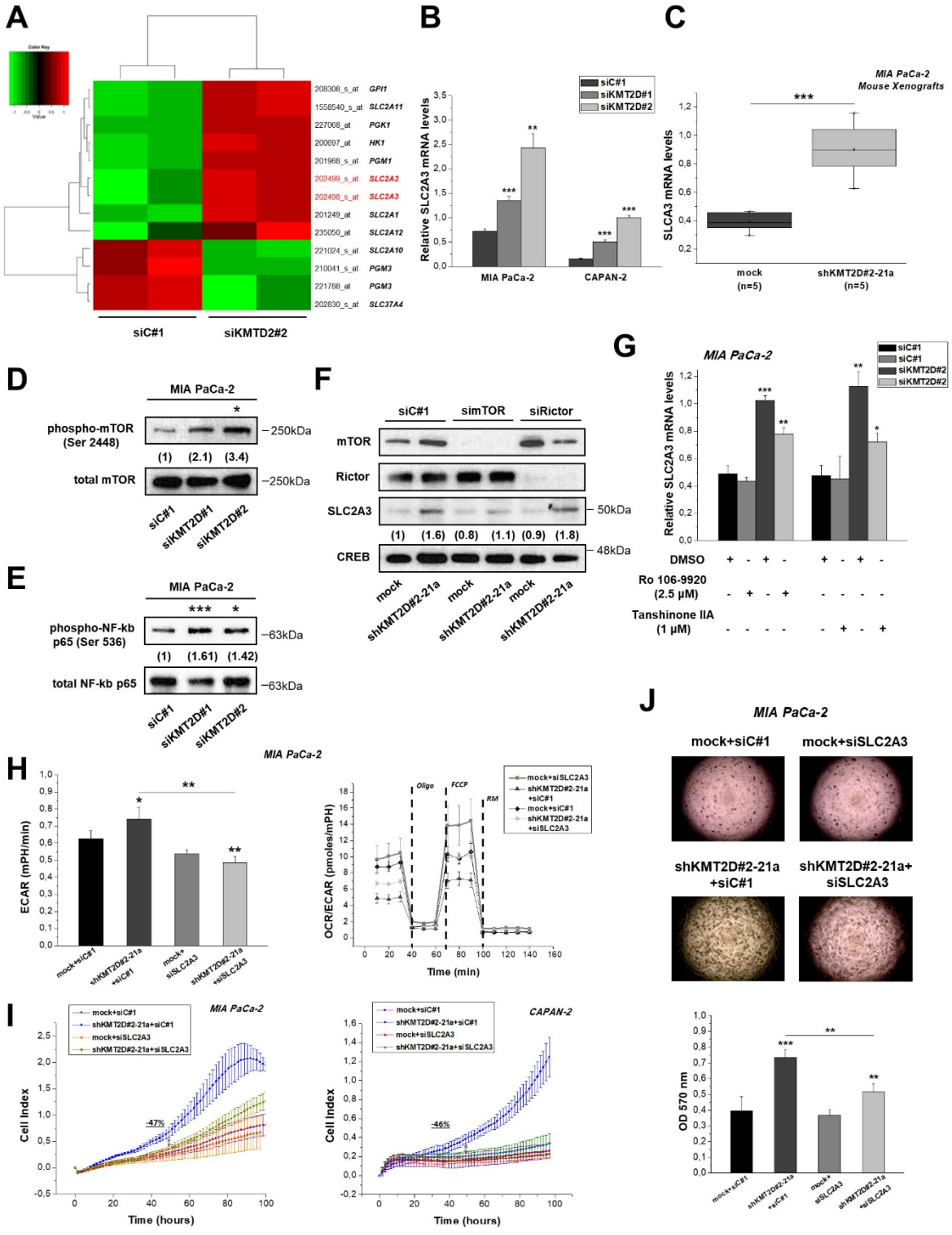
A
208308_s_at GPI1
1558540_s_at SLC2A11
227068_at PGK1
200697_at HK1
201988_s_at PGM1
202499_s_at SLC2A3
202498_s_at SLC2A3
201249_at SLC2A1
235050_at SLC2A12
221024_s_at SLC2A10
210041_s_at PGM3
221788_at PGM3
202830_s_at SLC37A4
siC#1
siKMTD2#2
B
siC#1
siKMT2D#1
siKMT2D#2
Relative SLC2A3 mRNA levels
MIA PaCa-2
CAPAN-2
C
MIA PaCa-2
Mouse Xenografts
SLCA3 mRNA levels
mock (n=5)
shKMT2D#2-21a (n=5)
D
MIA PaCa-2
phospho-mTOR (Ser 2448)
total mTOR
250kDa
(1) (2.1) (3.4)
siC#1
siKMT2D#1
siKMT2D#2
E
MIA PaCa-2
phospho-NF-kb p65 (Ser 536)
total NF-kb p65
63kDa
(1) (1.61) (1.42)
F
siC#1
simTOR
siRictor
mTOR
Rictor
SLC2A3
CREB
50kDa
48kDa
(1) (1.6) (0.8) (1.1) (0.9) (1.8)
mock
shKMT2D#2-21a
G
MIA PaCa-2
siC#1
siC#1
siKMT2D#2
siKMT2D#2
Relative SLC2A3 mRNA levels
DMSO
Ro 106-9920 (2.5 μM)
Tanshinone IIA (1 μM)
H
MIA PaCa-2
ECAR (mPH/min)
mock+siC#1
shKMT2D#2-21a +siC#1
mock+ siSLC2A3
shKMT2D#2-21a +siSLC2A3
OCR/ECAR (pmoles/mPH)
Oligo
FCCP
RM
Time (min)
I
MIA PaCa-2
mock+siC#1
shKMT2D#2-21a+siC#1
mock+siSLC2A3
shKMT2D#2-21a+siSLC2A3
Cell Index
-47%
Time (hours)
CAPAN-2
-46%
J
MIA PaCa-2
mock+siC#1
mock+siSLC2A3
shKMT2D#2-21a +siC#1
shKMT2D#2-21a+ siSLC2A3
OD 570 nm

FIGURE 5

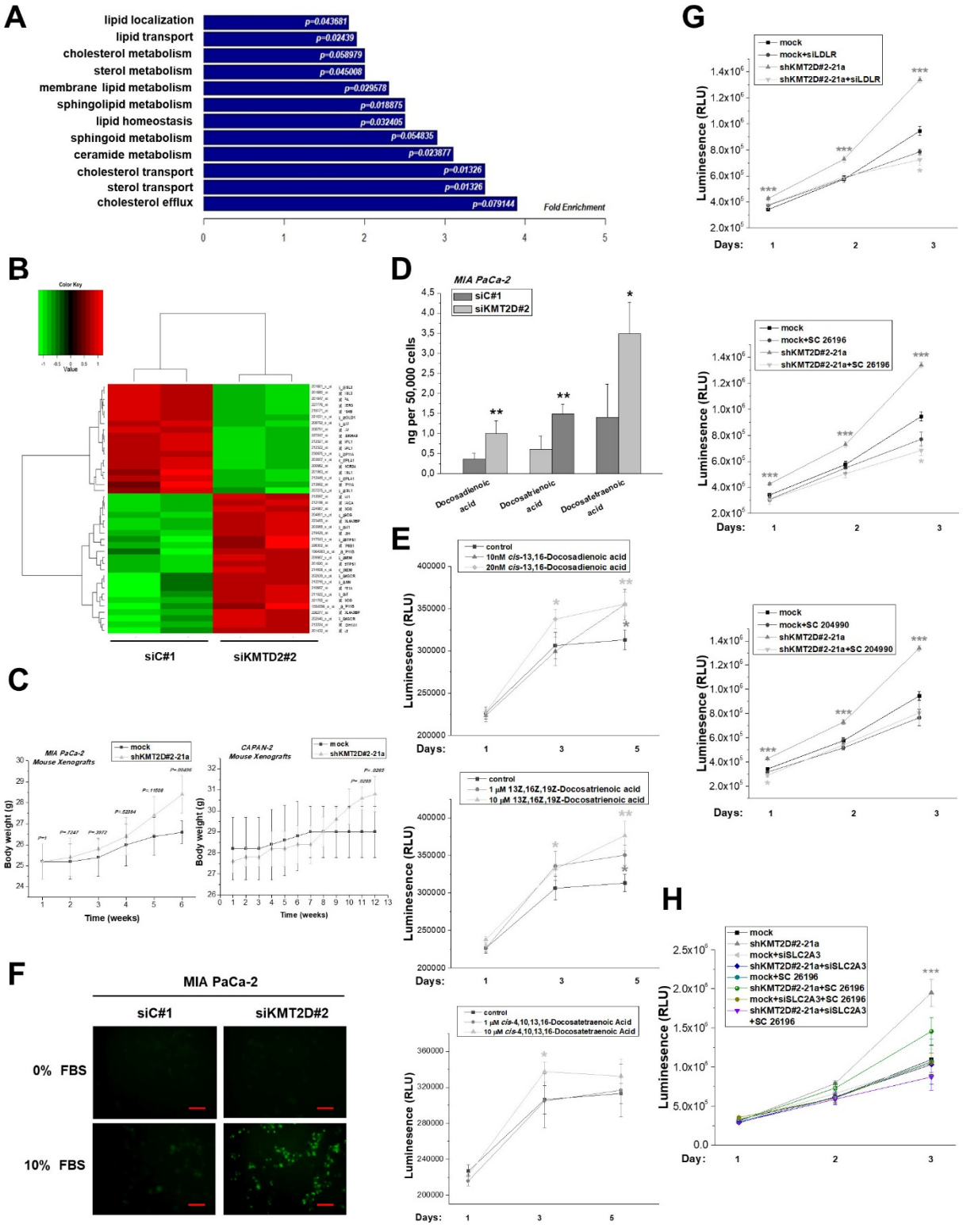
A
lipid localization
lipid transport
cholesterol metabolism
sterol metabolism
membrane lipid metabolism
sphingolipid metabolism
lipid homeostasis
sphingoid metabolism
ceramide metabolism
cholesterol transport
sterol transport
cholesterol efflux
p=0.043681
p=0.02439
p=0.058979
p=0.045008
p=0.029578
p=0.018875
p=0.032405
p=0.054835
p=0.023877
p=0.01326
p=0.01326
p=0.079144
Fold Enrichment
B
Color Key
Value
siC#1
siKMTD2#2
C
MIA PaCa-2
Mouse Xenografts
mock
shKMT2D#2-21a
Body weight (g)
Time (weeks)
CAPAN-2
Mouse Xenografts
D
MIA PaCa-2
siC#1
siKMT2D#2
ng per 50,000 cells
Docosadienoic acid
Docosatrienoic acid
Docosatetraenoic acid
E
control
10nM cis-13,16-Docosadienoic acid
20nM cis-13,16-Docosadienoic acid
control
1 μM 13Z,16Z,19Z-Docosatrienoic acid
10 μM 13Z,16Z,19Z-Docosatrienoic acid
control
1 μM cis-4,10,13,16-Docosatetraenoic Acid
10 μM cis-4,10,13,16-Docosatetraenoic Acid
Luminescence (RLU)
Days:
F
MIA PaCa-2
siC#1
siKMT2D#2
0% FBS
10% FBS
G
mock
mock+siLDLR
shKMT2D#2-21a
shKMT2D#2-21a+siLDLR
mock
mock+SC 26196
shKMT2D#2-21a
shKMT2D#2-21a+SC 26196
mock
mock+SC 204990
shKMT2D#2-21a
shKMT2D#2-21a+SC 204990
Luminescence (RLU)
Days:
H
mock
shKMT2D#2-21a
mock+siSLC2A3
shKMT2D#2-21a+siSLC2A3
mock+SC 26196
shKMT2D#2-21a+SC 26196
mock+siSLC2A3+SC 26196
shKMT2D#2-21a+siSLC2A3
+SC 26196
Luminescence (RLU)
Day:

FIGURE 6

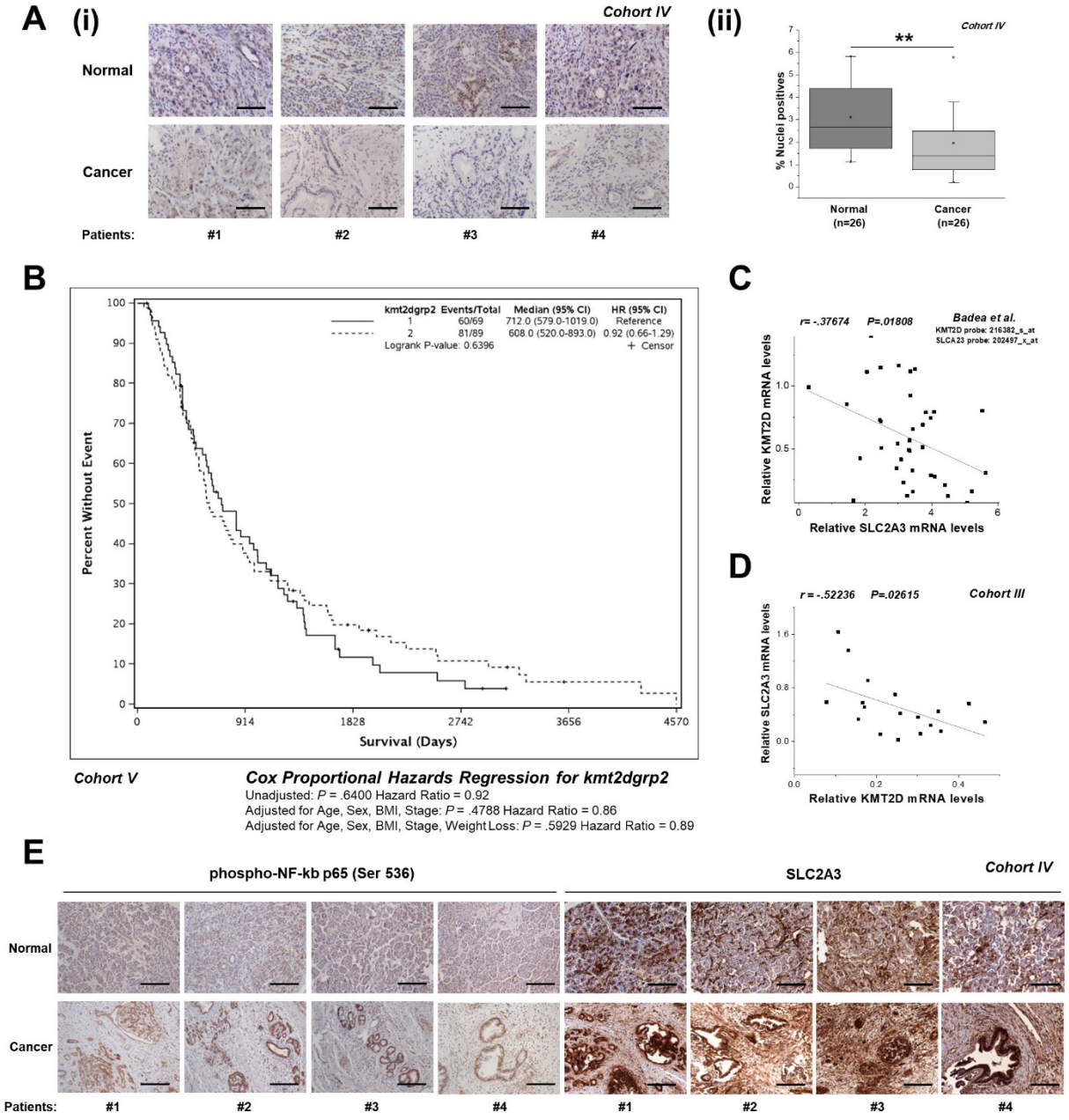
A (i)
Cohort IV
Normal
Cancer
Patients: #1 #2 #3 #4
(ii)
Cohort IV
**
% Nuclei positives
Normal (n=26)
Cancer (n=26)
B
kmt2dgrp2 Events/Total Median (95% CI) HR (95% CI)
1 60/69 712.0 (579.0-1019.0) Reference
2 81/89 608.0 (520.0-893.0) 0.92 (0.66-1.29)
Logrank P-value: 0.6396
+ Censor
Percent Without Event
Survival (Days)
Cohort V
Cox Proportional Hazards Regression for kmt2dgrp2
Unadjusted: P = .6400 Hazard Ratio = 0.92
Adjusted for Age, Sex, BMI, Stage: P = .4788 Hazard Ratio = 0.86
Adjusted for Age, Sex, BMI, Stage, Weight Loss: P = .5929 Hazard Ratio = 0.89
C
r= -.37674 P=.01808
Badea et al.
KMT2D probe: 216382_s_at
SLCA23 probe: 202497_x_at
Relative KMT2D mRNA levels
Relative SLC2A3 mRNA levels
D
r = -.52236 P=.02615
Cohort III
Relative SLC2A3 mRNA levels
Relative KMT2D mRNA levels
E
phospho-NF-kb p65 (Ser 536)
SLC2A3
Cohort IV
Normal
Cancer
Patients: #1 #2 #3 #4 #1 #2 #3 #4

FIGURE 7

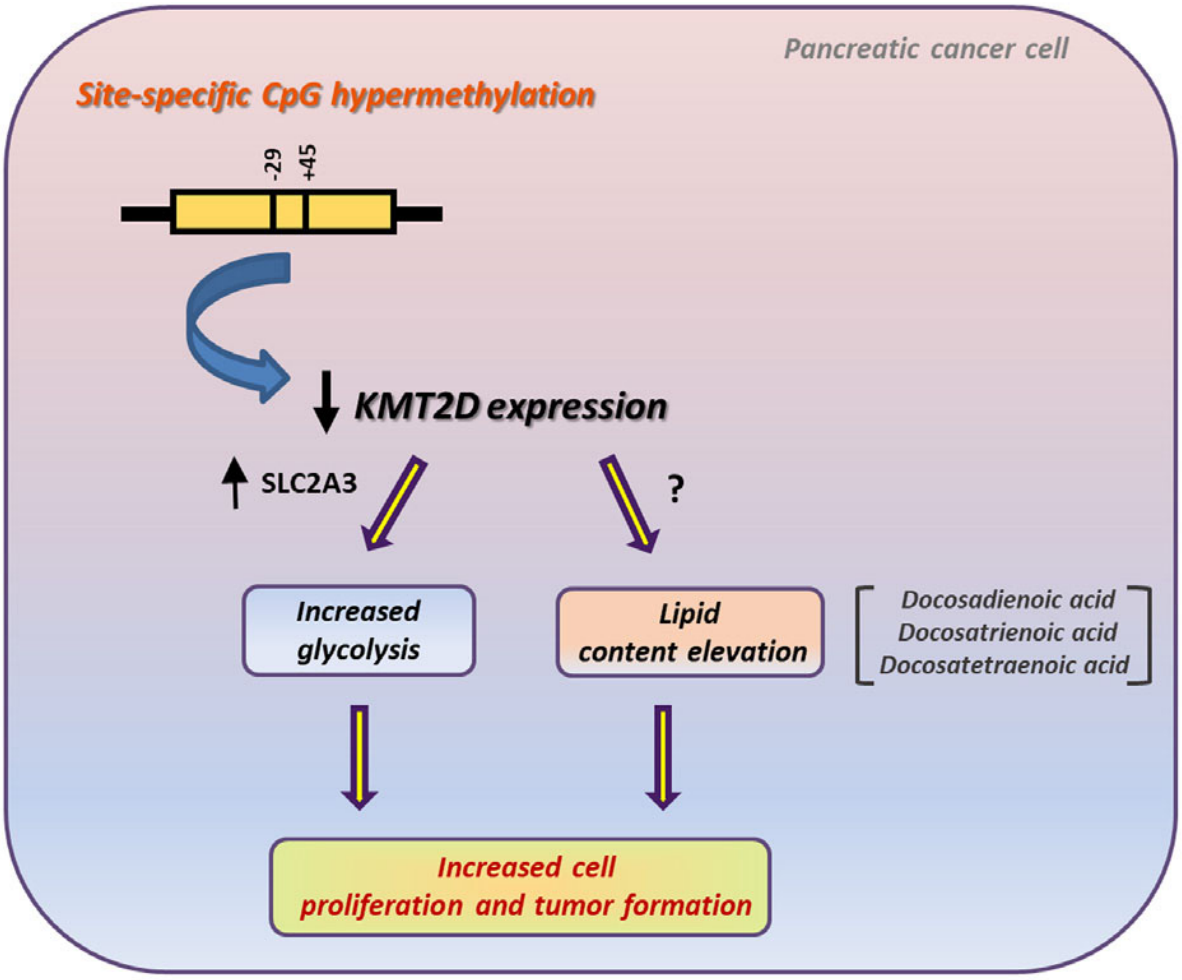
Pancreatic cancer cell
Site-specific CpG hypermethylation
-29
+45
KMT2D expression
SLC2A3
?
Increased glycolysis
Lipid content elevation
Docosadienoic acid
Docosatrienoic acid
Docosatetraenoic acid
Increased cell proliferation and tumor formation

SUPPLEMENTARY INFORMATION

SUPPLEMENTARY FIGURES

A

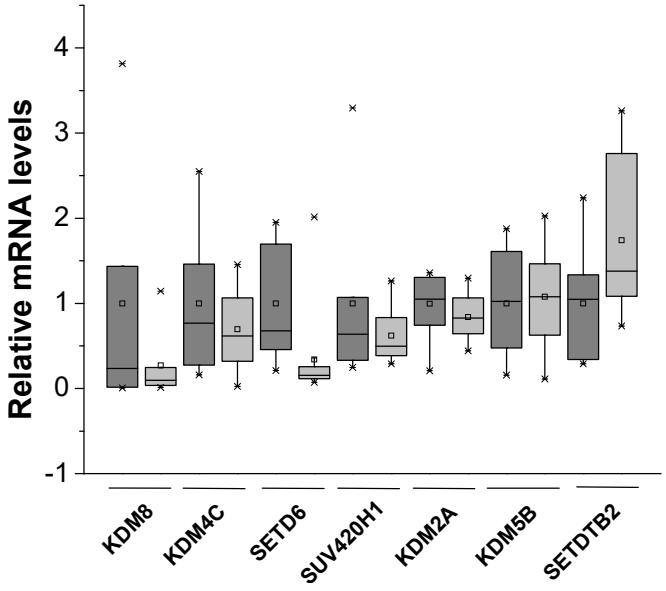

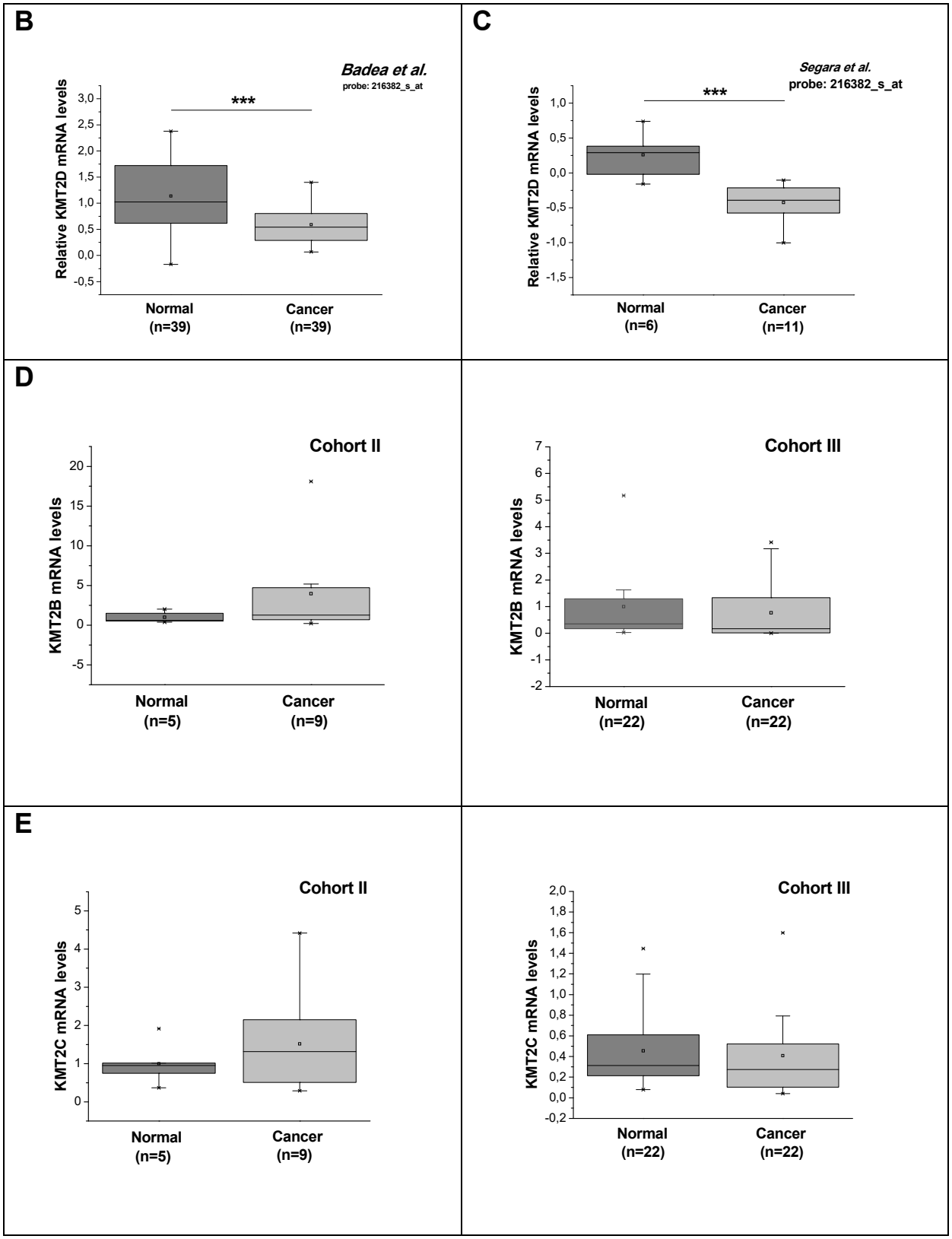
B
Badea et al.
probe: 216382_s_at
***
Relative KMT2D mRNA levels
3,0
2,5
2,0
1,5
1,0
0,5
0,0
-0,5
Normal
(n=39)
Cancer
(n=39)
C
Segara et al.
probe: 216382_s_at
***
Relative KMT2D mRNA levels
1,0
0,5
0,0
-0,5
-1,0
-1,5
Normal
(n=6)
Cancer
(n=11)
D
Cohort II
KMT2B mRNA levels
20
15
10
5
0
-5
Normal
(n=5)
Cancer
(n=9)
Cohort III
KMT2B mRNA levels
7
6
5
4
3
2
1
0
-1
-2
Normal
(n=22)
Cancer
(n=22)
E
Cohort II
KMT2C mRNA levels
5
4
3
2
1
0
Normal
(n=5)
Cancer
(n=9)
Cohort III
KMT2C mRNA levels
2,0
1,8
1,6
1,4
1,2
1,0
0,8
0,6
0,4
0,2
0,0
-0,2
Normal
(n=22)
Cancer
(n=22)

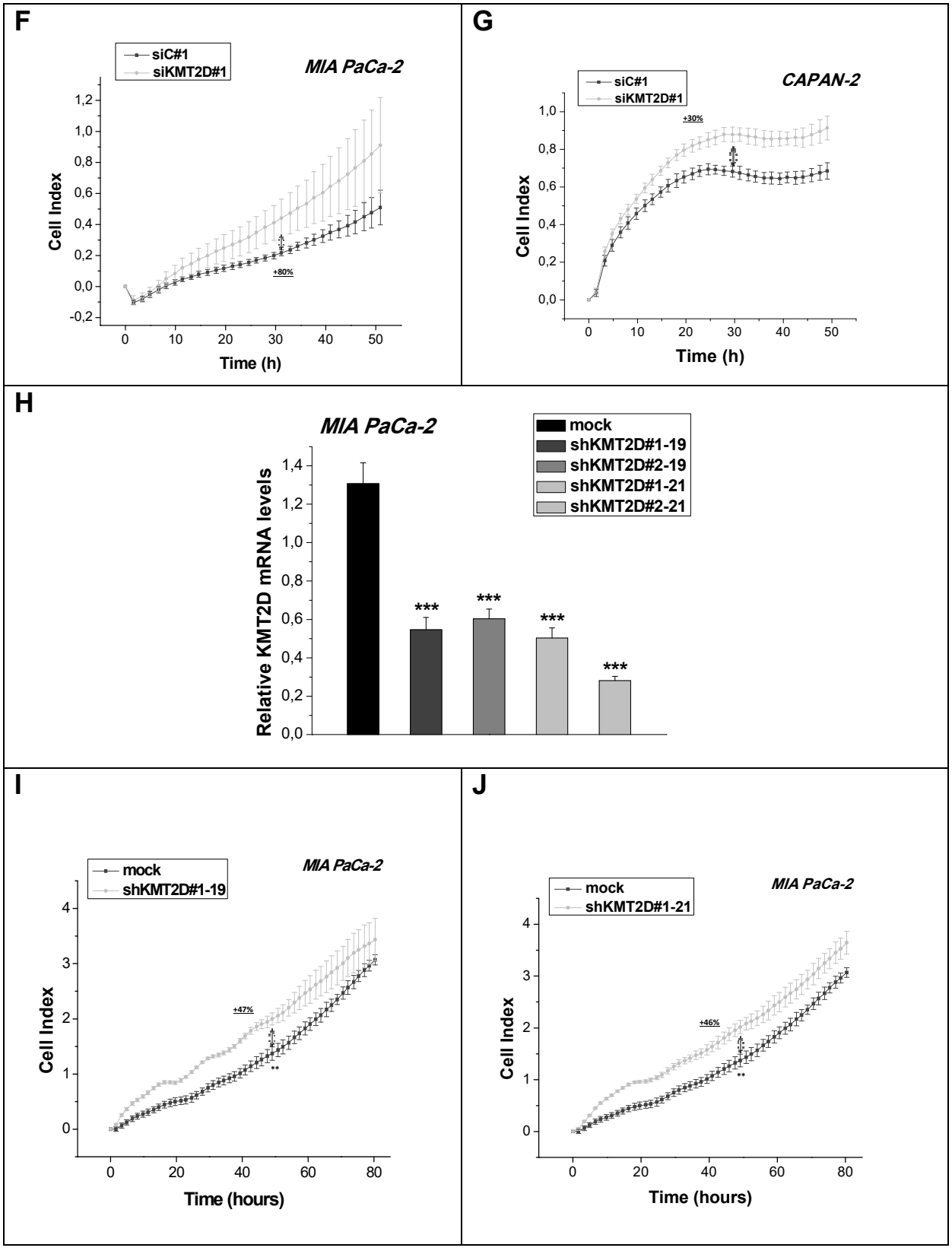
F
siC#1
siKMT2D#1
MIA PaCa-2
Cell Index
Time (h)
+80%
G
siC#1
siKMT2D#1
CAPAN-2
+30%
Cell Index
Time (h)
H
MIA PaCa-2
mock
shKMT2D#1-19
shKMT2D#2-19
shKMT2D#1-21
shKMT2D#2-21
Relative KMT2D mRNA levels
***
I
mock
shKMT2D#1-19
MIA PaCa-2
+47%
**
Cell Index
Time (hours)
J
mock
shKMT2D#1-21
MIA PaCa-2
+46%
**
Cell Index
Time (hours)

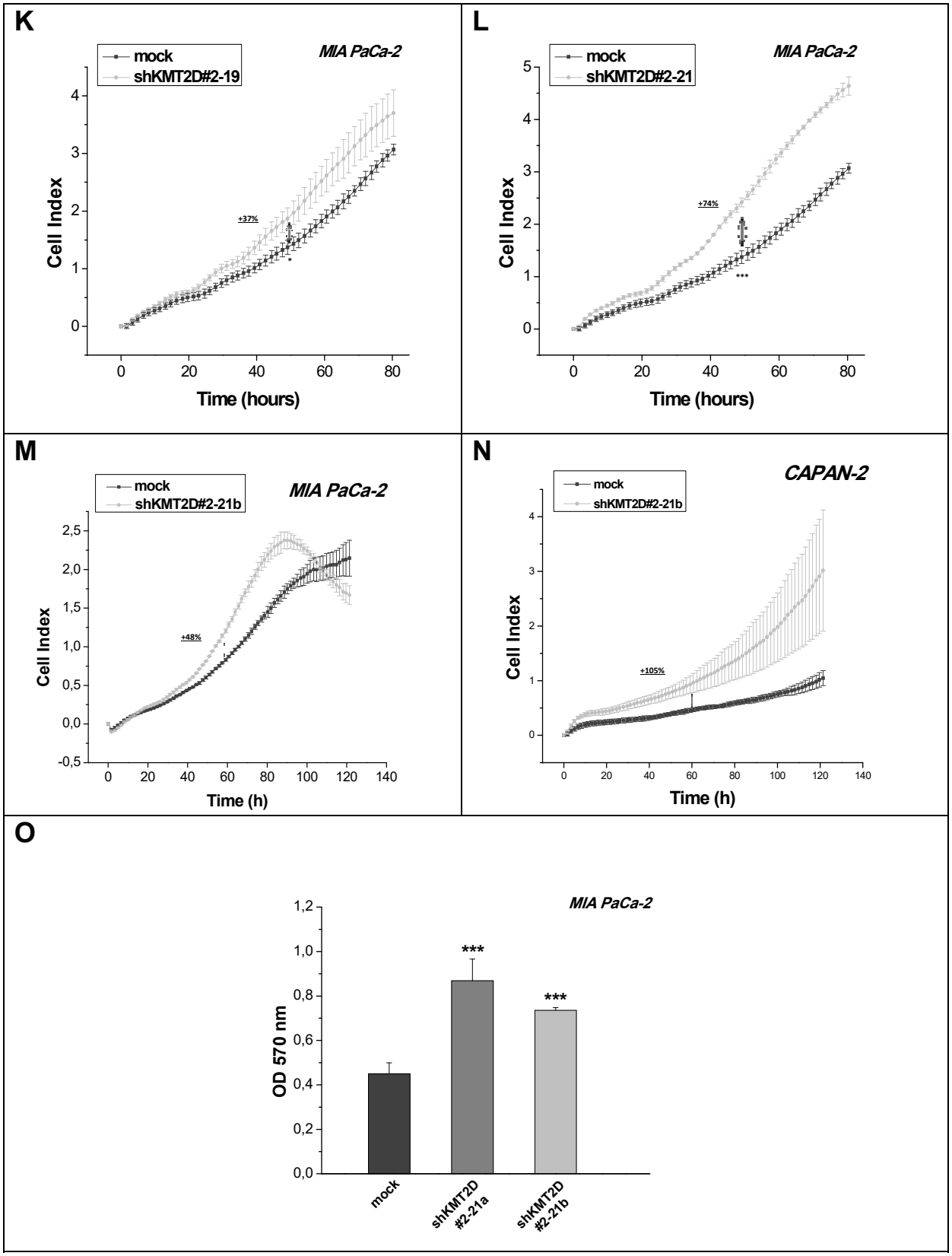
K
mock
shKMT2D#2-19
MIA PaCa-2
Cell Index
Time (hours)
+37%
L
mock
shKMT2D#2-21
MIA PaCa-2
Cell Index
Time (hours)
+74%
M
mock
shKMT2D#2-21b
MIA PaCa-2
Cell Index
Time (h)
+48%
N
mock
shKMT2D#2-21b
CAPAN-2
Cell Index
Time (h)
+105%
O
MIA PaCa-2
OD 570 nm
mock
shKMT2D #2-21a
shKMT2D #2-21b

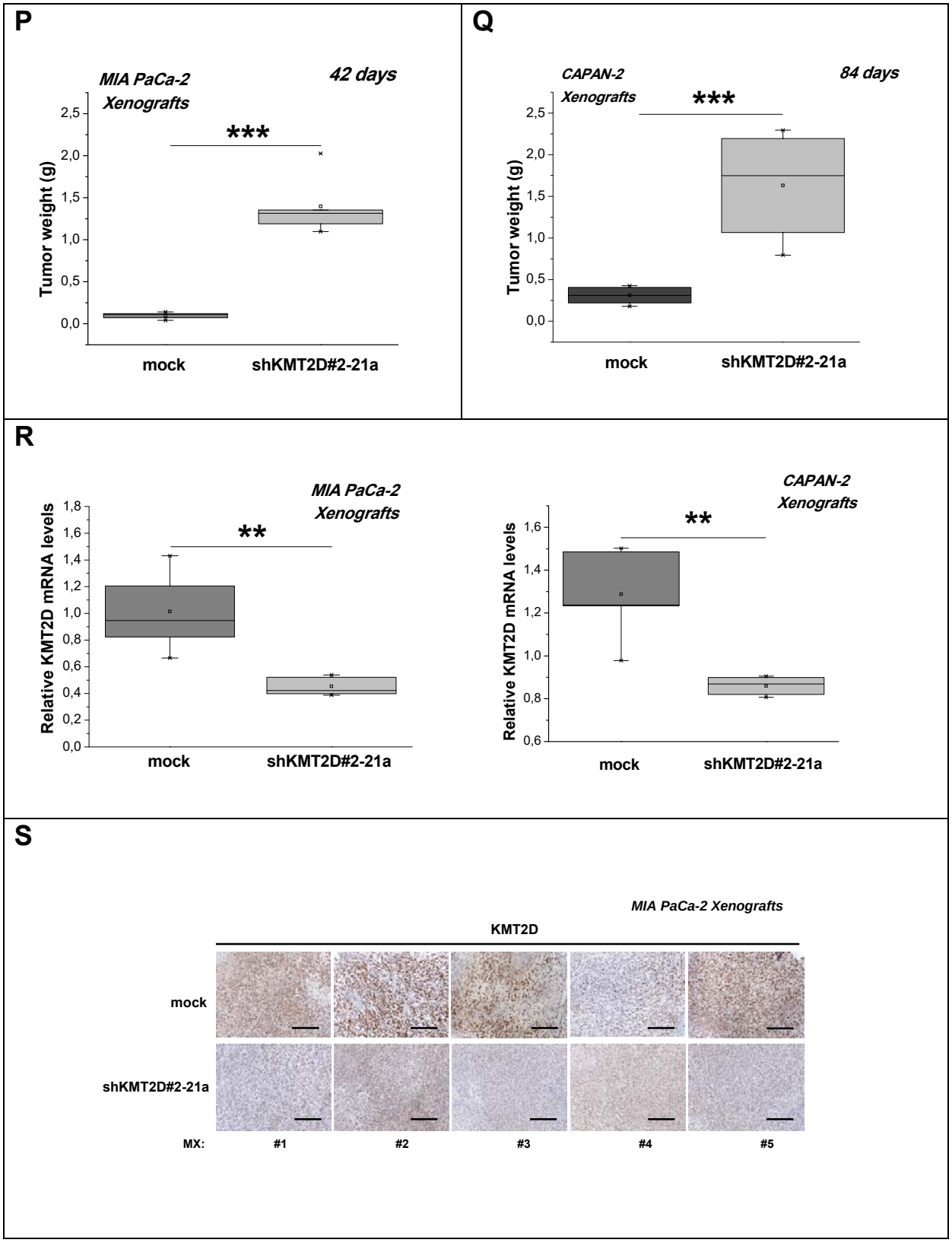
P
MIA PaCa-2 Xenografts
42 days
***
Tumor weight (g)
2,5
2,0
1,5
1,0
0,5
0,0
mock
shKMT2D#2-21a
Q
CAPAN-2 Xenografts
84 days
***
Tumor weight (g)
2,5
2,0
1,5
1,0
0,5
0,0
mock
shKMT2D#2-21a
R
MIA PaCa-2 Xenografts
**
Relative KMT2D mRNA levels
1,8
1,6
1,4
1,2
1,0
0,8
0,6
0,4
0,2
0,0
mock
shKMT2D#2-21a
CAPAN-2 Xenografts
**
Relative KMT2D mRNA levels
1,6
1,4
1,2
1,0
0,8
0,6
mock
shKMT2D#2-21a
S
MIA PaCa-2 Xenografts
KMT2D
mock
shKMT2D#2-21a
MX:
#1
#2
#3
#4
#5

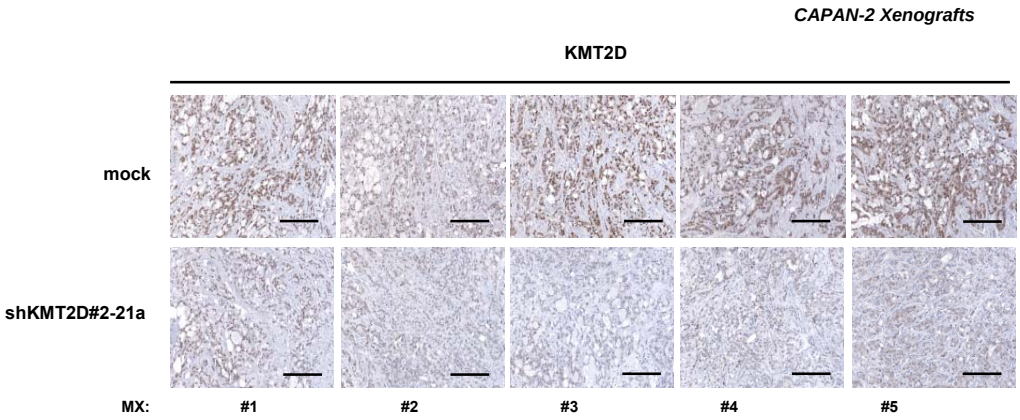
CAPAN-2 Xenografts
KMT2D
mock
shKMT2D#2-21a
MX:
#1
#2
#3
#4
#5

T


MIA PaCa-2 Xenografts
mock
shKMT2D#2-21b
CAPAN-2 Xenografts
mock
shKMT2D#2-21b

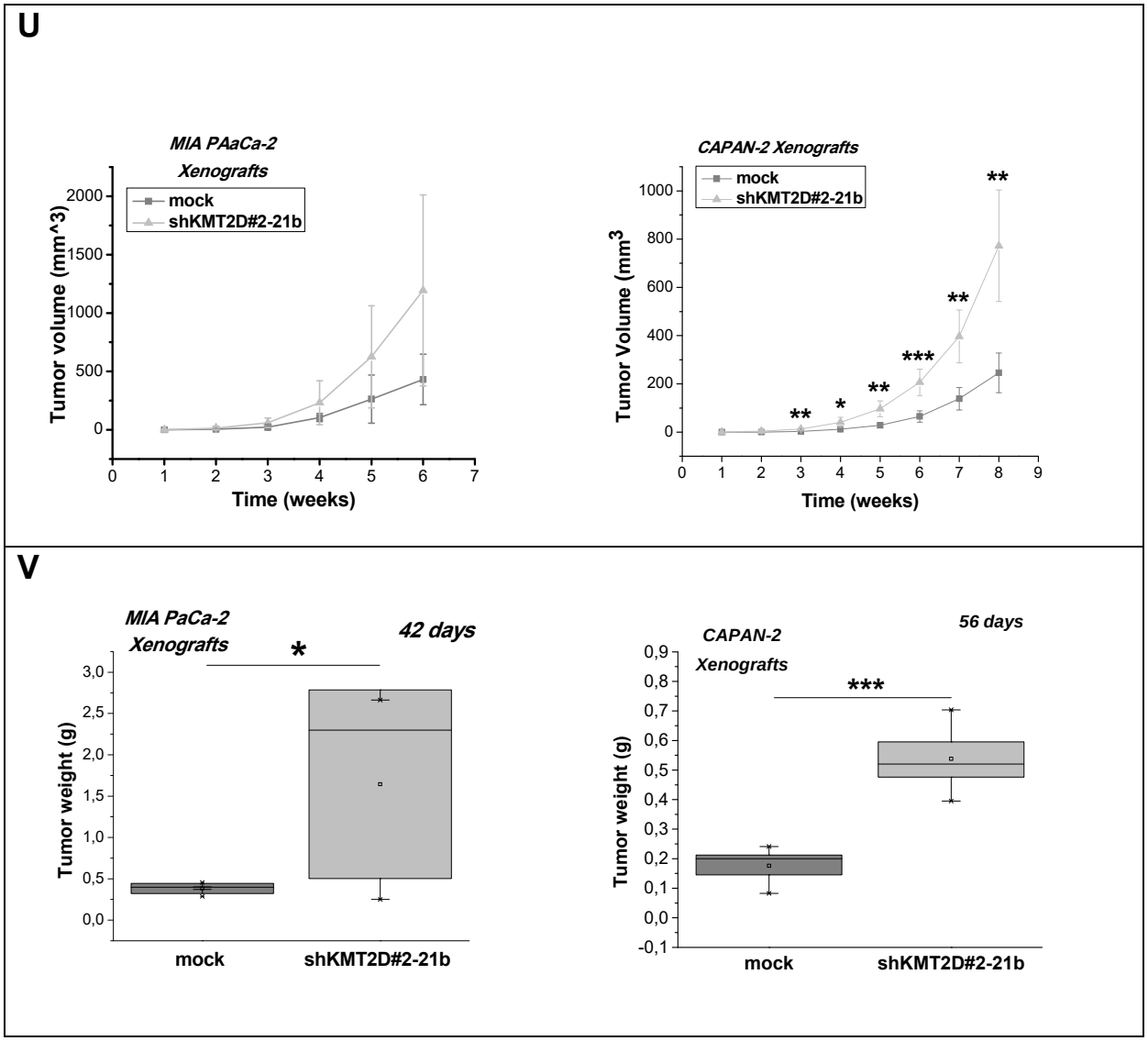

Supplementary Figure S1: Histone methyltransferase KMT2D acts as a tumor suppressor in pancreatic cancer.

(A) Differential expression of chromatin regulators including *KDM8, KDM4C, SETD6, SUV420H1, KDM2A, KDM5B and SETDB2* in pancreatic carcinoma versus normal tissues originating from Cohort II, as assessed by RT-qPCR. **(B, C)** Differential expression of *Lysine (K)-Specific Methyltransferase 2D (KMT2D)* in pancreatic

carcinoma versus normal tissues, based on 2 studies listed in Oncomine database [1 2]. **(D, E)** Relative mRNA levels of KMT2B and KMT2C in Cohorts II and III, as assessed by RT-qPCR. **(F, G)** Effect of transient *KMT2D* suppression by using siKMT2D#1 and the respective scramble control on pancreatic cancer cell proliferation, as assessed by the xCELLigence system. **(H)** Efficiency of *KMT2D* stable depletion by using 4 different shRNAs in MIA PaCa-2 cells, as assessed by RT-qPCR. **(I-L)** Effect of stable *KMT2D* suppression by using 4 different shRNAs on pancreatic cancer cell proliferation, as assessed by the xCELLigence system. **(M, N)** Assessment of the proliferative capacity of shKMT2D#2-21b clonal cell lines versus mock transfected cells. **(O)** Quantification of the colonies formed by shKMT2D#2-21 a and b clonal cell lines versus mock transfected cells. **(P, Q)** Tumor weight graphs of xenografts bearing KMT2D stably suppressed MIA PaCa-2 and CAPAN-2 cells (5 mice/group). *KMT2D* expression in MIA PaCa-2 and CAPAN-2 xenografts from mice injected with mock or shKMT2D#2-21a cells, as assessed by RT-qPCR **(R)** and IHC analysis **(S)**. **(T)** Representative images of the excised tumors and **(U)** tumor volume (mm^3) **(V)** and tumor weight graphs of xenografts from mice injected with mock or shKMT2D#2-21b cells. For establishing shKMT2D#2-21b xenografts, $3.5*10^6$ MIA PaCa-2 and $4.5*10^6$ CAPAN-2 cells were injected subcutaneously in the right flank of NOD-SCID mice (5 mice/group). siC#1, cells transfected with a negative control scramble siRNA; siKMT2D#1, cells transfected with siRNA#1 for KMT2D; mock, cells transfected with shRNA empty vector; shKMT2D#1-19, cells transfected with #1-19 shRNA for KMT2D; shKMT2D#1-21, cells transfected with #1-21 shRNA for KMT2D; shKMT2D#2-19, cells transfected with #2-19 shRNA for KMT2D; shKMT2D#2-21, cells transfected with #2-21 shRNA for KMT2D;

shKMT2D#2-21a or b, cells transfected with #2-21 shRNA for KMT2D that underwent clonal selection resulting in clones a and b; MX, Mouse Xenograft. Statistical analyses were performed using one-way ANOVA. Asterisks denote statistically significant differences, * *P*<.05, ** *P*<.01, *** *P*<.001

A

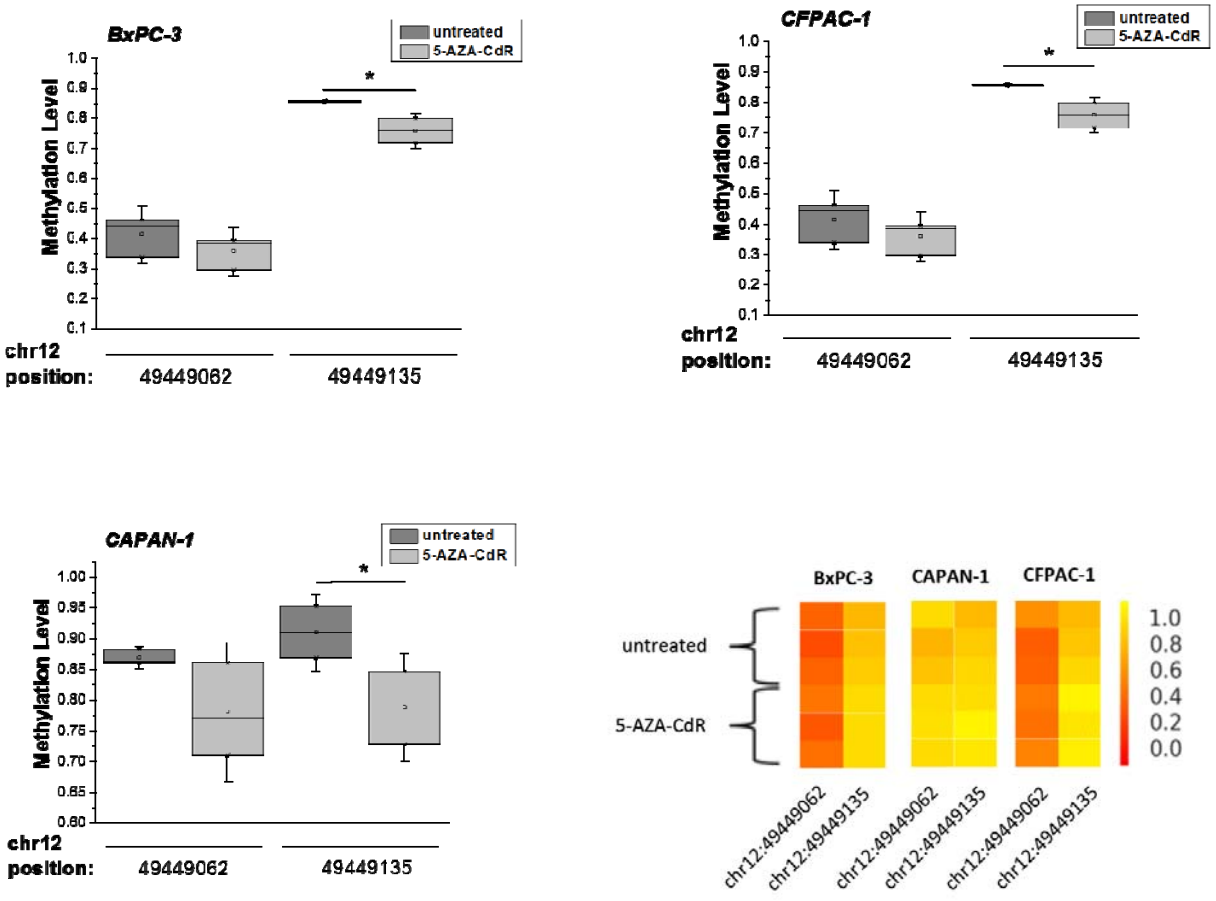

B

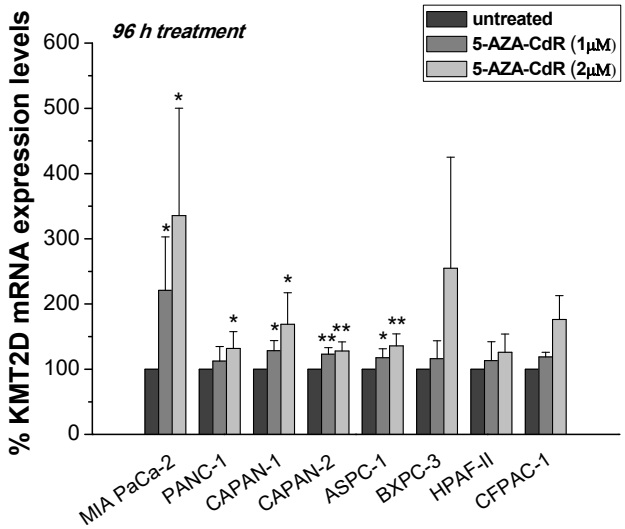

Supplementary Figure S2. Epigenetic regulation of KMT2D levels through DNA methylation of two different CpG sites.

(A) CpG methylation validation via Targeted Bisulfite Sequencing for the selected region of interest (ROI) (chr12: 49448986-49449286). Quantitative methylation measurements at the single-CpG-site level for untreated or 5-AZA-2'-deoxycytidine (5-AZA-CdR)-treated BxPC-3, CAPAN-1 and CFPAC-1 cells are box plotted or depicted as heatmaps of the methylation ratio. The color indicates the level of methylation from higher to lower in yellow > orange > red order. **(B)** Dose response evaluation of 5-AZA-CdR treatment for 96 h of KMT2D mRNA levels, as assessed by RT-qPCR. Statistical analyses were performed using one-way ANOVA. Asterisks denote statistically significant differences, * $P<.05$, ** $P<.01$

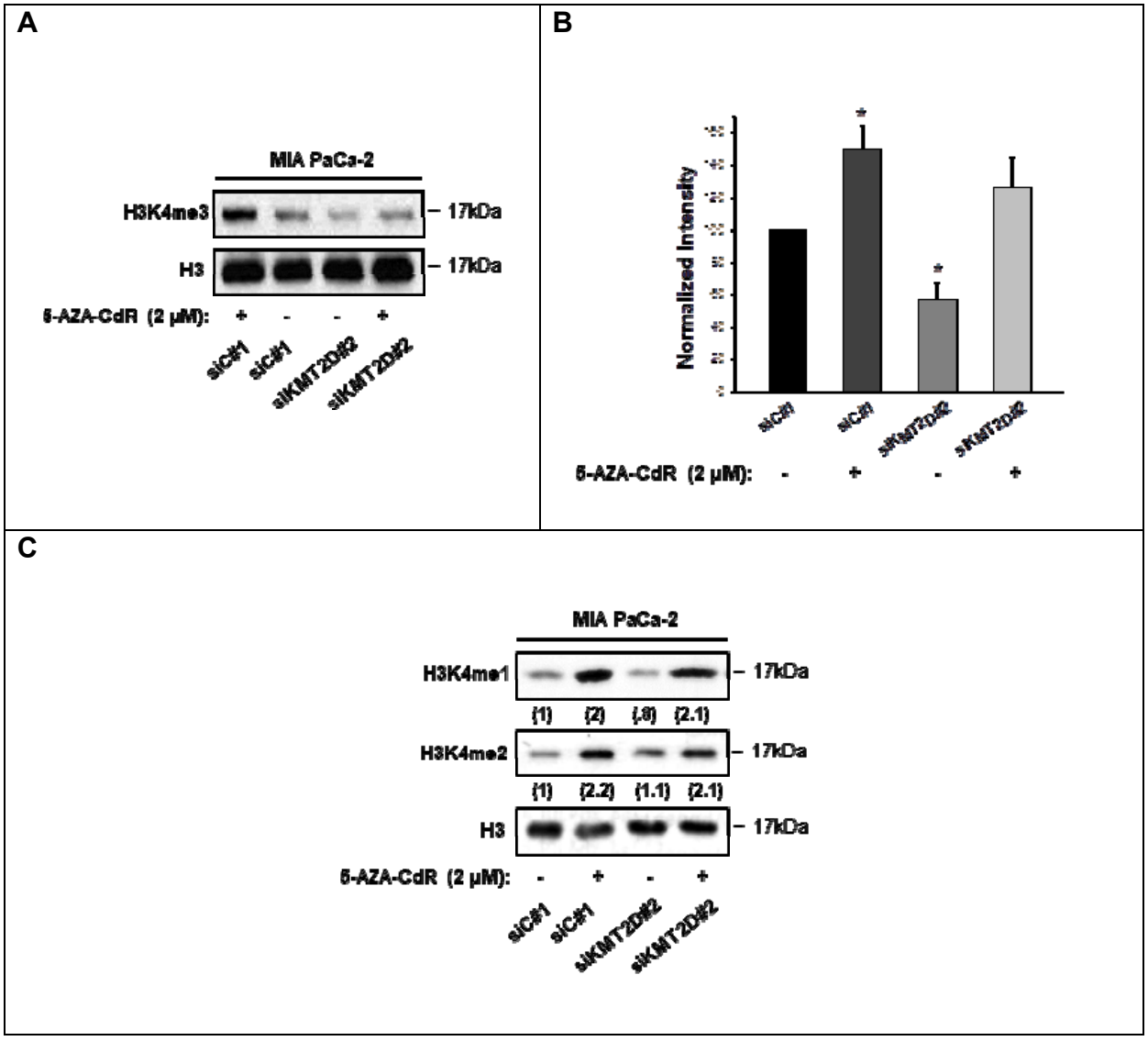

Supplementary Figure S3: Assessment of the global H3K4me3 levels of control or *KMT2D*-silenced cells upon 5-AZA-CdR treatment.

Effect of 5-AZA-CdR treatment for 48 h on the tri-methylated form of histone H3 at lysine 4 (H3K4me3) levels in control or *KMT2D*-silenced cells, as assessed by **(A)** Immunoblot (IB) analyses and **(B)** the quantification of the respective immunoreactive bands of 2 independent experiments. Statistical analyses were performed using one-

way ANOVA. Asterisk denotes statistically significant differences, * P<0.05. **(C)** Numbers in parentheses denote the average-fold change of the ratio H3K4me1:CREB total protein (upper lane) and H3K4me2:CREB (lower lane) of 5-AZA-CdR-treated cells versus non-treated cells (set as default 1). siKMT2D#2, cells transfected with siRNA#2 for KMT2D.

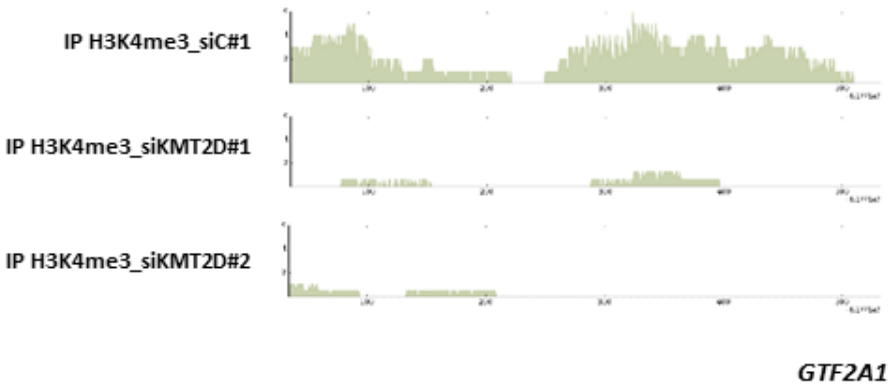

Supplementary Figure S4: ChIP-seq signals of H3K4me3 in *KMT2D*-silenced cells. Effects of *KMT2D* silencing measured by ChIP-seq on H3K4me3 occupancy of the *General Transcription Factor IIA Subunit 1 (GTF2A1)* genomic region. The enrichment values were tested with the Mann-Whitney U test (P<0.001).

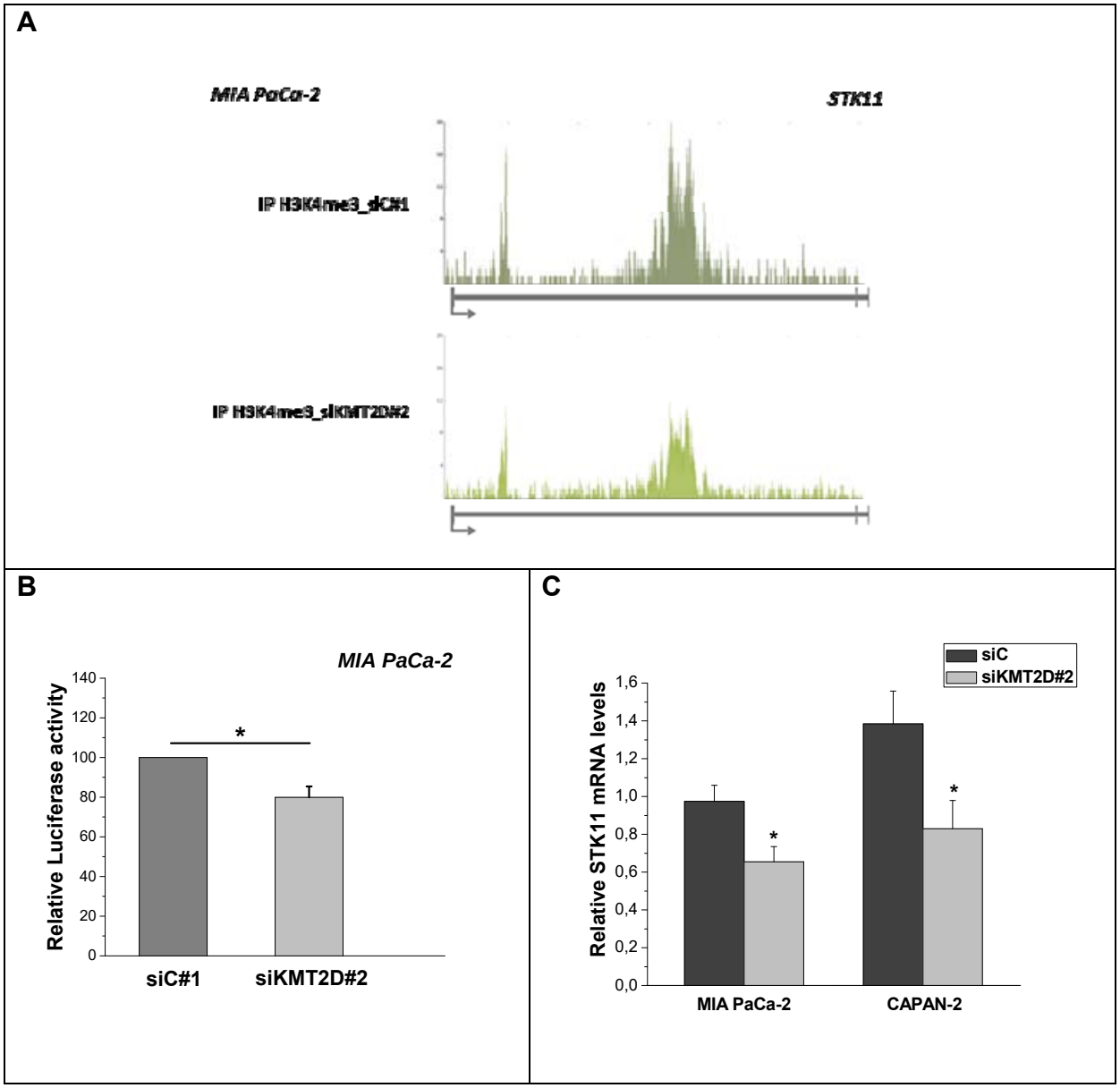

Supplementary Figure S5: Evaluation of *STK11* as a direct KMT2D transcriptional target.

(A) Profiles of H3K4me3 ChIP-seq peaks at the *Serine/Threonine Kinase 11 (STK11)* locus upon *KMT2D* suppression. The x-axes indicate the genomic region. The y-axes represent the fold enrichment of H3K4me3 peaks compared with 2% input control. The

enrichment values were tested with the Mann-Whitney U test (*P*<0.001). **(B)** Luciferase activity mediated by *STK11* promoter upon KMT2D silencing was evaluated 28 h after transfection of the STK11_pLightSwitch_ Prom Reporter or pLenti CMV Puro LUC vectors in MIAPaCa-2 cells. **(C)** *STK11* mRNA levels in pancreatic cancer cell lines transiently-silenced of KMT2D, as assessed by RT-qPCR. Statistical analyses were performed using one-way ANOVA. Asterisk denotes statistically significant differences, * *P*<0.05

A

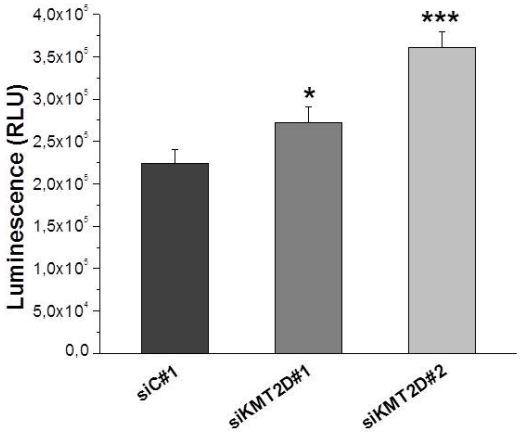

B

MIA PaCA-2

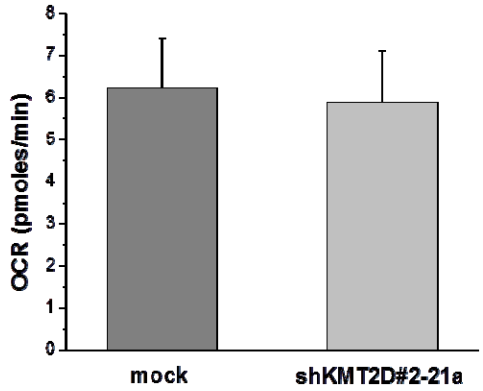

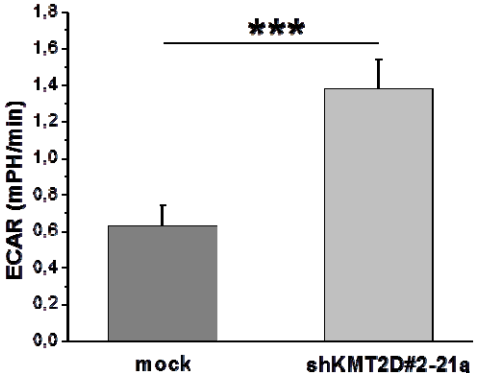

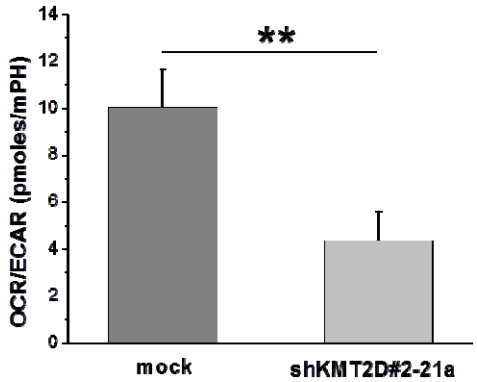

CAPAN-2

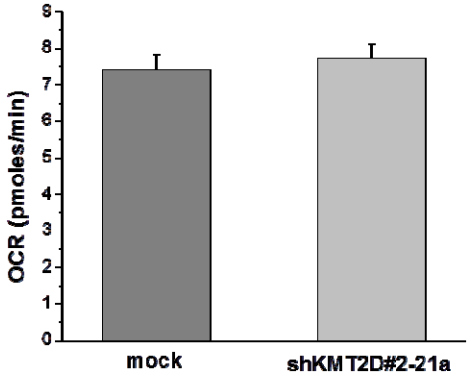

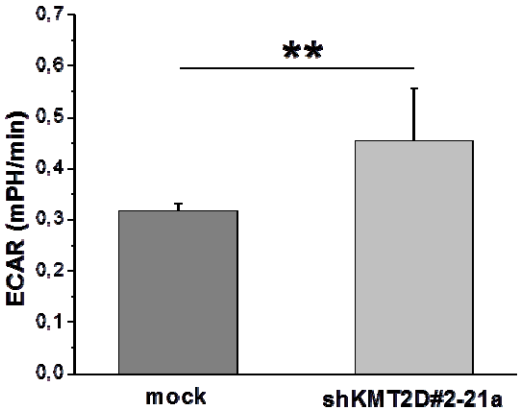

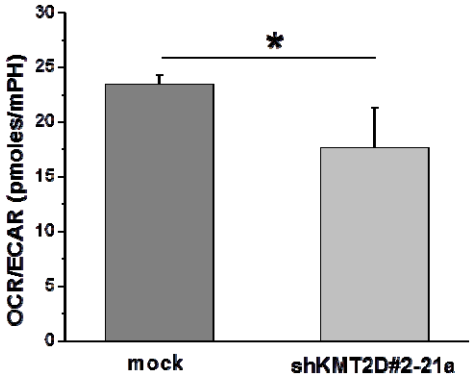

C

MIA PaCA-2 ***CAPAN-2***

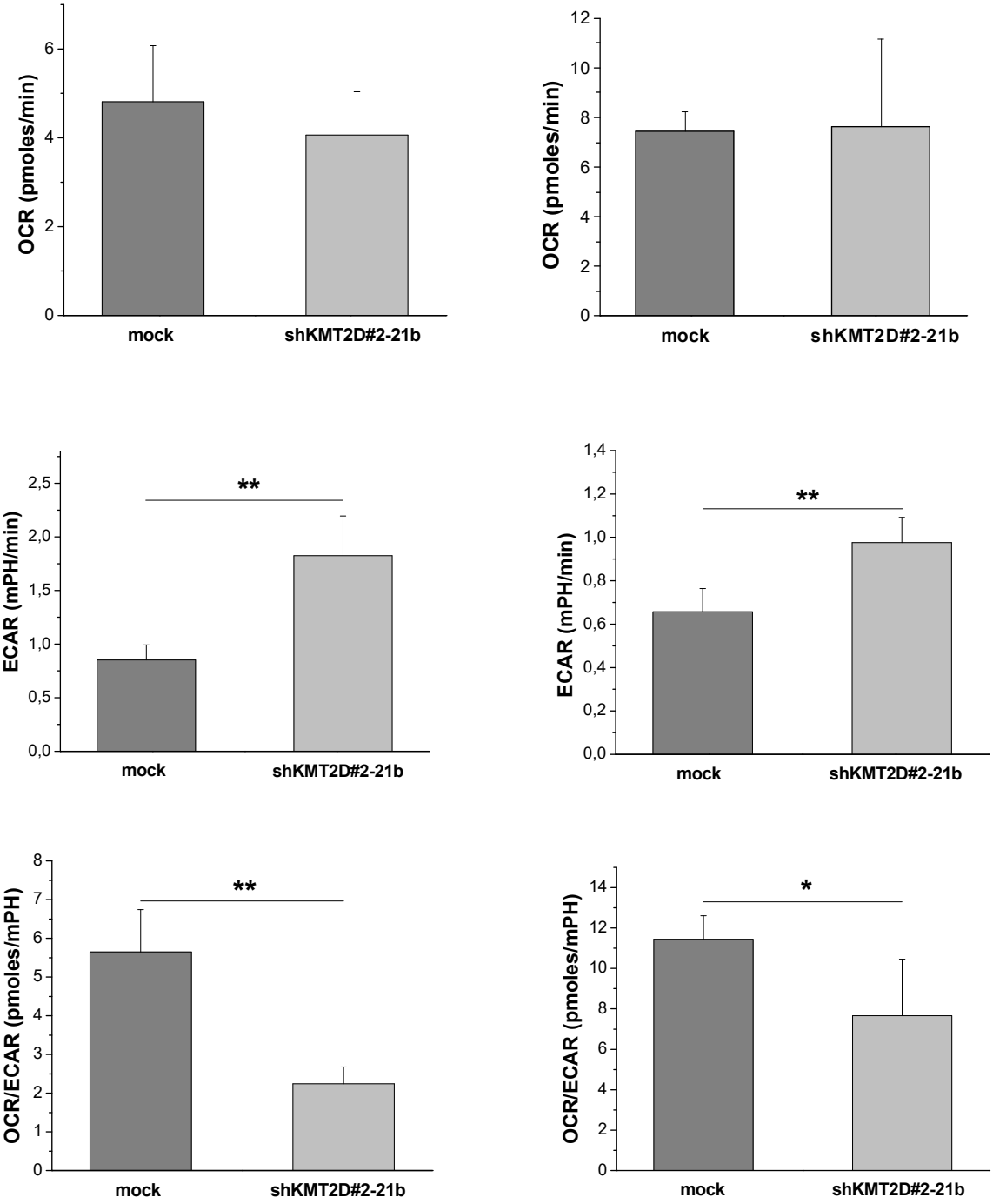

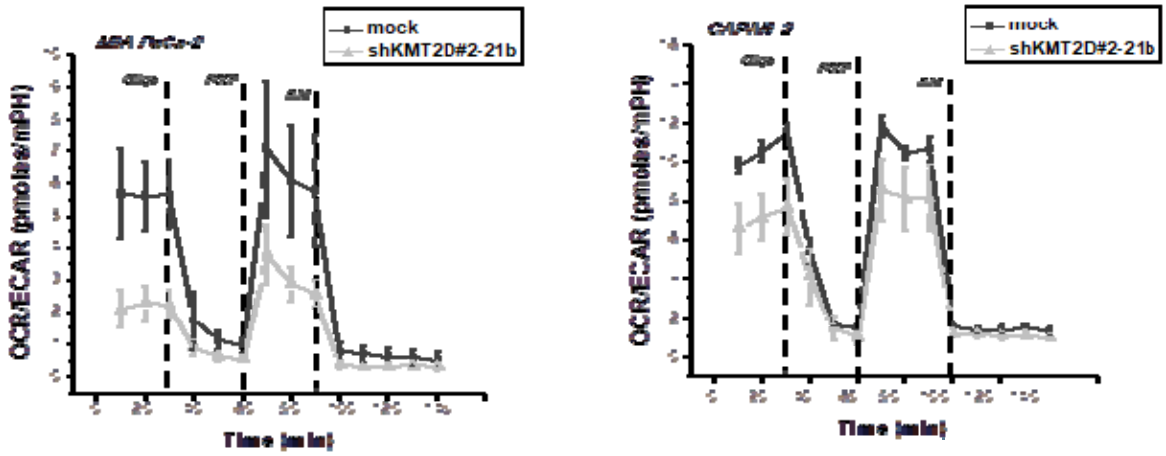
mock
shKMT2D#2-21b
OCR/ECAR (pmoles/mPH)
Time (min)

D

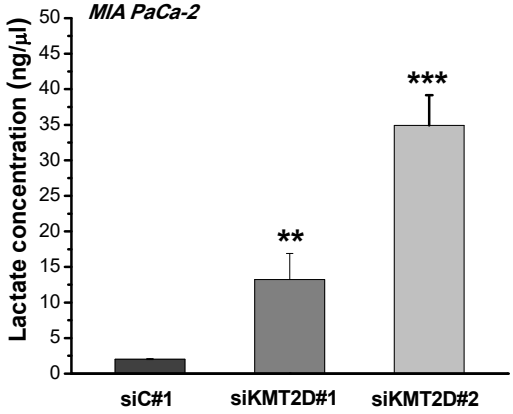
MIA PaCa-2
Lactate concentration (ng/μl)
**
***
siC#1
siKMT2D#1
siKMT2D#2

E

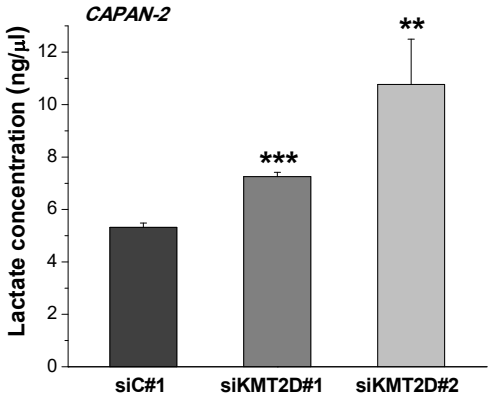
CAPAN-2
Lactate concentration (ng/μl)
***
**
siC#1
siKMT2D#1
siKMT2D#2

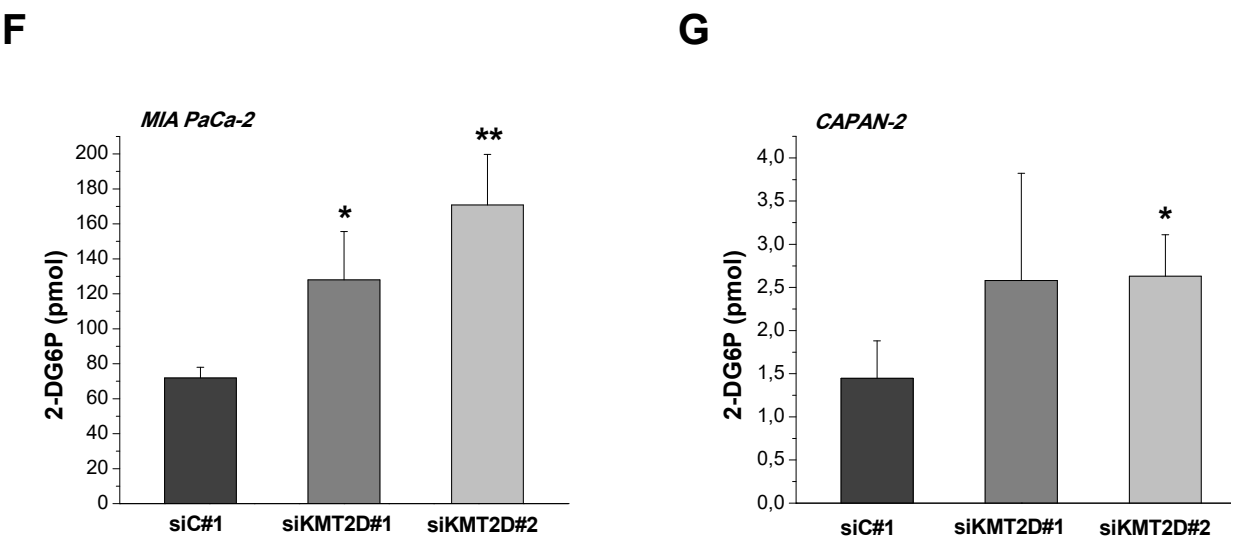

Supplementary Figure S6: KMT2D histone methyltransferase regulates pancreatic cancer cell metabolism.

(A) Endogenous nicotinamide adenine dinucleotide phosphate (NADPH) levels of MIA PaCa-2 cells pretreated with scramble siRNA or 2 different siRNAs against KMT2D, as assessed by the NADP/NADPH-Glo™ bioluminescent Assay. **(B-C)** Effects of *KMT2D* suppression, by using 2 different shKMT2D-stably transfected populations for each cell line on pancreatic cancer cells' bioenergetic profile, as assessed by the XF24-3 Analyzer. Effects of *KMT2D* silencing, by using 2 different siRNAs in **(D and E)** lactate production and **(F and G)** glucose uptake. Average basal OCR and ECAR were further normalized per protein for KMT2D stably-depleted cells. OCR, Oxygen Consumption Rate; ECAR, Extracellular Acidification Rate; 2-DG6P, the 2-deoxyglucose (2-DG) glucose analogue phosphorylated by hexokinase to 2-DG6P. Statistical analyses were

performed using one-way ANOVA. Asterisks denote statistically significant differences, * *P*<0.05, ** *P*<0.01, *** *P*<0.001

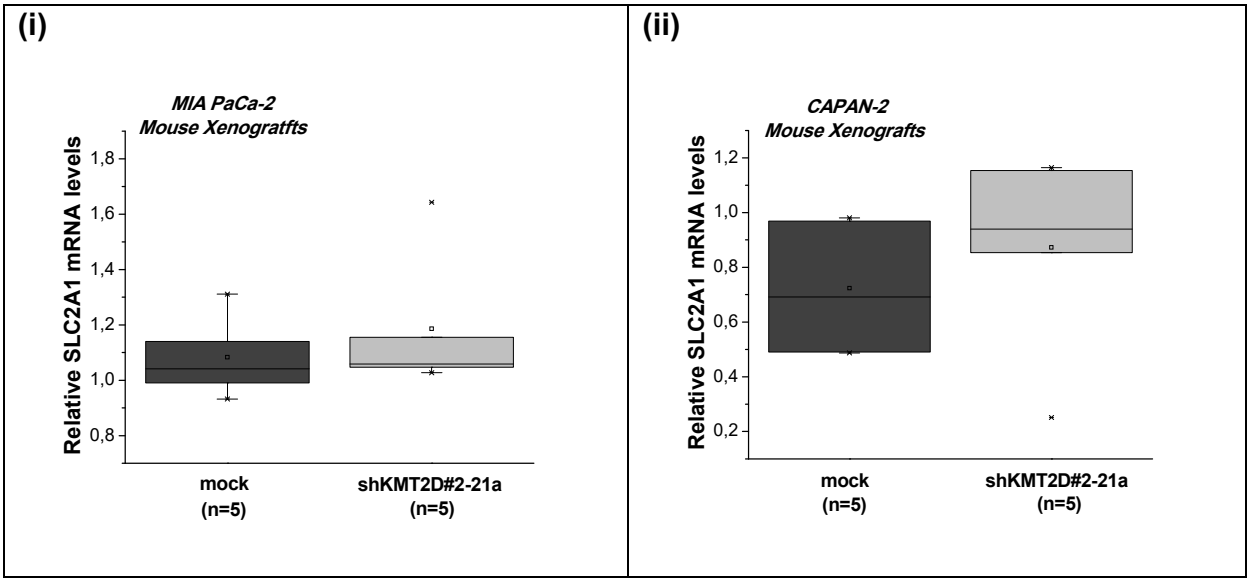

Supplementary Figure S7: Assessment of SLC2A1 mRNA levels in mouse xenografts.

Solute Carrier Family 2 Member 1 (SLC2A1) expression levels in xenografts from mice injected with mock or shKMT2D#2-21a **(i)** MIA PaCa-2 or **(ii)** CAPAN-2 cells, as assessed by RT-qPCR analysis. Statistical analyses were performed using one-way ANOVA.

(i)	**(ii)**

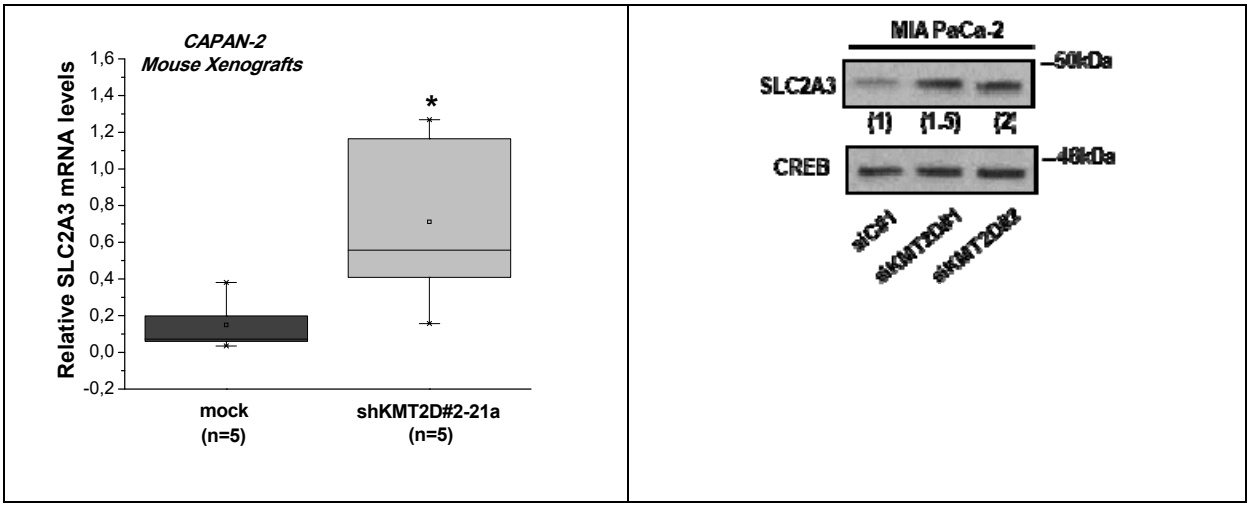

Supplementary Figure S8: Assessment of SLC2A3 mRNA levels and protein levels upon KMT2D genetic manipulation.

(i) *Solute Carrier Family 2 Member 3* (*SLC2A3)* expression levels in xenografts from mice injected with mock or shKMT2D#2-21a CAPAN-2 cells, as assessed by RT-qPCR analysis. **(ii)** Effect of *KMT2D* silencing by using 2 different siRNAs on SLC2A3 protein levels, as assessed by IB analysis. Numbers in parentheses denote the average-fold change of the ratio SLC2A3 : CREB total protein of siKMT2D-transiently transfected cells compared with siC#1-treated cells (set as default 1) of 2 independent experiments, as assessed by densitometric analysis of the immunoreactive bands. Statistical analyses were performed using one-way ANOVA. Asterisk denotes statistically significant differences, * $P<0.05$

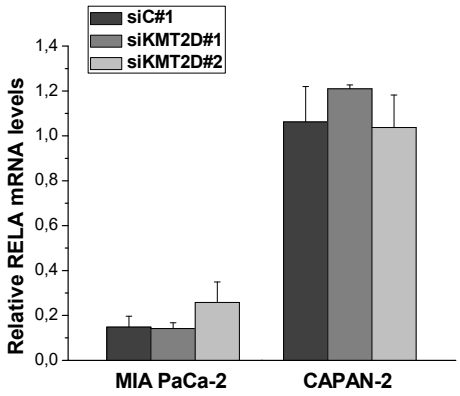

Supplementary Figure S9: Assessment of REL-associated protein mRNA levels upon KMT2D genetic manipulation.

Effect of *KMT2D* silencing on *REL-associated protein (p65)* expression, as assessed by RT-qPCR analysis. Statistical analyses were performed using one-way ANOVA.

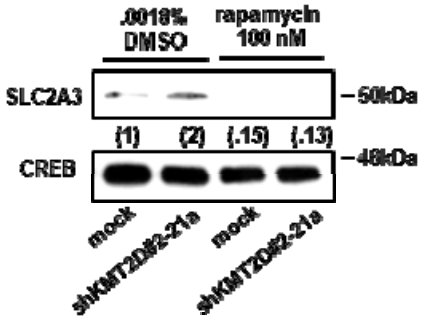

Supplementary Figure S10: Effect of pharmacological inhibition of mTORC1 on the SLC2A3 levels upon KMT2D suppression.

Representative IB images for the indicated antibodies upon treatment of MIA PacA-2 cells harboring differential KMT2D levels with 100 nM rapamycin for 24 h. Numbers in

parentheses denote the average-fold change of the ratio SLC2A3 : CREB total protein of drug-treated cells versus non-treated cells (set as default 1).

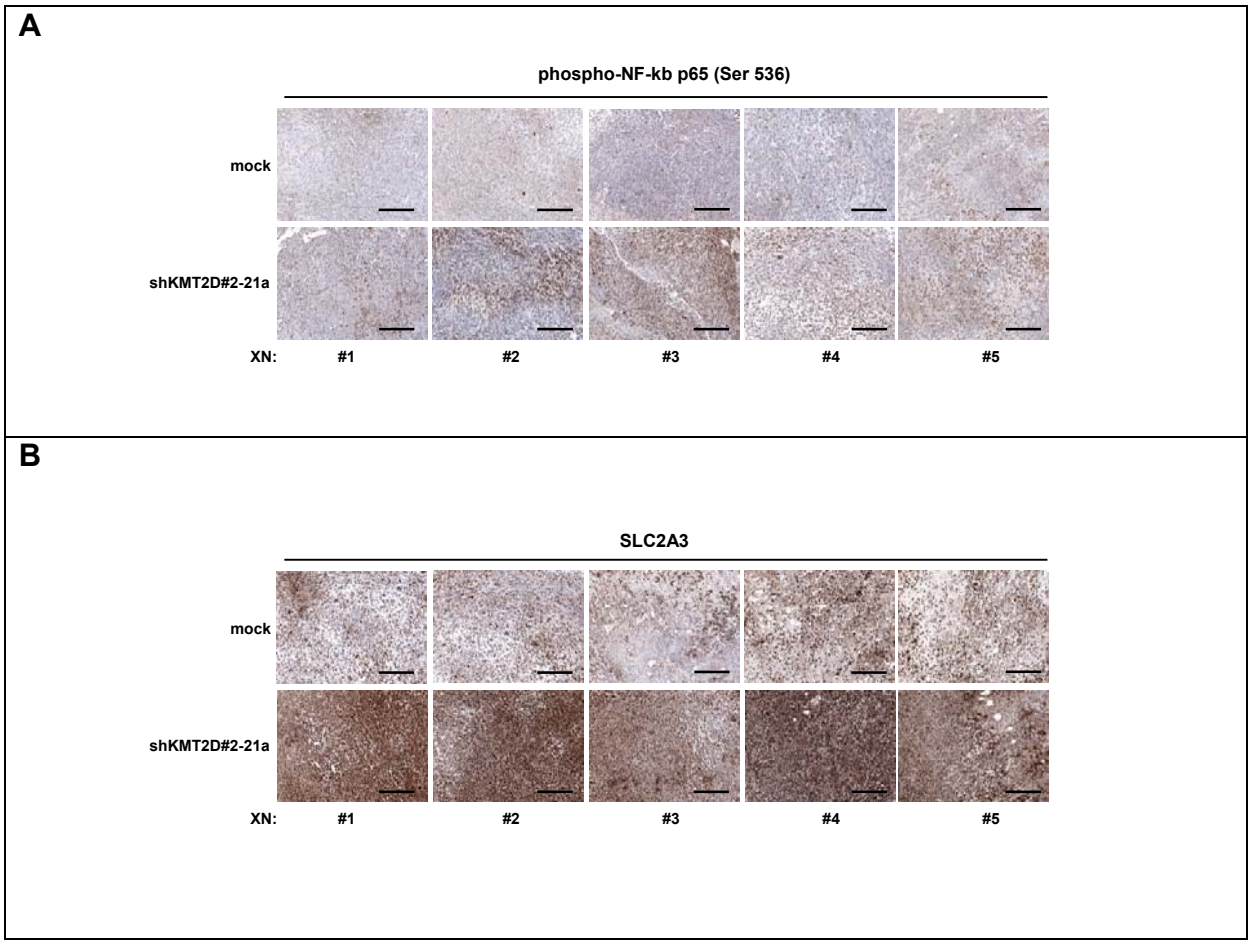

Supplementary Figure S11: Phospho-NF-kB (Ser 536) and SLC2A3 staining patterns in mouse xenografts bearing KMT2D-depleted or mock-transfected pancreatic cancer cells.

Representative images (10x magnification) of **(A)** phospho-NF-kb p65 (Ser 536) and **(B)** SLC2A3 expression, as assessed by IHC analysis, in tumors from xenografts bearing KMT2D stably-suppressed or mock-transfected MIA PaCa-2 cells. Scale bars represent 50 μm.

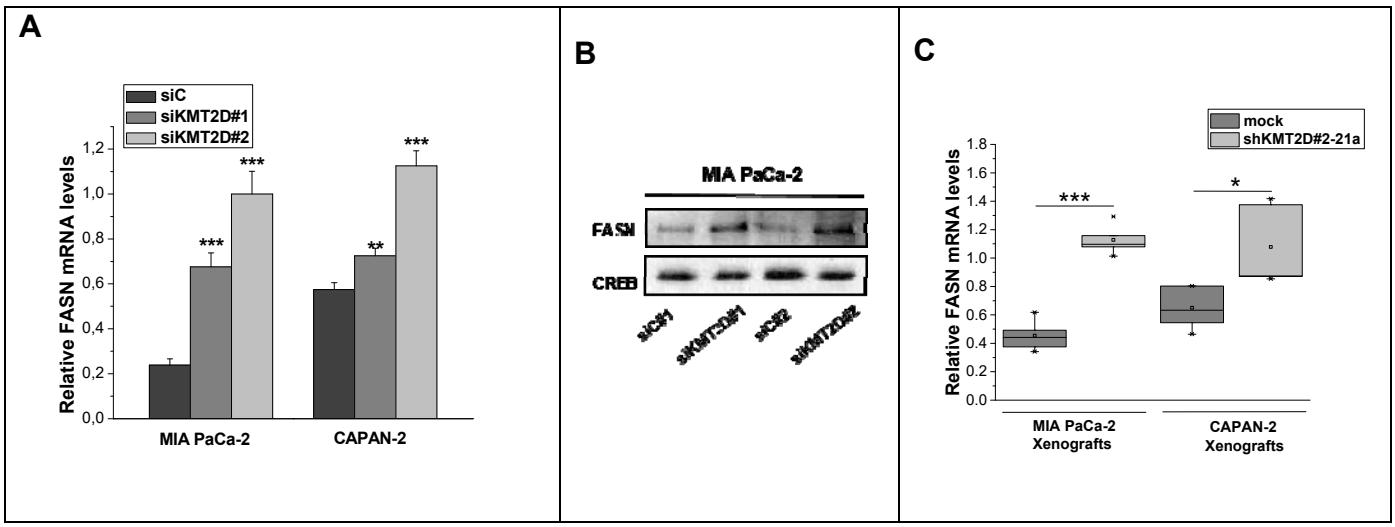

Supplementary Figure S12: Assessment of FASN expression levels upon KMT2D suppression.

(A) Fatty Acid Synthase (FASN*)* expression levels in *KMT2D* transiently-silenced pancreatic cancer cells, as assessed by RT-qPCR analysis. **(B)** FASN expression levels in KMT2D-transiently silenced pancreatic cancer cells, as assessed by IB analysis. **(C)** FASN mRNA levels in xenografts from mice injected with mock or shKMT2D#2-21a cells, as assessed by RT-qPCR analysis. Statistical analyses were performed using one-way ANOVA. Asterisks denote statistically significant differences, * *P<0*.05*,* ** *P<0*.01*,* *** *P<0*.001

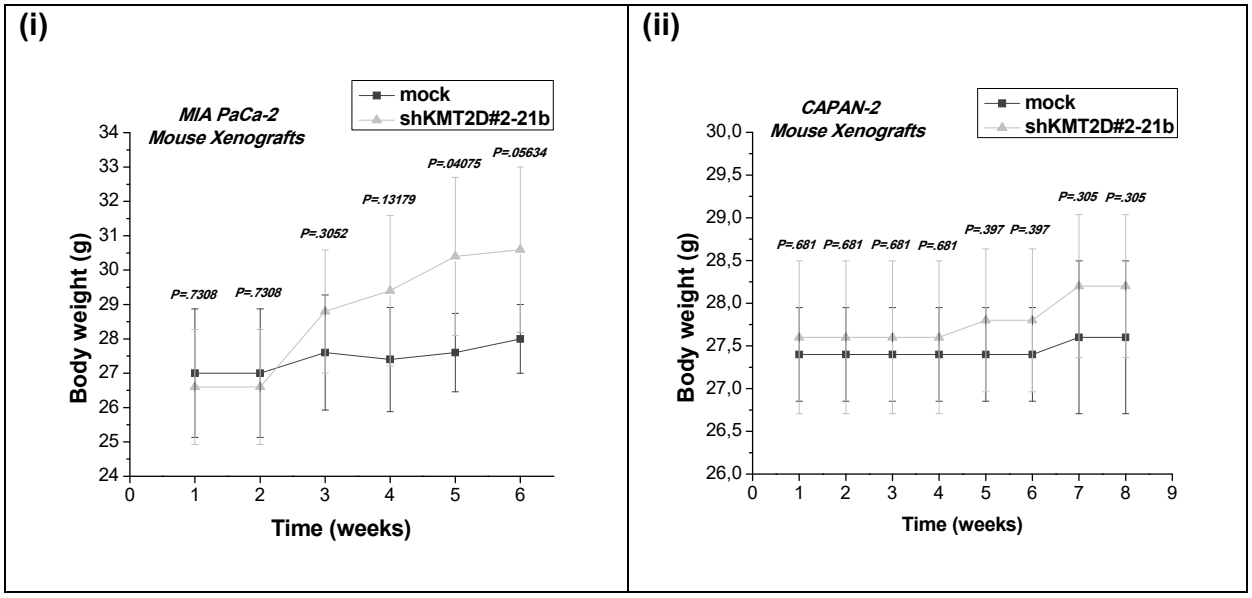

Supplementary Figure S13: Assessment of body weight changes in mice injected with control or KMT2D-lacking pancreatic cancer cells.

Body weight graphs of mouse xenografts bearing **(i)** MIAPaCa-2 or **(ii)** CAPAN-2 shKMT2D#2-21b clonal cell lines and mock-transfected cells (n=5 mice per group). Statistical analyses were performed using one-way ANOVA.

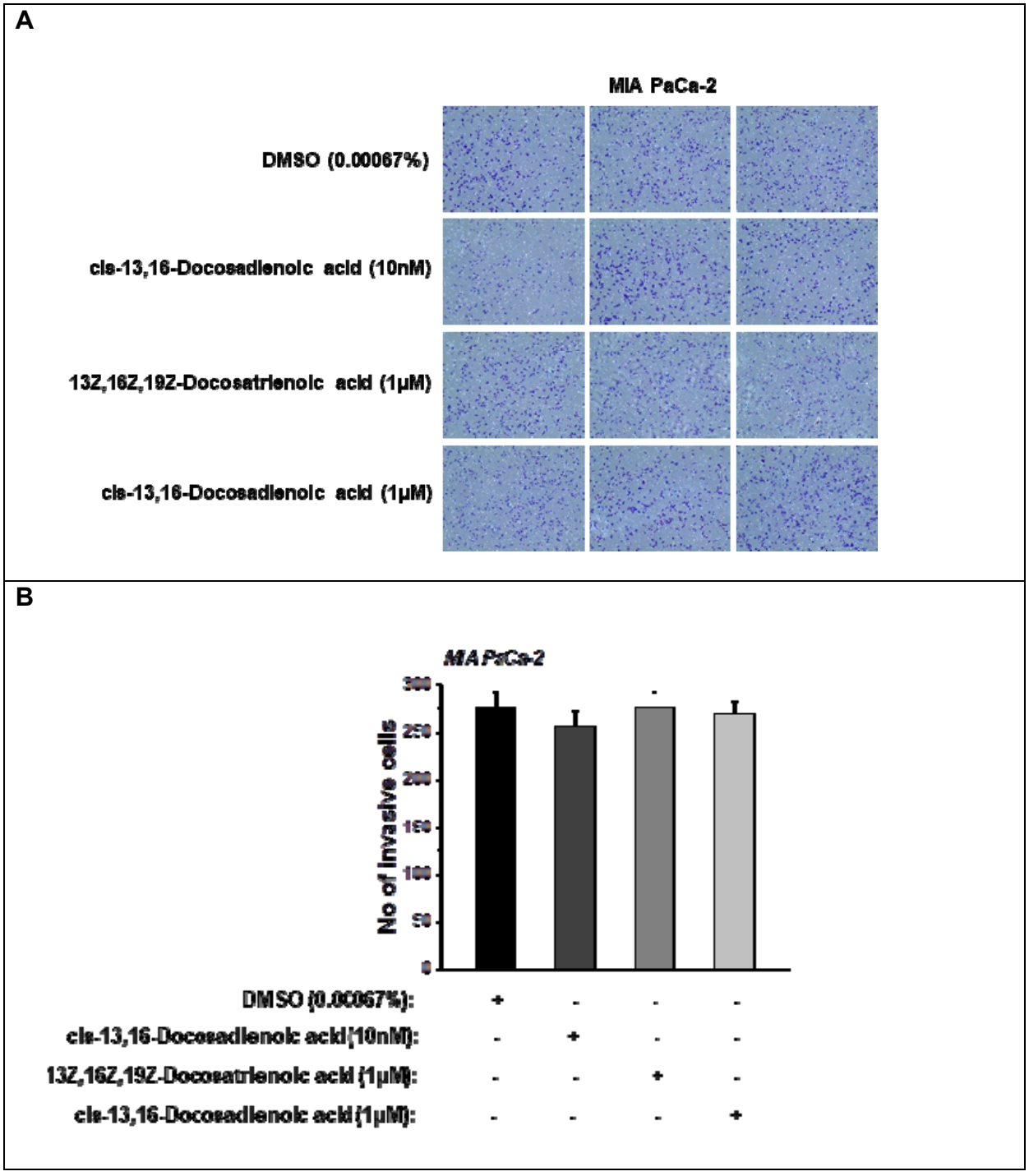
A
MIA PaCa-2
DMSO (0.00067%)
cis-13,16-Docosadienoic acid (10nM)
13Z,16Z,19Z-Docosatrienoic acid (1μM)
cis-13,16-Docosadienoic acid (1μM)
B
MIA PaCa-2
No of invasive cells
300
250
200
150
100
50
0
DMSO (0.00067%): + - - -
cis-13,16-Docosadienoic acid (10nM): - + - -
13Z,16Z,19Z-Docosatrienoic acid (1μM): - - + -
cis-13,16-Docosadienoic acid (1μM): - - - +

Supplementary Figure S14: Effects of docosadienoic, docosatrienoic and docosatretraenoic acid on pancreatic cancer cell invasiveness *in vitro*.

(A) Representative images of invading cells upon treatment with docosadienoic, docosatrienoic or docosatretraenoic acid for 22 h and **(B)** the respective quantification. Data are expressed as the mean number of invading cells per field±SE.

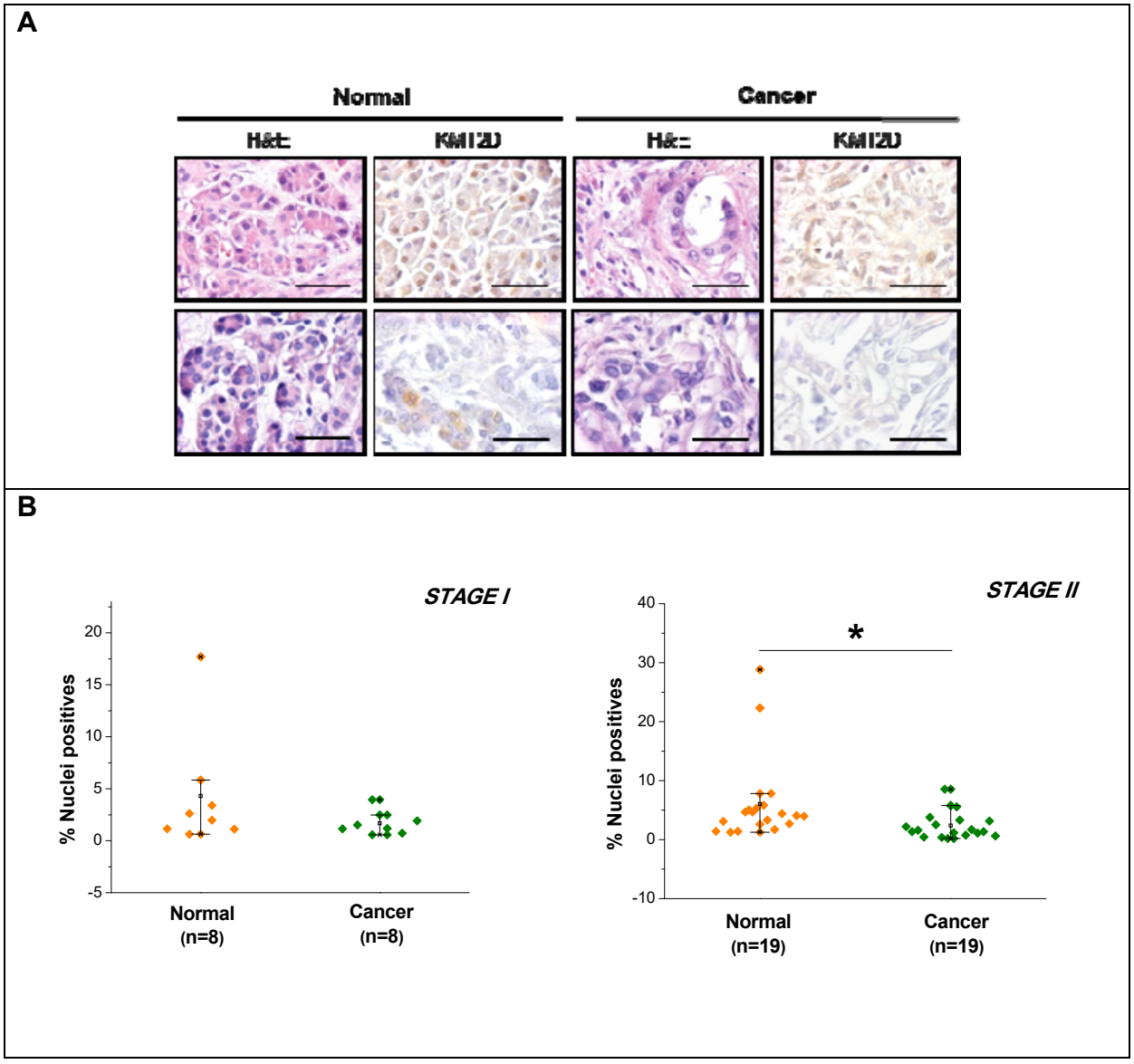

Supplementary Figure S15: KMT2D staining patterns in matched pancreatic cancer and normal human tissues.

(A) Representative images (4x magnification) of KMT2D expression as assessed by IHC analysis. Scale bars represent 40 μm. **(B)** Graphs for nuclear staining quantification of KMT2D expression in normal pancreata and matched tumors derived from Stage I or Stage II pancreatic cancer patients (Cohort IV).

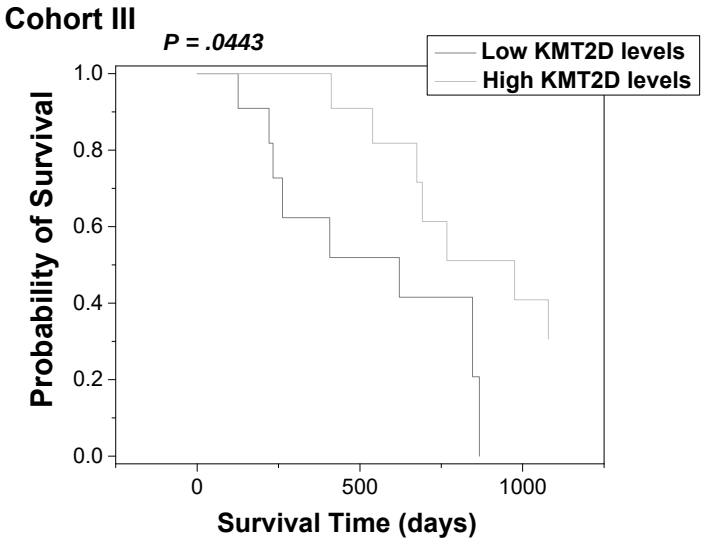

Supplementary Figure S16: Correlation of *KMT2D* expression with overall patient survival.

Kaplan-Meier survival curves of patients derived from Cohort III, harboring below median (<.25) and above median (>.25) *KMT2D* levels. 19 out of 22 cases were stratified as Stage III, 1 case as Stage IV pancreatic cancer and 1 case remains

uncharacterized. r, Pearson correlation coefficient; Statistical analyses were performed using Pearson correlation.

SUPPLEMENTARY TABLES

Table S1

Gene symbols	Fold change	*P* value	q value	Probes
KMT2D	-1.741141121	.095383814	.253115	227527_at
KDM2A	1.717960305	.223050879	.444714	208988_at
KDM4C	-1.848905517	.002576512	.041733	1556493_a_at
KDM5B	1.825971671	.020177382	.086848	201548_s_at
KDM8	-2.020680417	.0000928	.001968	220070_at
SETDB2	-1.72662285	.006398742	.03863	235339_at
SETD6	-1.849110572	.001285416	.01239	1554555_a_at
SETD6	-1.785867564	.001087622	.011024	219751_at
SUV420H1	-1.705577585	.0073486	.042803	222566_at

Supplementary Table S1: Differential expression of chromatin regulators in pancreatic cancer.

Table of standardized (Z-scores) expression of the corresponding histone methyltransferases (KMTs) and demethylases (KDMs) in pancreatic cancer as well as adjacent normal tissues originating from Cohort I, as assessed by DNA microarray analysis (Affymetrix U133 Gene ChIP Set). Multi-array analysis followed by filtering of uninformative and low variance probes revealed 8 epigenetic factors to be up- or down-regulated ≥1.5 fold relatively to normal samples. Array fold change is generally reported as log value but has been converted to an arithmetic value for comparison purposes.

Table S2

	MIA PaCa-2								
Time (hours)	**Cell Index siC#1** (n=4)				**Cell Index siKMT2D#2** (n=4)				***P* value siKMT2D#2 vs siC#1**
0	0	0	0	0	0	0	0	0	
1.556944444	0.01993	0.00307	0.0161	0.02633	0.01218	0.01417	0.04009	0.04838	0.2787
3.306944444	0.17238	0.10747	0.13113	0.17127	0.16564	0.14392	0.15754	0.16934	0.45282
4.806944444	0.23896	0.17123	0.188	0.23339	0.2298	0.19187	0.20576	0.21341	0.90455
6.556944444	0.28382	0.21657	0.23608	0.28436	0.27899	0.2319	0.23863	0.24487	0.75331
8.056944444	0.31366	0.24275	0.26066	0.31161	0.31102	0.25793	0.26227	0.26644	0.73415
9.806944444	0.34585	0.26983	0.29308	0.34035	0.34456	0.28638	0.285	0.29172	0.67265
11.55694444	0.37777	0.29253	0.31851	0.36801	0.38798	0.31856	0.3136	0.31742	0.86442
13.05694444	0.40391	0.32055	0.34242	0.39765	0.4221	0.34908	0.33966	0.34518	0.94257
14.80694444	0.43768	0.34307	0.37141	0.42657	0.4706	0.39153	0.38318	0.38488	0.69096
16.30694444	0.46548	0.36034	0.39357	0.44251	0.51015	0.42361	0.42656	0.4204	0.39104
18.05694444	0.48411	0.37485	0.40839	0.46096	0.55653	0.46225	0.46366	0.45651	0.17771
19.55694444	0.49563	0.38574	0.4169	0.46539	0.58461	0.49454	0.49707	0.47523	0.08277
21.30694444	0.51023	0.39866	0.42816	0.47528	0.62531	0.51577	0.51739	0.5098	0.0539
22.80694444	0.53428	0.42219	0.4468	0.49818	0.65059	0.54778	0.54651	0.53385	0.04379
24.55694444	0.57582	0.45676	0.48193	0.53862	0.68852	0.58323	0.5879	0.56766	0.0515
26.05694444	0.61471	0.49414	0.52977	0.57605	0.73841	0.62387	0.62212	0.60624	0.05856
27.80694444	0.66688	0.55229	0.58403	0.6156	0.79959	0.67146	0.68054	0.65628	0.05531
29.55694444	0.71799	0.58852	0.62445	0.66588	0.8643	0.74643	0.7338	0.69781	0.0502
31.05694444	0.76111	0.6173	0.65519	0.69779	0.91719	0.78763	0.78436	0.74619	0.04052
32.80694444	0.79299	0.65679	0.68778	0.72991	0.97381	0.86092	0.82865	0.80414	0.01992
34.30694444	0.82135	0.6842	0.71556	0.75847	1.02194	0.90791	0.88465	0.83918	0.01372
36.05694444	0.84057	0.7155	0.73749	0.78684	1.07253	0.94268	0.9306	0.88986	0.00792
37.55694444	0.87557	0.73416	0.77224	0.82506	1.11671	0.9901	0.97506	0.91518	0.00931
39.30694444	0.92721	0.77848	0.81946	0.86033	1.15278	1.04075	1.0271	0.95036	0.00954
40.80694444	0.97444	0.82619	0.8596	0.90322	1.20265	1.06349	1.06287	0.99585	0.01243
42.55694444	1.03478	0.87915	0.92693	0.9688	1.25158	1.13502	1.13759	1.05507	0.01024

44.05694444	1.08756	0.91975	0.98197	1.02528	1.30741	1.18536	1.19222	1.10988	0.01116
45.80694444	1.14759	0.97162	1.03087	1.0803	1.38722	1.24957	1.26116	1.17628	0.0105
47.55694444	1.20711	1.0233	1.078	1.13413	1.44859	1.32177	1.33128	1.24172	0.00813
49.05694444	1.24837	1.07129	1.1352	1.19125	1.51097	1.38801	1.3996	1.30525	0.00558
50.80694444	1.30284	1.12654	1.19836	1.24521	1.57876	1.45095	1.47003	1.37221	0.0045

Supplementary Table S2: Xcelligence Cell Index and *P* values of siKMT2D#2-treated versus control MIA PaCa-2 cells.

List of Cell Index values derived from the measured impedances and continuously displayed on the Xcelligence Software user interface. Each experimental condition was performed in quadruplicates. Statistical analyses were performed using one-way ANOVA and the *P* values corresponding to the comparison of siRNA-treated versus control cells are shown at every single time point. *P* values ≤.05 are marked in red. Differences in Cell Index measurements are significant after 31 hours of monitoring MIA PaCa-2 cells.

Table S3

	CAPAN-2								
Time (hours)	**Cell Index siC#1** (n=4)				**Cell Index siKMT2D#2** (n=4)				***P* value siKMT2D#2 vs siC#1**
0	0	0	0	0	0	0	0	0	
1.556944444	-0.020073	0.034304	0.050577	0.05816	0.06867	0.059427	0.083027	0.085488	0.05928
3.306944444	0.037766	0.079534	0.099732	0.094963	0.141033	0.122201	0.144497	0.157935	0.00721
4.806944444	0.068535	0.10916	0.125919	0.113986	0.179764	0.165437	0.179974	0.200587	0.00175
6.556944444	0.08927	0.128111	0.139508	0.129772	0.205867	0.190239	0.200832	0.231135	9.12692E-4
8.056944444	0.099004	0.1331	0.155176	0.1359	0.219105	0.201924	0.214894	0.244162	8.90077E-4
9.806944444	0.101722	0.127247	0.158144	0.137542	0.229755	0.212719	0.219634	0.253497	5.65592E-4
11.55694444	0.098911	0.13078	0.15315	0.137105	0.230603	0.214544	0.22037	0.258289	5.14131E-4
13.05694444	0.098725	0.125915	0.146574	0.134241	0.233402	0.220184	0.221467	0.260783	2.389E-4

14.80694444	0.097222	0.124272	0.145863	0.134348	0.238026	0.220155	0.222833	0.264834	2.67765E-4
16.30694444	0.096102	0.122436	0.143388	0.131518	0.239895	0.219975	0.226634	0.263344	1.746E-4
18.05694444	0.094791	0.12158	0.140609	0.130565	0.241798	0.215101	0.232633	0.262699	1.63212E-4
19.55694444	0.087017	0.122059	0.139195	0.126579	0.241056	0.216168	0.227237	0.2572	1.79476E-4
21.30694444	0.082258	0.119865	0.137669	0.128171	0.241253	0.21935	0.225254	0.259881	2.21228E-4
22.80694444	0.080472	0.123005	0.136547	0.128523	0.243548	0.218359	0.230869	0.259986	2.22074E-4
24.55694444	0.075172	0.121803	0.132296	0.132782	0.243325	0.221071	0.22565	0.262633	3.19085E-4
26.05694444	0.074455	0.122927	0.134319	0.129331	0.244887	0.22282	0.226275	0.266265	3.30394E-4
27.80694444	0.0737	0.119391	0.131049	0.125469	0.242504	0.223553	0.223904	0.271749	3.16723E-4
29.55694444	0.072791	0.11973	0.12722	0.125928	0.242003	0.229328	0.218143	0.263189	2.28539E-4
31.05694444	0.072043	0.120048	0.124046	0.119541	0.24577	0.22249	0.225408	0.258103	1.34237E-4
32.80694444	0.066999	0.11541	0.12315	0.11772	0.244751	0.227915	0.220318	0.259354	1.52409E-4
34.30694444	0.062007	0.116527	0.121774	0.12072	0.244203	0.231497	0.223175	0.263073	2.01022E-4
36.05694444	0.061464	0.112372	0.116357	0.120599	0.24808	0.225763	0.225829	0.241364	1.1443E-4
37.55694444	0.065181	0.11423	0.102967	0.115519	0.245032	0.227805	0.22235	0.239662	4.57436E-5
39.30694444	0.06347	0.117356	0.09523	0.116264	0.245516	0.233652	0.219364	0.232157	6.4013E-5
40.80694444	0.063181	0.113218	0.090033	0.112343	0.244225	0.236082	0.223486	0.232254	3.19248E-5
42.55694444	0.063229	0.11298	0.080251	0.116045	0.250371	0.236341	0.229732	0.235528	3.98296E-5
44.05694444	0.066098	0.116247	0.079267	0.117831	0.249681	0.240117	0.232087	0.238075	3.97361E-5
45.80694444	0.064277	0.121713	0.084177	0.124887	0.248549	0.242266	0.234827	0.24359	7.50008E-5
47.55694444	0.06762	0.124783	0.082257	0.123198	0.252865	0.243433	0.241608	0.247328	5.8002E-5
49.05694444	0.070556	0.125857	0.083957	0.124076	0.249066	0.247302	0.249124	0.245079	4.609E-5
50.80694444	0.071493	0.12713	0.078742	0.124957	0.250745	0.24804	0.252373	0.25484	5.28337E-5

Supplementary Table S3: Xcelligence Cell Index and *P* values of siKMT2D#2-treated versus control CAPAN-2 cells.

List of Cell Index values derived from the measured impedances and continuously displayed on the Xcelligence Software user interface. Each experimental condition was performed in quadruplicates. Statistical analyses were performed using one-way ANOVA and the *P* values corresponding to the comparison of siRNA-treated versus control cells are shown at every

single time point. *P* values ≤.05 are marked in red. Differences in Cell Index measurements are significant after 3.3 hours of monitoring CAPAN-2 cells.

Table S4

	MIA PaCa-2						
Time (hours)	**Cell Index mock** (n=3)			**Cell Index shKMT2D#2-21a** (n=3)			***P* value shKMT2D#2-21a vs mock**
0	0	0	0	0	0	0	
1.64611	-0.03548	-6.7E-4	0.04437	0.02274	0.03943	0.06906	0.20064
3.39611	0.02795	0.05192	0.11561	0.18392	0.17674	0.21105	0.01122
4.89611	0.08816	0.105	0.17799	0.27335	0.25557	0.29962	0.0074
6.64611	0.15481	0.16696	0.25148	0.35875	0.32387	0.3673	0.00872
8.14611	0.20299	0.20718	0.29803	0.40881	0.36791	0.41359	0.00934
9.89611	0.2414	0.24242	0.3348	0.45946	0.41235	0.45553	0.00791
11.39611	0.27765	0.27711	0.37328	0.51275	0.45182	0.50053	0.0084
13.14611	0.32252	0.31923	0.41425	0.57925	0.51468	0.56412	0.00546
14.64611	0.36765	0.36132	0.46573	0.63069	0.56235	0.60952	0.00676
16.39611	0.41964	0.3977	0.5132	0.67095	0.6043	0.65111	0.00806
18.14611	0.45588	0.42176	0.5516	0.69757	0.62371	0.67342	0.01334
19.64611	0.48118	0.43805	0.57682	0.71668	0.64357	0.68661	0.01645
21.39611	0.49712	0.46084	0.59246	0.76491	0.67262	0.72969	0.01243
22.89611	0.51328	0.47107	0.61206	0.82401	0.73223	0.78193	0.00751
24.64611	0.54207	0.50643	0.65696	0.92238	0.82223	0.879	0.00474
26.14611	0.59431	0.56295	0.69114	1.00921	0.90233	0.96789	0.00227
27.89611	0.66012	0.62616	0.7551	1.1097	1.01301	1.06958	0.0013
29.64444	0.74236	0.68291	0.82783	1.1898	1.11702	1.1598	0.00101
31.14444	0.78123	0.73267	0.88596	1.26025	1.19066	1.23467	9.85588E-4
32.89444	0.82113	0.78133	0.9338	1.32393	1.26901	1.29878	7.2956E-4
34.39444	0.86096	0.81316	0.96802	1.38432	1.32704	1.34736	6.35982E-4
36.14444	0.90486	0.85244	1.01082	1.46964	1.41646	1.44576	4.44133E-4

37.64444	0.93605	0.88429	1.0517	1.55654	1.52442	1.54173	3.166E-4
39.39444	0.98666	0.94622	1.1091	1.68043	1.66193	1.6784	1.80687E-4
40.89444	1.04982	0.9958	1.172	1.79348	1.78453	1.81634	1.64543E-4
42.64444	1.10853	1.06787	1.24812	1.91062	1.96863	1.96647	1.52504E-4
44.39444	1.16738	1.12633	1.3259	2.01828	2.11814	2.1126	2.20452E-4
45.89333	1.21602	1.1799	1.38965	2.12459	2.24856	2.21155	2.33143E-4
47.64333	1.26615	1.24707	1.46187	2.21607	2.3618	2.33057	2.79254E-4
49.14167	1.31626	1.28497	1.50996	2.32416	2.48603	2.44008	2.53257E-4
50.88972	1.37807	1.34948	1.57186	2.45744	2.59205	2.58472	1.74688E-4
52.38972	1.43097	1.40787	1.63916	2.55202	2.71498	2.70421	2.09778E-4
54.13972	1.50776	1.4887	1.70548	2.70808	2.85097	2.89939	1.54796E-4
55.88972	1.61186	1.58677	1.79364	2.84836	2.98378	3.06371	1.36266E-4
57.38972	1.67382	1.66723	1.86846	2.96868	3.13848	3.19889	1.38547E-4
59.13972	1.76102	1.75566	1.96147	3.13693	3.29247	3.29779	7.90511E-5
60.63972	1.83668	1.84181	2.03916	3.27238	3.39747	3.41639	5.49798E-5
62.38972	1.92252	1.93019	2.12654	3.42067	3.51613	3.55384	4.18829E-5
63.88972	1.98447	2.00046	2.20477	3.52858	3.63979	3.66438	4.71E-5
65.63972	2.081	2.10635	2.31714	3.69513	3.75112	3.79362	3.91071E-5
67.13972	2.16031	2.20805	2.37155	3.81512	3.85113	3.88427	1.80775E-5
68.88972	2.27924	2.32252	2.45216	3.9797	3.95671	4.00217	6.98761E-6
70.63972	2.3875	2.41904	2.59425	4.08349	4.03866	4.14571	2.22305E-5
72.13972	2.48343	2.50893	2.70639	4.21164	4.11882	4.21704	3.09696E-5
73.88972	2.58672	2.61139	2.80666	4.32744	4.22684	4.2726	2.86289E-5
75.38972	2.72494	2.71189	2.88812	4.45171	4.32179	4.37495	1.90687E-5
77.13944	2.8011	2.83126	3.01627	4.59121	4.37858	4.4798	6.16085E-5
78.63944	2.91401	2.90089	3.0763	4.69108	4.42792	4.56312	7.22673E-5
80.38944	3.02859	3.00459	3.17597	4.83053	4.48886	4.5994	1.61295E-4
81.88944	3.13508	3.08395	3.24635	4.87581	4.53915	4.64591	1.55821E-4
83.63944	3.26149	3.17539	3.31704	4.98727	4.6286	4.68768	2.14344E-4
85.38944	3.39014	3.26267	3.42184	5.10971	4.70364	4.74254	4.15676E-4
86.88944	3.49607	3.32432	3.48201	5.156	4.74067	4.76751	5.56886E-4
88.63944	3.55179	3.40723	3.55229	5.20273	4.78268	4.80914	5.83157E-4

90.13944	3.68251	3.47698	3.62795	5.22825	4.83796	4.83767	6.76022E-4
91.88944	3.80046	3.55814	3.72993	5.40447	4.8729	4.88635	0.00199
93.38944	3.87641	3.6527	3.81331	5.46153	4.88317	4.93434	0.00261
95.13944	3.98026	3.72709	3.87598	5.55389	4.93473	4.9804	0.00365
96.88944	4.09917	3.79225	3.97422	5.58058	4.95065	5.0155	0.00498
98.38944	4.20116	3.86002	4.01449	5.60487	4.95606	5.02309	0.00689
100.13917	4.31632	3.92505	4.10531	5.61392	4.95159	5.04212	0.01001
101.63917	4.43169	3.98702	4.17207	5.68448	4.98647	5.00756	0.01735
103.38917	4.54915	4.03133	4.20871	5.70852	4.99687	5.00298	0.02571
104.88917	4.65601	4.05039	4.27636	5.75427	4.98478	4.98693	0.04245
106.63917	4.71997	4.08675	4.32626	5.76795	4.94804	4.93416	0.06472
108.13917	4.81067	4.13599	4.35874	5.79617	4.90208	4.91447	0.09709
109.88917	4.88043	4.13423	4.38586	5.80425	4.8672	4.86941	0.13465
111.63917	4.98009	4.16329	4.4206	5.82269	4.80838	4.8519	0.19337
113.13917	5.03647	4.18176	4.41413	5.83088	4.74924	4.80327	0.25046
114.88917	5.13655	4.20232	4.42149	5.7937	4.66986	4.75638	0.34815
116.38917	5.18354	4.19483	4.42152	5.77905	4.6451	4.7042	0.40361
118.13917	5.23074	4.18789	4.45534	5.76533	4.57388	4.6051	0.51611
119.63917	5.25751	4.19731	4.42753	5.72818	4.5083	4.57409	0.57714
121.38917	5.35591	4.17537	4.41114	5.70622	4.44587	4.49845	0.68849

Supplementary Table S4: Xcelligence Cell Index and *P* values of shKMT2D#2-21a versus mock MIA PaCa-2 cells.

List of Cell Index values derived from the measured impedances and continuously displayed on the Xcelligence Software user interface. Each experimental condition was performed in triplicates. Statistical analyses were performed using one-way ANOVA and the *P* values corresponding to the comparison of shRNA-stably transfected versus control cells are shown at every single time point. *P* values ≤0.05 are marked in red. Differences in Cell Index measurements are significant after 3.3 hours of monitoring.

Table S5

	CAPAN-2								
Time (hours)	**Cell Index mock** (n=4)				**Cell Index shKMT2D#2-21a** (n=4)				***P* value shKMT2D#2-21a vs mock**
0	0	0	0	0	0	0	0	0	
1.64611	0.01462	0.01218	0.03884	0.06201	0.07853	0.04418	0.02288	0.03539	0.45515
3.39611	0.07544	0.05766	0.07975	0.10362	0.1246	0.08982	0.07047	0.0966	0.31017
4.89611	0.11267	0.08142	0.10833	0.13384	0.15458	0.11595	0.10411	0.13383	0.2854
6.64611	0.13282	0.09975	0.13087	0.15106	0.17986	0.13594	0.12981	0.1606	0.19468
8.14611	0.14139	0.10637	0.13721	0.15648	0.19189	0.14788	0.13682	0.17371	0.14612
9.89611	0.1525	0.10688	0.1374	0.1588	0.20485	0.15644	0.14623	0.18281	0.10382
11.39611	0.15252	0.10846	0.13751	0.15606	0.21631	0.16728	0.15531	0.19419	0.04309
13.14611	0.15796	0.10767	0.13622	0.15512	0.22899	0.1757	0.16183	0.20175	0.03085
14.64611	0.15662	0.10242	0.13536	0.15155	0.23498	0.18659	0.17484	0.20937	0.01139
16.39611	0.15975	0.09829	0.13219	0.14733	0.24868	0.19501	0.18465	0.21619	0.00748
18.14611	0.15871	0.09698	0.13278	0.14415	0.25905	0.21019	0.18786	0.22294	0.00473
19.64611	0.15639	0.09199	0.13041	0.1444	0.27136	0.22274	0.1972	0.23074	0.00301
21.39611	0.15989	0.09242	0.13139	0.13816	0.28585	0.23164	0.1939	0.23603	0.00402
22.89611	0.16406	0.08835	0.13004	0.13723	0.29695	0.24713	0.20966	0.23996	0.00258
24.64611	0.1619	0.08548	0.12986	0.13359	0.30964	0.25627	0.21183	0.25081	0.0023
26.14611	0.1678	0.0876	0.12719	0.1307	0.32135	0.27093	0.23042	0.2566	0.00136
27.89611	0.16923	0.08459	0.12604	0.13104	0.3342	0.28139	0.2374	0.26743	0.00124
29.64444	0.17416	0.08085	0.12452	0.12672	0.34964	0.29744	0.24991	0.27925	0.00104
31.14444	0.1824	0.07759	0.126	0.12553	0.35925	0.3033	0.25879	0.28762	0.00116
32.89444	0.18152	0.07712	0.12331	0.12159	0.36834	0.31755	0.2705	0.29826	7.34904E-4
34.39444	0.18649	0.07346	0.11996	0.11769	0.37439	0.32594	0.27598	0.30492	7.57403E-4
36.14444	0.18978	0.07419	0.12101	0.11213	0.37185	0.33697	0.28399	0.3099	5.85979E-4
37.64444	0.19512	0.06979	0.11535	0.11125	0.38244	0.35255	0.29787	0.32168	5.18973E-4
39.39444	0.19763	0.06798	0.10924	0.10578	0.39243	0.36354	0.30484	0.32708	5.16712E-4
40.89444	0.19881	0.06364	0.11474	0.09785	0.39526	0.37742	0.3182	0.33605	4.11666E-4
42.64444	0.20051	0.0574	0.10941	0.09803	0.40709	0.39498	0.33898	0.34726	3.17093E-4

44.39444	0.20842	0.05262	0.10969	0.09621	0.42697	0.41296	0.35257	0.35588	3.92894E-4
45.89333	0.21108	0.03697	0.11015	0.09583	0.44859	0.42364	0.36593	0.36544	4.67138E-4
47.64333	0.21688	0.03923	0.11628	0.09659	0.46535	0.44283	0.39169	0.3835	3.54637E-4
49.14167	0.22108	0.04193	0.11735	0.09839	0.48161	0.47117	0.40379	0.40015	3.13406E-4
50.88972	0.23155	0.04425	0.11829	0.09668	0.50937	0.48388	0.42265	0.41374	3.36406E-4
52.38972	0.23578	0.04409	0.12151	0.09185	0.52924	0.49896	0.44429	0.42949	2.90154E-4
54.13972	0.24363	0.04808	0.12219	0.08561	0.54634	0.5207	0.45773	0.4489	2.73627E-4
55.88972	0.253	0.05448	0.12579	0.08556	0.57381	0.54568	0.46975	0.46185	3.10678E-4
57.38972	0.25673	0.05762	0.13062	0.08629	0.58611	0.56827	0.49624	0.48122	2.27898E-4
59.13972	0.26142	0.06335	0.13304	0.08675	0.60869	0.60007	0.50725	0.49634	2.2984E-4
60.63972	0.26829	0.06477	0.13566	0.09055	0.62504	0.61133	0.53163	0.51868	1.79323E-4
62.38972	0.27364	0.06557	0.13821	0.089	0.64896	0.63632	0.54708	0.53735	1.76477E-4
63.88972	0.27408	0.07054	0.14284	0.0914	0.67956	0.66286	0.55842	0.54902	1.77675E-4
65.63972	0.28038	0.07291	0.14651	0.09407	0.7024	0.68778	0.57252	0.56675	1.79125E-4
67.13972	0.28963	0.07739	0.14796	0.09153	0.72935	0.71003	0.58763	0.58466	1.92732E-4
68.88972	0.29532	0.07692	0.15511	0.08452	0.75266	0.72862	0.60422	0.60104	1.99467E-4
70.63972	0.29942	0.08279	0.15458	0.08815	0.7841	0.76832	0.63173	0.62832	1.65234E-4
72.13972	0.30537	0.08631	0.1581	0.08772	0.80715	0.79405	0.65885	0.64177	1.55946E-4
73.88972	0.31327	0.09277	0.16368	0.08601	0.83972	0.81829	0.68513	0.67534	1.3085E-4
75.38972	0.3182	0.08969	0.16533	0.08903	0.85848	0.85382	0.71023	0.7047	1.09467E-4
77.13944	0.33027	0.09882	0.16565	0.09587	0.89576	0.90812	0.73604	0.72969	1.22138E-4
78.63944	0.33924	0.10003	0.16911	0.09508	0.94837	0.94157	0.77601	0.76276	1.10465E-4
80.38944	0.3487	0.10577	0.17359	0.0987	1.00222	0.98485	0.80443	0.79951	1.11257E-4
81.88944	0.35949	0.11137	0.18091	0.09913	1.03302	1.03145	0.84508	0.82332	1.06542E-4
83.63944	0.36418	0.11618	0.18941	0.10619	1.06645	1.07785	0.86758	0.8391	1.17714E-4
85.38944	0.37339	0.12079	0.19537	0.10567	1.11719	1.12588	0.89975	0.8771	1.16753E-4
86.88944	0.38011	0.12661	0.19735	0.10701	1.1595	1.18502	0.92108	0.90369	1.36251E-4
88.63944	0.39188	0.13656	0.20597	0.11024	1.2158	1.23839	0.96176	0.94011	1.36401E-4
90.13944	0.3994	0.14292	0.21497	0.10799	1.28016	1.3008	0.99606	0.97683	1.51674E-4
91.88944	0.4124	0.14896	0.22115	0.11206	1.35973	1.35436	1.02401	1.01358	1.84004E-4
93.38944	0.41764	0.15343	0.2324	0.11258	1.42202	1.43345	1.06019	1.0492	2.09515E-4
95.13944	0.42643	0.16578	0.23832	0.11547	1.52347	1.56719	1.07862	1.09339	3.56668E-4

96.88944	0.43567	0.17158	0.24716	0.11923	1.60117	1.63223	1.12655	1.1347	3.58733E-4
98.38944	0.44724	0.17464	0.25659	0.12718	1.68784	1.75962	1.18409	1.18649	4.1616E-4
100.13917	0.46331	0.17956	0.26242	0.13036	1.77026	1.84637	1.23422	1.22194	4.72084E-4
101.63917	0.46731	0.18361	0.27419	0.1322	1.86374	1.9746	1.27434	1.27042	5.86156E-4
103.38917	0.48137	0.18737	0.28146	0.13378	1.95985	2.08392	1.32145	1.31949	6.71452E-4
104.88917	0.49534	0.19351	0.29001	0.13492	2.07408	2.28446	1.37379	1.37304	9.59862E-4
106.63917	0.51044	0.19558	0.29743	0.13514	2.18489	2.39506	1.40685	1.41617	0.00115
108.13917	0.52609	0.21009	0.3009	0.1425	2.32248	2.58844	1.46406	1.47154	0.00149
109.88917	0.53772	0.21542	0.31296	0.14786	2.45081	2.78011	1.51131	1.51776	0.00193
111.63917	0.54959	0.22733	0.32882	0.14885	2.67416	2.93264	1.56531	1.60026	0.00217
113.13917	0.56386	0.23495	0.33118	0.15368	2.86434	3.1599	1.62501	1.65958	0.00272
114.88917	0.57123	0.24506	0.34073	0.15369	3.10717	3.39293	1.70519	1.75151	0.00306
116.38917	0.58829	0.25	0.35437	0.16194	3.29853	3.66115	1.7787	1.82755	0.00361
118.13917	0.60761	0.2572	0.36414	0.16934	3.511	4.04172	1.85226	1.90569	0.00469
119.63917	0.62744	0.26197	0.36525	0.17169	3.77049	4.463	1.9252	2.01165	0.00587
121.38917	0.638784	0.27081	0.376880	0.177430	4.07119	5.0249788	2.02605	2.09975	0.00781

Supplementary Table S5: Xcelligence Cell Index and *P* values of shKMT2D#2-21a versus mock CAPAN-2 cells.

List of Cell Index values derived from the measured impedances and continuously displayed on the Xcelligence Software user interface. Each experimental condition was performed in triplicates. Statistical analyses were performed using one-way ANOVA and the *P* values corresponding to the comparison of shRNA-stably transfected versus control cells are shown at every single time point. *P* values ≤0.05 are marked in red. Differences in Cell Index measurements are significant after 11 hours of monitoring.

Table S6

Gene symbols	Mean difference	*P* value	q value	Probes
SETD3	0.264457	.0000027	.000353114	cg16694837
KMT2D	0.293902	.000394	.003574961	cg13007988
KMT2D	0.276747	.0000201	.000762928	cg00522588
KDM3A	0.254105	.000000979	.000258094	cg01878308
KDM2B	-0.26654	.0000164	.000694	cg15234492
SETDB2	-0.31333	.0000133	.002972	cg05743713

Supplementary Table S6: Differential methylation of chromatin regulators in pancreatic cancer.

Table of standardized (Z-scores) expression of the corresponding KMTs and KDMs in pancreatic cancer as well as adjacent normal tissues, as assessed by the Infinium Human Methylation 450 Bead ChIP Array. Wilcoxon rank-sum tests were conducted to compare methylation array data between pancreatic cancer patients and healthy controls. Genes shown are up- or down-regulated ≥1.5 fold relatively to normal samples and with statistical significance $P \leq 0.001$

Table S7

(i)

Chr	Start	End	Ref	Alt	Func. refGene	ExonicFunc. refGene	AAChange.refGene
12	49421179	49421179	G	C	intronic	na	na
12	49422795	49422795	G	A	intronic	na	na
12	49427919	49427919	T	C	exonic	synonymous SNV	KMT2D:NM_003482:exon38:c.A10671G:p.P3557P
12	49439659	49439659	C	T	intronic	na	na
12	49445447	49445447	T	A	exonic	synonymous SNV	KMT2D:NM_003482:exon10:c.A2019T:p.P673P

12	49445536	49445536	T	G	exonic	nonsynonymous SNV	KMT2D:NM_003482:exon10:c.A1930C:p.M644L
12	49445540	49445540	T	A	exonic	synonymous SNV	KMT2D:NM_003482:exon10:c.A1926T:p.S642S
12	49447819	49447819	T	C	exonic	synonymous SNV	KMT2D:NM_003482:exon5:c.A615G:p.L205L

(ii)

Chr	Start	End	Ref	Alt	Func. refGene	ExonicFunc. refGene	AAChange.refGene
12	49413208	49413208	-	A	UTR3	na	na
12	49415026	49415026	G	A	UTR3	na	na
12	49416048	49416048	C	-	intronic	na	na
12	49419677	49419677	G	C	intronic	na	na
12	49421179	49421179	G	C	intronic	na	na
12	49422094	49422094	A	G	intronic	na	na
12	49424616	49424616	G	A	intronic	na	na
12	49424878	49424881	TCTG	-	intronic	na	na
12	49425978	49425978	T	C	exonic	synonymous SNV	KMT2D:NM_003482:exon39:c.A12510G:p.P4170P
12	49427652	49427652	C	T	exonic	synonymous SNV	KMT2D:NM_003482:exon39:c.G10836A:p.Q3612Q
12	49434074	49434074	C	A	exonic	synonymous SNV	KMT2D:NM_003482:exon31:c.G7479T:p.G2493G
12	49436724	49436724	A	G	intronic	na	na
12	49439521	49439521	A	G	intronic	na	na
12	49439659	49439659	C	T	intronic	na	na
12	49441382	49441382	T	-	intronic	na	na
12	49442359	49442359	-	A	intronic	na	na
12	49442813	49442813	T	C	intronic	na	na
12	49444545	49444545	G	A	exonic	synonymous SNV	KMT2D:NM_003482:exon11:c.C2826T:p.I942I

12	49448881	49448881	T	G	intronic	na	na

Table S7: *KMT2D* mutational status.

Sequence alterations in *KMT2D* gene, as assessed by Whole Exome Sequencng, in **(i)** MIA PaCa-2 and **(ii)** CAPAN-2 cell lines. Chr, Chromosome number; Start, Start position; End, End position; Ref, Reference base(s); Alt, Alternate non-reference alleles called on at least one of the samples; Func.refGene, Regions (e.g., exonic, intronic, non-coding RNA)) that one variant hits; ExonicFunc.refGene, Exonic variant function, e.g., nonsynonymous, synonymous, frameshift insertion; AAChange.refGene, Amino acid change. For example, KMT2D : NM_003482:exon38:c.A10671G:p.P3557P stands for gene name, Known RefSeq accession, region, cDNA level change, protein level change.

Table S8

(i)

Chr	Start	End	Ref	Alt	Func. refGene	ExonicFunc. refGene	AAChange.refGene
12	8072008	8072008	T	C	UTR3	na	na
12	8073496	8073496	T	-	UTR3	na	na
12	8074192	8074192	G	A	exonic	synonymous SNV	SLC2A3:NM_006931:exon10:c.C1308T:p.T436T
12	8075117	8075117	A	G	intronic	na	na
12	8075286	8075286	C	T	intronic	na	na
12	8083541	8083541	C	T	intronic	na	na
12	8085547	8085547	T	C	intronic	na	na
12	8086083	8086083	C	A	intronic	na	na

	8088227	8088227	T	C	intronic	na	na
	8088766	8088766	T	C	UTR5	na	na

(ii)

Chr	Start	End	Ref	Alt	Func. refGene	ExonicFunc. refGene	AAChange.refGene
12	8072562	8072562	A	G	UTR3	na	na
12	8073496	8073496	T	-	UTR3	na	na
12	8074192	8074192	G	A	exonic	synonymous SNV	SLC2A3:NM_006931:exon10:c.C1308T:p.T436T
12	8075117	8075117	A	G	intronic	na	na
12	8075286	8075286	C	T	intronic	na	na
12	8086062	8086062	G	C	intronic	na	na
12	8088766	8088766	T	C	UTR5	na	na

Table S8: SLC2A3 mutational status.

Sequence alterations in *SLC2A3* gene, as assessed by Whole Exome Sequencng, in **(i)** MIA PaCa-2 and **(ii)** CAPAN-2 cell lines.

Table S9

	MIA PaCa-2								
Time (hours)	**Cell Index shKMT2D#2-21a+siC#1** (n=4)				**Cell Index shKMT2D#2-21a+siSLC2A3** (n=4)				***P* value shKMT2D#2-21a+siSLC2A3 vs shKMT2D#2-21a+siC#1**
0	0	0	0	0	0	0	0	0	
1.64611	-0.09461	-0.10544	-0.10934	-0.09085	-0.06418	-0.08382	-0.1064	-0.09298	0.2297
3.39611	-0.07183	-0.08472	-0.08991	-0.06829	-0.04211	-0.06424	-0.08378	-0.0497	0.12519

4.89611	-0.03959	-0.05402	-0.05856	-0.0265	-0.01929	-0.04226	-0.05887	-0.01414	0.41835
6.64611	-0.00333	-0.02005	-0.02692	0.00252	-0.00723	-0.02847	-0.04887	0.00368	0.5636
8.14611	0.03037	0.01308	0.00741	0.02951	0.00352	-0.01821	-0.03962	0.0122	0.05644
9.89611	0.06093	0.03873	0.03554	0.05915	0.01221	-0.00894	-0.02679	0.02	0.00747
11.39611	0.08987	0.06699	0.06234	0.08699	0.02703	0.00411	-0.0171	0.03304	0.00291
13.14611	0.11748	0.09022	0.08578	0.1108	0.03469	0.0146	-0.00307	0.04192	8.19E-04
14.64611	0.14544	0.11846	0.11708	0.13531	0.04826	0.02964	0.0146	0.05787	2.46E-04
16.39611	0.17055	0.14461	0.13905	0.15488	0.06123	0.04342	0.03029	0.07208	1.29E-04
18.14611	0.19574	0.17415	0.1595	0.18154	0.07805	0.05888	0.04607	0.08932	1.09E-04
19.64611	0.21736	0.19735	0.17909	0.20363	0.09044	0.07096	0.05506	0.10093	8.85E-05
21.39611	0.24085	0.21538	0.20297	0.22107	0.1039	0.08493	0.06319	0.11479	8.77E-05
22.89611	0.26035	0.23619	0.21879	0.23155	0.10422	0.09528	0.07271	0.12445	5.91E-05
24.64611	0.28008	0.2552	0.23872	0.24416	0.11326	0.10717	0.08278	0.13412	4.69E-05
26.14611	0.29911	0.26855	0.2621	0.25453	0.12754	0.11606	0.09111	0.14491	5.39E-05
27.89611	0.32114	0.28338	0.27851	0.2651	0.14007	0.12484	0.09979	0.15369	8.00E-05
29.64444	0.34657	0.30347	0.2998	0.27632	0.15044	0.13389	0.11386	0.1615	8.82E-05
31.14444	0.35513	0.32492	0.3265	0.28211	0.16899	0.1474	0.13319	0.17644	9.34E-05
32.89444	0.38004	0.34996	0.34583	0.30357	0.18761	0.16214	0.15399	0.18929	7.82E-05
34.39444	0.42083	0.38988	0.37766	0.32976	0.21553	0.16931	0.17833	0.20924	1.50E-04
36.14444	0.451	0.42665	0.41102	0.34823	0.23936	0.18943	0.19445	0.23121	2.47E-04
37.64444	0.49111	0.46056	0.45351	0.38222	0.27224	0.21294	0.21425	0.25569	2.74E-04
39.39444	0.51728	0.4972	0.4868	0.40949	0.29648	0.23014	0.22787	0.27045	2.56E-04
40.89444	0.5545	0.52714	0.51567	0.43311	0.31419	0.24799	0.24713	0.29207	2.92E-04
42.64444	0.59323	0.54773	0.54368	0.44909	0.32836	0.26515	0.25549	0.30506	4.09E-04
44.39444	0.6212	0.58563	0.5737	0.4755	0.34719	0.28024	0.27408	0.31986	3.47E-04
45.89333	0.65597	0.62375	0.60767	0.48826	0.3702	0.28844	0.29087	0.3374	6.08E-04
47.64333	0.70713	0.67223	0.64871	0.51336	0.39095	0.2897	0.31313	0.36012	8.35E-04
49.14167	0.75288	0.71725	0.69244	0.53825	0.41959	0.31031	0.33353	0.38414	0.00108
50.88972	0.82426	0.77215	0.75003	0.57887	0.4602	0.33434	0.36341	0.41361	0.00133
52.38972	0.87652	0.83089	0.79804	0.61428	0.48923	0.35649	0.38867	0.44307	0.0014
54.13972	0.94527	0.89607	0.87458	0.66318	0.5208	0.38831	0.41366	0.4755	0.00124
55.88972	0.98306	0.96064	0.93668	0.70036	0.5501	0.41436	0.42933	0.49565	0.00114

57.38972	1.06	1.03367	1.00026	0.74032	0.58465	0.43986	0.44855	0.51596	0.00128
59.13972	1.12301	1.09276	1.07692	0.7769	0.60392	0.46201	0.46392	0.53602	0.00124
60.63972	1.20626	1.14633	1.13268	0.81675	0.63557	0.49094	0.48428	0.56445	0.00136
62.38972	1.28918	1.20455	1.18868	0.84646	0.65848	0.50778	0.50738	0.58652	0.0016
63.88972	1.37471	1.28074	1.27408	0.89532	0.69283	0.53255	0.53213	0.61546	0.00162
65.63972	1.44241	1.35446	1.32066	0.92819	0.72384	0.5516	0.55807	0.64672	0.00184
67.13972	1.54195	1.44198	1.41084	0.97504	0.76773	0.58073	0.59579	0.68441	0.0021
68.88972	1.62172	1.51839	1.47243	1.03179	0.80514	0.6037	0.62269	0.7066	0.0019
70.63972	1.72848	1.62262	1.55557	1.0837	0.85393	0.6376	0.65647	0.7417	0.00213
72.13972	1.80786	1.69168	1.62729	1.13608	0.89613	0.66294	0.68323	0.77687	0.0021
73.88972	1.88601	1.77459	1.70508	1.18451	0.93812	0.70083	0.71112	0.80651	0.00213
75.38972	1.9323	1.84716	1.77276	1.23341	0.97532	0.73422	0.73653	0.83511	0.00196
77.13944	2.00516	1.93677	1.84752	1.27405	1.02062	0.77242	0.75711	0.87031	0.00217
78.63944	2.0589	1.98732	1.91977	1.31567	1.05548	0.80312	0.77064	0.8978	0.00211
80.38944	2.1331	2.01494	2.02523	1.36859	1.08688	0.83444	0.80255	0.93638	0.00197
81.88944	2.1557	2.07281	2.05688	1.41857	1.11514	0.85874	0.822	0.96617	0.00168
83.63944	2.19256	2.13124	2.05782	1.47013	1.16515	0.89392	0.85701	1.00212	0.00158
85.38944	2.23593	2.17164	2.10071	1.5153	1.19504	0.9209	0.88714	1.03901	0.00147
86.88944	2.2729	2.1846	2.13259	1.577	1.23163	0.96151	0.92578	1.06566	0.00116
88.63944	2.27382	2.20528	2.13942	1.61148	1.26288	0.99543	0.95666	1.09706	0.00105
90.13944	2.27634	2.21071	2.12413	1.66209	1.30815	1.02607	0.99548	1.12739	8.67E-04
91.88944	2.26027	2.19989	2.13127	1.70817	1.34063	1.04828	1.02661	1.16042	6.55E-04
93.38944	2.22563	2.17577	2.08407	1.74883	1.3773	1.07453	1.05412	1.19905	5.11E-04
95.13944	2.1836	2.15322	2.07722	1.77086	1.38817	1.09131	1.07173	1.22476	3.82E-04
96.88944	2.13645	2.12463	1.99197	1.77793	1.42416	1.12489	1.09436	1.26069	4.36E-04

Supplementary Table S9: Xcelligence Cell Index and *P* values of shKMT2D#2-21a+siSLC2A3 versus shKMT2D#2-21a+siC#1 MIA PaCa-2 cells.

List of Cell Index values derived from the measured impedances and continuously displayed on the Xcelligence Software user interface. Each experimental condition was performed in triplicates. Statistical analyses were performed using one-way ANOVA and the *P* values

corresponding to the comparison of siRNA- transfected versus control cells are shown at every single time point. *P* values ≤.05 are marked in red. Differences in Cell Index measurements are significant after 9.9 hours of monitoring.

Table S10

	CAPAN-2								
Time (hours)	**Cell Index shKMT2D#2-21a+siC#1** (n=4)				**Cell Index shKMT2D#2-21a+siSLC2A3** (n=4)				***P* value shKMT2D#2-21a+siSLC2A3 vs shKMT2D#2-21a+siC#1**
0	0	0	0	0	0	0	0	0	
1.64611	-0.00518	0.02887	0.02781	0.05786	0.0328	0.05089	0.05253	0.08391	0.14817
3.39611	0.04612	0.07247	0.03966	0.09728	0.12267	0.11334	0.1014	0.14091	0.01182
4.89611	0.08429	0.10152	0.05783	0.13086	0.1671	0.14826	0.12715	0.16902	0.01723
6.64611	0.09141	0.12081	0.07221	0.15163	0.18629	0.1777	0.14465	0.19019	0.01749
8.14611	0.10227	0.13077	0.08522	0.16305	0.19681	0.19102	0.15491	0.19491	0.0175
9.89611	0.10822	0.14479	0.10014	0.17095	0.20304	0.19155	0.15909	0.20452	0.0243
11.39611	0.11602	0.14908	0.10879	0.18075	0.20815	0.19342	0.15649	0.20683	0.04243
13.14611	0.12673	0.15749	0.11432	0.19297	0.20311	0.19383	0.15725	0.20882	0.08766
14.64611	0.13734	0.16688	0.12238	0.20425	0.20318	0.1959	0.16033	0.20762	0.15637
16.39611	0.13679	0.1788	0.12986	0.21527	0.20663	0.19367	0.16094	0.20704	0.28
18.14611	0.13963	0.18715	0.13867	0.22552	0.20577	0.19182	0.15731	0.21143	0.46563
19.64611	0.13908	0.20014	0.15055	0.24238	0.20772	0.18509	0.15691	0.21236	0.79081
21.39611	0.15199	0.20827	0.16008	0.25841	0.21072	0.18474	0.15826	0.21277	0.91564
22.89611	0.16439	0.22046	0.16757	0.26948	0.20681	0.18091	0.15888	0.2217	0.65516
24.64611	0.17178	0.22879	0.17618	0.27906	0.21022	0.17862	0.15943	0.22131	0.4854
26.14611	0.18233	0.24194	0.18778	0.28877	0.20975	0.17247	0.16625	0.22506	0.31264
27.89611	0.19079	0.25002	0.19631	0.29901	0.21337	0.16567	0.16833	0.22944	0.23377
29.64444	0.19871	0.26096	0.20498	0.31507	0.21382	0.16072	0.16708	0.22533	0.14486
31.14444	0.20416	0.26983	0.20815	0.32568	0.2169	0.15077	0.17228	0.22927	0.13198
32.89444	0.21547	0.27794	0.21468	0.33238	0.21841	0.14868	0.17111	0.22952	0.09304

34.39444	0.2292	0.2868	0.22262	0.32484	0.22026	0.155	0.17275	0.22971	0.05689
36.14444	0.23987	0.29629	0.23187	0.32977	0.21612	0.153	0.17661	0.2296	0.03314
37.64444	0.25174	0.31045	0.24004	0.33863	0.21891	0.14798	0.16968	0.23424	0.02475
39.39444	0.25973	0.3197	0.24715	0.3491	0.21942	0.14642	0.17331	0.23079	0.01765
40.89444	0.27946	0.33161	0.25708	0.36537	0.21993	0.14594	0.17611	0.23741	0.01242
42.64444	0.29606	0.34571	0.26887	0.37698	0.22579	0.14306	0.17781	0.23661	0.00828
44.39444	0.30998	0.35912	0.28344	0.39855	0.22584	0.14444	0.1766	0.24021	0.00591
45.89333	0.32379	0.36613	0.29789	0.40662	0.23146	0.14379	0.1792	0.2435	0.00422
47.64333	0.34235	0.38699	0.31054	0.42459	0.23412	0.14304	0.17697	0.2435	0.00293
49.14167	0.36082	0.39765	0.32663	0.44115	0.23574	0.14884	0.18105	0.24735	0.00187
50.88972	0.37941	0.42018	0.34334	0.46218	0.2378	0.14949	0.18381	0.25057	0.00136
52.38972	0.39413	0.41995	0.36094	0.48011	0.24189	0.15193	0.18888	0.25398	0.00104
54.13972	0.41497	0.43158	0.37869	0.49187	0.24582	0.14865	0.19262	0.25755	7.32891E-4
55.88972	0.43311	0.44867	0.39118	0.50838	0.24916	0.15321	0.19742	0.2592	5.46944E-4
57.38972	0.45302	0.47498	0.41281	0.53264	0.25755	0.15661	0.19852	0.2666	4.56875E-4
59.13972	0.46446	0.49226	0.4216	0.54882	0.26464	0.15728	0.20195	0.26656	4.56939E-4
60.63972	0.47616	0.50906	0.44211	0.5688	0.26744	0.15994	0.20132	0.27022	3.60677E-4
62.38972	0.49577	0.53169	0.46098	0.59144	0.27397	0.15731	0.20344	0.27539	3.3748E-4
63.88972	0.50828	0.54829	0.47664	0.60875	0.27296	0.15572	0.20593	0.27813	2.84032E-4
65.63972	0.5195	0.56537	0.48394	0.63331	0.27788	0.15846	0.21138	0.28111	3.37041E-4
67.13972	0.53669	0.58838	0.49631	0.66112	0.2775	0.1593	0.21224	0.28775	3.56313E-4
68.88972	0.5662	0.61035	0.51694	0.69972	0.28775	0.15971	0.21376	0.28993	3.59497E-4
70.63972	0.584	0.62813	0.54239	0.73745	0.29622	0.16154	0.21927	0.29396	3.72348E-4
72.13972	0.59859	0.65662	0.56239	0.74433	0.30039	0.1621	0.22218	0.29927	2.69419E-4
73.88972	0.61695	0.68457	0.59003	0.79462	0.31094	0.16276	0.22757	0.29996	3.21261E-4
75.38972	0.64572	0.71715	0.62019	0.82155	0.31558	0.16979	0.22811	0.30751	2.27107E-4
77.13944	0.67032	0.75109	0.64926	0.87338	0.32503	0.16878	0.22842	0.30924	2.60778E-4
78.63944	0.70091	0.77414	0.68272	0.91828	0.33496	0.17422	0.23751	0.31654	2.47164E-4
80.38944	0.719	0.817	0.71987	0.96488	0.34224	0.1776	0.24023	0.32514	2.55432E-4
81.88944	0.73772	0.84741	0.76302	0.99968	0.35463	0.17843	0.24233	0.33096	2.3224E-4
83.63944	0.76381	0.88565	0.79464	1.03528	0.36315	0.18018	0.2539	0.33904	2.13786E-4
85.38944	0.79156	0.92192	0.84333	1.08365	0.37281	0.18552	0.25962	0.34019	1.86516E-4

86.88944	0.82089	0.95469	0.89068	1.14278	0.3834	0.18351	0.26606	0.34651	2.03876E-4
88.63944	0.86111	0.98606	0.93542	1.22052	0.39078	0.19116	0.27524	0.35727	2.36421E-4
90.13944	0.88858	1.02288	0.98232	1.2608	0.40177	0.19443	0.27683	0.36444	2.11559E-4
91.88944	0.92279	1.07905	1.0497	1.32095	0.40469	0.19637	0.28283	0.36852	1.79287E-4
93.38944	0.94733	1.12063	1.10369	1.37082	0.41868	0.19939	0.28276	0.37743	1.86388E-4
95.13944	0.98508	1.15215	1.17704	1.46032	0.43141	0.20711	0.28999	0.38536	2.29796E-4
96.88944	1.01497	1.19294	1.25461	1.51927	0.44505	0.21306	0.3005	0.39972	2.39577E-4

Supplementary Table S10: Xcelligence Cell Index and *P* values of shKMT2D#2-21a+siSLC2A3 versus shKMT2D#2-21a+siC#1 CAPAN-2 cells.

List of Cell Index values derived from the measured impedances and continuously displayed on the Xcelligence Software user interface. Each experimental condition was performed in triplicates. Statistical analyses were performed using one-way ANOVA and the *P* values corresponding to the comparison of siRNA- transfected versus control cells are shown at every single time point. *P* values ≤0.05 are marked in red. Differences in Cell Index measurements are significant after 36.1 hours of monitoring.

Table S11

Top Networks	
ID Associated Network Functions Score	**Score**
Cell Cycle, Cell Death and Survival, RNA Post-Transcriptional Modification	47
Cell Morphology, Connective Tissue Disorders, Developmental Disorder	44
Cellular Assembly and Organization, DNA Replication, Recombination and Repair, Cell Cycle	43
Cancer, Endocrine System Disorders, Nervous System Development and Function	39
Lipid Metabolism, Small Molecule Biochemistry, Vitamin and Mineral Metabolism	36

Supplementary Table S11: Bioinformatics prediction of the top networks regulated by KMT2D.

The list of the top 5 networks derived from IPA GO algorithms for the KMT2D-regulated genes (Figure 3G). “Score” refers to the numerical value used to rank networks according to how relevant they are to the genes in the input dataset.

Table S12

Relative Hazard ($Surv_1/Surv_2$)	Median Survival Group 2	Total events needed
.90 (1.11)	667 (540)	2828
.85 (1.18)	706 (510)	1189
.80 (1.25)	750 (480)	631
.75 (1.33)	800 (450)	379
.70 (1.43)	857 (420)	247
.67 (1.50)	900 (400)	191
.65 (1.54)	923 (390)	169
.60 (1.67)	1000 (360)	120
.57 (1.75)	1050 (343)	100
.55 (1.82)	1090 (330)	88
.50 (2.00)	1200 (300)	65

Table S12: Sample Size Calculations.

2-tail test has been conducted by the Mayo Clinic Pancreatic Cancer SPORE Biostatistics Core, for sample size calculations (Cohort V). To correctly reject a false null hypothesis, critical values have been set as follows: α .05, Power=.80, 50% allocation per group.

Table S13

KMT2D Expression	Quartile 1 (≤1.743) (N=54)	Quartile 2 (>1.743, ≤3.917) (N=55)	Quartile 3 (>3.917, ≤26.986) (N=55)	Quartile 4 (>26.986) (N=56)	*P* value
Age at Diagnosis					.7052
N	41	45	48	54	
Mean (SD)	64.78 (12.12)	64.53 (11.48)	64.98 (12.61)	63.15 (10.51)	
Median	67.00	66.00	64.50	62.00	
Q1, Q3	55.00, 75.00	55.00, 74.00	53.50, 75.00	57.00, 72.00	
Range	(41.00-88.00)	(37.00-81.00)	(41.00-89.00)	(43.00-92.00)	
Vital Status					.2316
Missing	6	4	4	1	
Alive	8 (16.7%)	6 (11.8%)	2 (3.9%)	6 (10.9%)	
Deceased	40 (83.3%)	45 (88.2%)	49 (96.1%)	49 (89.1%)	
Survival (Days)					
N	30	39	39	50	
Events	25	35	37	44	
Median Survival Days	949.0 (588.0-1239.0)	602.0 (413.0-874.0)	788.0 (409.0-1127.0)	565.0 (487.0-751.0)	
5 Yr Survival Rate	19.1% (4.0%-34.2%)	6.0% (0.0%-14.1%)	17.9% (5.9%-30.0%)	21.4% (9.6%-33.3%)	
Year 5 N at Risk	4	2	7	8	
Sex					.2540
Missing	6	4	4	1	
Female	21 (43.8%)	31 (60.8%)	24 (47.1%)	24 (43.6%)	
Male	27 (56.3%)	20 (39.2%)	27 (52.9%)	31 (56.4%)	
Race					.6593
Missing	9	5	4	1	
1=American Indian/Alaskan Native	0 (0.0%)	0 (0.0%)	0 (0.0%)	1 (1.8%)	
2=Asian/Asian-American	1 (2.2%)	1 (2.0%)	0 (0.0%)	0 (0.0%)	
3=Black/African-American	0 (0.0%)	1 (2.0%)	0 (0.0%)	1 (1.8%)	
5=White	44 (97.8%)	48 (96.0%)	51 (100.0%)	53 (96.4%)	
Usual Adult BMI					.0252
N	35	39	44	51	
Mean (SD)	27.01 (5.12)	27.59 (5.69)	30.21 (6.09)	29.67 (5.27)	
Median	26.63	28.34	29.32	28.80	
Q1, Q3	24.24, 29.23	23.81, 31.46	26.24, 32.03	25.06, 33.66	
Range	(15.31-43.72)	(16.46-38.80)	(20.60-46.18)	(18.88-43.02)	
Usual Adult BMI (<30,30+)					.1108
Missing	19	16	11	5	
<30	28 (80.0%)	27 (69.2%)	24 (54.5%)	32 (62.7%)	
30+	7 (20.0%)	12 (30.8%)	20 (45.5%)	19 (37.3%)	
Weight Loss					.0060
Missing	6	4	4	1	
No	22 (45.8%)	21 (41.2%)	11 (21.6%)	11 (20.0%)	
Yes	26 (54.2%)	30 (58.8%)	40 (78.4%)	44 (80.0%)	
Pounds Lost					.0004
N	48	51	51	55	
Mean (SD)	8.63 (10.71)	13.78 (15.62)	20.10 (19.31)	21.16 (17.58)	

KMT2D Expression	Quartile 1 (≤1.743) (N=54)	Quartile 2 (>1.743, ≤3.917) (N=55)	Quartile 3 (>3.917, ≤26.986) (N=55)	Quartile 4 (>26.986) (N=56)	*P* value
Median	5.00	11.00	15.00	20.00	
Q1, Q3	0.00, 13.50	0.00, 22.00	7.00, 30.00	10.00, 30.00	
Range	(0.00-40.00)	(0.00-60.00)	(0.00-85.00)	(0.00-70.00)	
Stage at Surgery					.7224
Missing	26	23	18	8	
IA	0 (0.0%)	0 (0.0%)	1 (2.7%)	0 (0.0%)	
IB	3 (10.7%)	3 (9.4%)	3 (8.1%)	3 (6.3%)	
IIA	5 (17.9%)	7 (21.9%)	13 (35.1%)	15 (31.3%)	
IIB	20 (71.4%)	22 (68.8%)	20 (54.1%)	29 (60.4%)	
IV	0 (0.0%)	0 (0.0%)	0 (0.0%)	1 (2.1%)	

Table S13: Quartile-based correlation of *KMT2D* expression with demographic and clinical characteristics of pancreatic cancer patients (Cohort V).

Pancreatic carcinomas were subdivided in 2 groups: carcinomas with below median (<3.917) *KMT2D* expression and carcinomas with above median (>3.917) *KMT2D* expression. N: number of patients with clinical information; BMI: Body Mass Index. Clinical correlations were examined using the SAS software.

Table S14

Primer	Sequence	Tm (°C)
FASN Forward	CTT GGC CTT GGG TGT GTA CT	57.4
FASN Reverse	CTG ATC ATC AAG AGC CAC CA	54.6
KMT2D Forward	ATG CAG CCA AGG ACC TAG AA	56.4
KMT2D Reverse	ATG CCT CGA TTC TGC TCT TC	56
KDM8 Forward	TCA GTG CAG AGA GCC AGA GA	54.1
KDM8 Reverse	ATC GGC CTC GTG TAA CAA GT	55.9
KDM4C Forward	TGG ATC CCA GAT AGC AAT GA	53.1
KDM4C Reverse	TGT CTT CAA ATC GCA TGT CA	52.3
KDM2A Forward	CCT CAG TGG CAT CAT CAA GA	54.5
KDM2A Reverse	TTT CAG TCC TGG CAG CCT AT	56.1
KDM5B Forward	CCT TGC CAA ATG GAA AG AAA	51.5
KDM5B Reverse	CTT CCC CAA GAG TTG CCA TA	54.6
KMT2B Forward	ACT TCG AGG ACA TGG AGG TG	55.6
KMT2B Reverse	GCG GCT ACA ATC TCT TCC TG	55.6
KMT2C Forward	GAA TCA CTT CCT GGG GTT GA	54.5
KMT2C Reverse	GGC AAG AGG AAG TTC CAT GA	54.8
RELA Forward	CCA GAC CAA CAA CAA CCC CT	57.6

RELA Reverse	TCA CTC GGC AGA TCT TGA GC	57.0
SETD6 Forward	GCT TTC AGG AAC CAC TGG AG	55.8
SETD6 Reverse	GGC GTT GTG ATT GGC TAA GT	55.8
SLC2A3 Forward	TCC ACG CTC ATG ACT GTT TC	55.1
SLC2A3 Reverse	GCC TGG TCC AAT TTC AAA GA	53.3
SLC2A1 Forward	GTG GAG ACT AAG CCC TGT CG	57.3
SLC2A1 Reverse	CAT AGC CAC CTC CTG GGA TA	55.8
STK11 Exon 6 Forward	TCG AAA TGA AGC TAC AAC ATC	50.7
STK11 Exon 6 Reverse	TTT CAG CAG GTC AGA GAG	51.3
SUV420H1 Forward	TCA ACT GGT CGA GAT ACA GCA	55.6
SUV420H1 Reverse	CTC CAA AGA ACC CAT CTC CA	54.3
TSC1 Forward	CTG GAG GAC TGC AGG AAC AT	56.9
TSC1 Reverse	GAG CAG CAG CTC AGT GTG AC	58.5
β-actin Forward	CCC AGC ACA ATG AAG ATC AA	57.1
β-actin Reverse	ACA TCT GCT GGA AGG TGG AC	53.0
GAPDH Forward	ATG TTC GTC ATG GGT GTG AA	54.4
GAPDH Reverse	GGT GCT AAG CAG TTG GTG GT	57.9

Supplementary Table S14 Primers used in qPCR analysis.

The list of all primer sequences used for real-time PCR analysis.

SUPPLEMENTARY MATERIALS AND METHODS

Cell Cultures and Treatments

Pancreatic cancer cell lines (MIAPaCa-2, PANC-1, CAPAN-1, CAPAN-2, AsPC-1, BxPC-3, HPAF-II and CFPAC-1) were purchased from ATCC. MIA PaCa-2 and PANC-1 were grown in DMEM, CAPAN-1 and CFPAC-1 in IMDM, CAPAN-2 in McCoy's 5A, AsPC-1 and BxPC-3 in RPMI 1640 (Gibco), HPAF-II in EMEM (ATCC), all supplemented with 10% FBS (Gemini Bioproducts). In the case of MIA PaCa-2, medium was also supplemented with 2.5% horse serum (Gibco). STR analysis has been performed as a method for human cell line authentication.

Pancreatic cancer cells were plated ($2.5*10^5$ cells in 35mm dishes) and after 24 h were treated with 1 or 2 μM of 5-AZA-CdR (A3656, Sigma-Aldrich). Cells were incubated for 0 to 4 days before DNA, RNA or protein extraction.

Around 80% confluent MIA PaCa-2 cells were pretreated with 100 nM rapamycin (#1292, TOCRIS) for 24 h. Cell lysates were analyzed by IB analysis.

KMT2D-silenced MIA PaCa-2 cells were treated with the inhibitors of NF-κB activation, Tanshinone IIA (4426) and RO 106-9920 (1778) purchased from TOCRIS, for 24 h before RNA extraction.

MIA PaCa-2 cells were plated in 96-well dishes ($1*10^3$ cells/well) and treated with a) different doses of lipids including: cis-13,16-Docosadienoic (Hebei Zhongzhuo Import and Export Trade Co, Ltd), 13Z,16Z,19Z-Docosatrienoic (SC-200782, Santa Cruz Biotechnology, Inc) or 4,10,13,16-Docosatetraenoic acid (D3659, Sigma-Aldrich) and b) the lipid synthesis inhibitors SC 26196 (4189, TOCRIS) and SB 204990 (4962, TOCRIS). Cells were incubated for 1, 3 or 5 days before measurement of cell viability and for 3 days before performing *in vitro* invasion assays.

Real-Time PCR Analysis

RNA purified from cells and tissues with TRIZOL (Life Technologies) was reverse-transcribed to form cDNA using the iSCRIPT RT Supermix (Bio-Rad), which was subjected to real-time PCR analysis using the iQ SYBR Green Supermix (Bio-Rad) on a CFX384 Touch Real-Time PCR Detection System (Bio-Rad). The primer sequences used for real-time PCR were acquired from previous studies [3] or designed using the NCBI Nucleotide Database (http://www.ncbi.nlm.nih.gov/nuccore), Primer3 v.0.4.0

(http://bioinfo.ut.ee/primer3-0.4.0) and UCSC In-Silico PCR (http://genome.ucsc.edu/cgi-bin/hgPcr) and are included in Table S14. Gene expression levels were normalized to the levels of GAPDH and β-actin. Normalized gene expression levels were quantified to the respective control. Bars represent means ± SE; experiments were performed in quadruplicates for each condition.

For Kaplan-Meir studies in patients' Cohort V, transcript expression for human KMT2D was determined using PerfeCTa SYBR Green FastMix (Quanta BioSciences Inc.,Gaithersburg, MD) and the following primer sets: KMT2D, 5'-AACCATATCGGCCTGGCATT -3' (forward) and 5'- CAGCAGGTATCACCTCGTCG -3' (reverse); 18S, 5'- AACCCGTTGAACCCCATTCGTGAT -3' (forward) and 5'-AGTCAAGTTCGACCGTCTTCTCAG -3' (reverse). 500 ng RNA was reverse transcribed using High Capacity cDNA synthesis kit (Applied Biosystems). 10 ng cDNA from each sample was used for qPCR analysis. Amplification was performed using the C1000 Thermal Cycler (Bio-Rad). RNA levels were normalized by comparison with the corresponding housekeeping RNA level in the same sample. The results are calculated following the 2ΔCt (where ΔCt represents the difference in threshold cycles between the target and control gene).

Whole Exome Sequencing

Genomic DNA was isolated from human MIA PaCa-2 and CAPAN-2 pancreatic cancer cell lines using QIAamp DNA Mini Kit (51304) and used for Whole Exome Sequencing that was conducted at the UCLA Clinical Microarray Core. The library construction was performed using the SeqCap EZ System from NimbleGen according to the

manufacturer's instructions. Briefly, genomic DNA was sheared, size selected to roughly 300 base pairs, and the ends were repaired and ligated to specific adapters and multiplexing indexes. Fragments were then incubated with SeqCap biotinylated DNA baits after LM-PCR and the hybrids were purified using streptavidin-coated magnetic beads. After amplification of 18 or less PCR cycles, the libraries were then sequenced on the HiSeq 3000 platform from Illumina, using 100-bp pair-ended reads. The sequence data were aligned to the GRCh37 human reference genome using BWA v0.7.7-r411. PCR duplicates were marked using MarkDuplicates program in Picard-tools-1.115 tool set. GATK v3.2-2 was used for INDEL (insertions and deletions) realignment and base quality recalibration. Exome coverage was calculated using the bedtools. Samtools was used to call the SNVs (single nucleotide variants) and small INDELs. Varscan2 was used to call the somatic SNVs. All variants were annotated using the Annovar program.

Immunoblot Analysis

Total cell extracts were separated by SDS-PAGE and transferred to PVDF membranes following standard procedures. Frozen tissue biopsies were homogenized using RIPA buffer (Cell Signaling Technology), followed by sonication. In the case of KMT2D, protein levels were monitored by 5% SDS-PAGE using modified long apparatus for extended running time. Transfer time reached 24 h at 4^0C and the buffering system contained 15% methanol. The following antibodies were used for immunoblot analysis: KMT2D (R0118-1, Abiocode), mono-methyl-Histone H3 (Lys4) (5326), di-methyl-Histone H3 (9725), tri-methyl-Histone H3 (Lys4) (9751), Histone H3 (14269), FASN

(3180), phospho-mTOR (Ser2448) (5536), mTOR (2983), RICTOR (2114), phospho-NF-κB p65 (Ser536) (3033), NF-κB p65 (8242), CREB (9104) (Cell Signaling Technology). The protein levels that corresponded to the immunoreactive bands were quantified using the Scion Image analysis software (Scion Corp., Frederick, MD).

Cell Viability Assay

MIA PaCa-2 cells were plated in quadruplicates and treated with exogenously added lipids in 96-well plate ($1*10^3$ cells/well) and cell growth was assessed 1, 3 or 5 days later using the CellTiter Glo Luminescence Cell Viability Assay (Promega). Data are expressed as mean fluorescence (arbitrary units) ± S.D.

Anchorage-Independent Cell Growth Assay

Triplicate samples of $25*10^3$ MIA PaCa-2 cells from each treatment were assayed in 48-well plates for colony formation using the CytoSelect Cell Transformation kit (Cell Biolabs, Inc). Colorimetric quantitation of colonies has been performed according to the manufacturer's instructions. Data were expressed ± SE of the mean of at least 2 independent experiments.

Invasion assay

Invasion in matrigel has been conducted by using standardized conditions with BD BioCoat Matrigel invasion chambers (354480; BD Biosciences) according to the manufacturer's protocol. Assays for MIA PaCa-2 cells were conducted using 10% FBS-containing media as chemoattractant. Noninvading cells on the top side of the

membrane were removed, whereas invading cells were fixed and stained with .1% crystal violet, 22 h after seeding. The cells that migrated through the filter were quantified by counting the entire area of each filter divided in four fields, using a grid and an Evos microscope at a X20 magnification. Data are expressed as the mean number of invading cells per field ± SD.

Dynamic Monitoring of Cell Proliferation

Real-time cell proliferation analysis based on the application of electrical cell substrate impedance changes (https://lifescience.roche.com/wcsstore/RASCatalogAssetStore/Articles/BIOCHEMICA_4_08_p14-16.pdf) was performed using the xCELLigence RTCA instrument (ACEA Biosciences). The presence of cells affects the local ionic environment at the electrode solution interface. Cell status is represented by a dimensionless parameter termed Cell Index, which is derived as the relative change in measured electrical impedance, after subtraction of the background measurements from media alone. Local ionic environment varies according to cell size, cell morphology and strength of adhesion of the cells to the surface of the electrode, resulting in changes of the electrode impedance. $5*10^3$ cells were seeded in quadruplicates of an E-Plate 96 with interdigitated microelectrode arrays integrated in the bottom of each well. Subsequently, the E-Plate 96 was mounted on the SP Station of the xCELLigence RTCA system which is placed in a standard temperature-controlled CO_2 incubator under humidity saturation. The RTCA Software preinstalled on the RTCA control unit allows automatic selection of wells for measurement and real-time data acquisition within preprogrammed 15 min

time intervals. Bars represent means±SD; experiments were performed in quadruplicates for each condition.

Immunohistochemistry and Digital Pathology Analysis

For immunohistochemical analysis of KMT2D in matched normal and cancer human tissues, deparaffinized 5-µm sections were incubated sequentially in accordance with the instructions of the LSAB kit (DAKO Corporation). For digital automated morphometry, the immunohistochemically stained sections were digitized at 40x magnification using an Aperio Scanscope CS (Aperio). The final immunohistochemical score was calculated from a combination of the intensity and percentage scores [4]. Antigen retrieval was performed by incubating the slides in boiling .01% sodium citrate pH 6.0 for 5 min. The endogenous peroxidase activity was inhibited by immersing the slides in 3% H_2O_2-methanol for 25 min and the background nonspecific binding was reduced by incubating with 1% BSA in PBS for 60 min. The slides were incubated overnight with antibody against KMT2D (1:200) (HPA035977, Sigma-Aldrich). In order to reduce the variability, all samples from each group were processed at the same time in a single experiment using a single batch of diluted antibody. The slides were then washed 5 times in PBS, followed by sequential incubations with biotinylated secondary antibody for 30 min at RT, streptavidin-HRP conjugate for 30 min at RT and 3,3'-diaminobenzidine tetrahydrochloride (liquid DAB) for 3 min in the dark. The reaction was arrested with distilled water and the slides were counterstained with hematoxylin. Thereafter, the tissues were washed in tap water for 5 min, dehydrated through ethanol

baths (70, 90 and 100%) and xylene. Slides were finally mounted with E-2 Mount medium (Shandon lab).

The Aperio Scanscope CS obtains 40X images with a spatial resolution of 0.45 μm/pixels. The images were reviewed using an ImageScope (Aperio). Once the areas were recorded (500 μm for each tissue), they were sent for automated image analysis using the Spectrum Software V11.1.2.752 (Aperio). For the within tissue intensity, an algorithm was developed to quantify the total or nuclear protein expression. The output from the algorithm gives a number of quantitative measurements, namely the intensity, concentration and percentage of positive staining. The quantitative scales for the intensity and percentage were categorized into 4 and 5 classes, respectively, after the cut-off values were determined. The staining intensity was categorized as 0 (no staining), 2+ (moderate) and 3+ (strong).

All other immunostainings of formalin fixed paraffin embedded (FFPE) sections have been performed by the Translational Pathology Core Laboratory, UCLA. The endogenous peroxidase activity was blocked with 3% hydrogen peroxide in methanol for 10 min. Heat-induced antigen retrieval was carried out for all sections in .01M Citrate buffer, pH=6.0 by using a Biocare decloaker at 95^{o}C for 25 min. The slides were incubated for 1h with antibodies against KMT2D (1:200) (HPA035977, Sigma-Aldrich), SLC2A3 (1:100) (20403-1-AP, Proteintech), phosphorylated NF-κB p65 (536) (1:100) (ab86299, Abcam) and Ki-67 (1:100) (M7240, Agilent). The signal was detected using Mach3 rabbit, HRP conjugated polymer for 30 min (Biocare Medical) and visualized with the diaminobenzidine reaction. Images were further captured with an Axio Imager.Z1 upright microscope (Carl-Zeiss).

HM450 Methylation array

For global methylation profiling, the Illumina Infinium HumanMethylation450 (HM450) BeadChIP has been used (Illumina, San Diego, CA). Bisulfite conversion has been performed on 1 µg of genomic DNA from each sample using the EZ-96 DNA Methylation Kit (Zymo Research, Irvine, CA) according to the manufacturer's instructions. Bisulfite-converted DNA was whole genome amplified and enzymatically fragmented prior to hybridization to BeadChIP arrays. The oligomer probe designs of HM450 arrays follow the Infinium I and II chemistries, in which locus-specific base extension follows hybridization to a methylation-specific oligomer. The level of DNA methylation at each CpG locus was scored as beta (β) value calculated as (M/(M+U)), ranging from 0 to 1, with 0 indicating no DNA methylation and 1 indicating fully methylated DNA. The data were extracted using Illumina Genome Studio Methylation Module and quantile normalized using 'preprocesscore' R package (https://cran.r-project.org/). Of the 485,577 CpG probes on the array, we filtered out probes with high detection *P* values, probes with a SNP within 10 base pairs of the target CpG [5] and repeat regions and probes on X and Y chromosomes, leaving 371,478 probes. The term 'hyper-methylation' was used when there was an increased DNA methylation in patients compared to controls and, the term 'hypo-methylation' was used when we observed a decreased DNA methylation in patients compared to controls.

For statistical and bioinformatics analyses, Wilcoxon rank-sum tests were conducted to compare methylation array data between pancreatic cancer patients and healthy controls. Magnitude of DNA methylation changes was assessed using methylation beta values. Correction for multiple comparisons was performed using FDR (Benjamini-

Hochberg) approach. A corrected *P* value, denoted as, 'q'≤.05 was considered significant. The mean difference in betas, associated *P* and q values for chromatin modifiers are presented in Table EV1.

Targeted Bisulfite Sequencing and Data Analysis

Next-generation sequencing for the evaluation of DNA methylation at single-nucleotide resolution has been conducted by Zymo Research Corporation, Irvine, CA. Assays were designed targeting CpG sites in the specified ROI using primers created with Rosefinch, Zymo Research's proprietary sodium bisulfite converted DNA-specific primer design tool. The primer sequences used are as follows: (Forward: TTTAGTTTATGTTTTTGTGTTAGGATTAGAA, Reverse: AATAAACATATAAATCTCTTTCTTAACACCAA). Sequence reads were aligned back to the reference genome using Bismark (http://www.bioinformatics.babraham.ac.uk/projects/bismark/), an aligner optimized for bisulfite sequence data and methylation calling (Krueger & Andrews, 2011). The methylation level of each sampled cytosine was estimated as the number of reads reporting a C, divided by the total number of reads reporting a C or T. Following primer validation, provided samples were bisulfite converted using the EZ DNA Methylation-LightningTM Kit (D5030, Zymo Research) according to the manufacturer's instructions. Multiplex amplification of all samples using ROI specific primer pair and the Fluidigm Access ArrayTM System was performed according the to the manufacturer's instructions. The resulting amplicons were pooled for harvesting and subsequent barcoding according to the Fluidigm instrument's guidelines. After barcoding, samples

were purified using ZR-96 DNA Clean & Concentrator™-5 (D4023, Zymo Research) and then prepared for massively parallel sequencing using a MiSeq V2 300bp Reagent Kit and paired-end sequencing protocol according to the manufacturer's guidelines. Sequence reads were identified using standard Illumina base-calling software and then analyzed using a Zymo Research proprietary analysis pipeline. Low quality nucleotides and adapter sequences were trimmed off during analysis QC. Paired-end alignment was used as default. Index files were constructed using the *bismark_genome_preparation* command and the entire reference genome. The *--non_directional* parameter was applied while running Bismark. All other parameters were set to default. Nucleotides in primers were trimmed off from amplicons during methylation calling.

Plasmid Construction and *in vitro* Methylation

Linear 300 bp DNA fragments between nt: -179 and +122 relatively to the transcription start site in the human *KMT2D* genomic region were constructed by Genewiz either in the wild type form (unmodified), or modified by a C to A mutation at CpG sites -29 (Mut 1) or +145 (Mut 2) or both (double Mut). Artificial SacI and HindIII restriction sites have been incorporated using Native Taq Polymerase (18038-018, Life Technologies) and the following primers: sense, 5'-GTAGATCAGAGCTCACTTTCTTG-3'; antisense, 5'-CTAGTCATAAGCTTTCCTTGTGC- 3'. The resulting PCR products were subsequently cloned into the pCR 2.1-TOPO vector (450641, Life Technologies) using the TOPO TA cloning kit (Life Technologies). The pCR 2.1 TOPO plasmids containing the *KMT2D* genomic inserts (hereafter referred to as TOPO*KMT2D*) were linearized with SacI

(R3156M, New England Biolabs) and *in vitro* methylated using SssI methylase (M0226L, New England Biolabs), which nonspecifically methylates all CpG dinucleotides. The efficiency of *in vitro* methylation was confirmed by resistance to cleavage by the methylation-sensitive restriction enzyme HpaII (R0171L, New England Biolabs) that has recognition site(s) in the analyzed regions and no sites within the sequence of pCR 2.1 TOPO vector. The linearized methylated and unmethylated TOPO*KMT2D* vectors were then digested with HindIII (R3104T, New England Biolabs) to excise the *KMT2D* inserts. After fractionation on a 1.8 % agarose gel, the DNA bands corresponding to 300 bp were cut from the gel, isolated using NucleoSpin® GeI and PCR Clean-up columns (Macherey-Nagel). To determine whether global or site-specific CpG methylation of the *KMT2D* genomic region affected gene expression in a reporter gene construct, the methylated and unmethylated control fragments were then ligated into the pGL4.82 [hRluc/Puro] Vector (E750A, Promega) between the SacI and HindIII restriction sites. The pGL4.82 [hRluc/Puro] plasmid is designed for high expression and reduced anomalous transcription. The vector encodes the luciferase reporter gene *hRluc* but lacks eukaryotic promoter and enhancer sequences. T4 DNA Ligase (M0202S, New England Biolabs) was used to perform the ligation reaction according to the manufacturer's instructions, at 1:3 vector to insert ratio. The efficiency of ligation and equivalence of incorporated DNA into the methylated and unmethylated constructs were confirmed by agarose gel electrophoresis. For further validation, DNA sequence analysis across the multiple cloning site region located upstream of the *hRluc* gene was performed using RVprimer3 clockwise primer (E448A, Promega) by Genewiz. The effect of total methylation on the transcriptional activity of the inserted *KMT2D*

fragments was expressed as the relative change in reporter gene activity. Data were presented as the mean of Luminescence Units ± SE of 3 independent experiments performed in triplicates.

Chromatin Immunoprecipitation, Sequencing and Analysis

Chromatin immunoprecipitation was carried out using the SimpleChIP Plus Enzymatic Chromatin IP Kit (Cell Signaling Technology). Briefly, the chromatin fragments, derived from siC#1, siKMT2D#1 and siKMT2D#2 treated cells, were immunoprecipitated with antibody against tri-methyl-Histone H3 (Lys4) (9751, Cell Signaling Technology) at a ratio 1:50 or 1:100, respectively. After purification, libraries for next generation sequencing were prepared using NEBNext® ChIP-seq Library Prep Master Mix Set for Illumina® (E6240, New England BioLabs) and further analyzed using Illumina NextSeq500 system (single-end 75bp protocol). Both ChIP-seq and Bioinformatics Analyses were performed by the Center for Cancer Computational Biology, Dana-Farber Cancer Institute, Boston, MA. Sequencing reads in fastq-format were aligned to the UCSC hg19 reference genome using BWA (version 0.7.9a bwa mem with default options). Duplicate reads were removed with Picard tools (v. 1.115) MarkDuplicates and were filtered to retain only primary alignments with samtools (v0.1.19, view command with -F 0x100 flag). ChIP-seq peaks were called using HOMER (v4.7) findPeaks by selecting matched input samples with default settings (Poisson *P* value of <=1E-4 and fold change >=4.0). Histone option was employed. Further, peaks were annotated using HOMER's annotatePeaks utility using the hg19 annotations database provided with the software. Analysis of differentially bound peaks was performed using HOMER's

getDifferentialPeaks command, which examines the distributions of reads to determine enrichment in a particular condition (Poisson *P* value <1E-4, fold-change >=4.0), suggesting a differentially bound peak. Plots of the distribution of distances to the annotated transcription start site were created directly from the annotated peak data provided as output by HOMER. Similar approach was applied for the pie charts representing the distribution of annotated peak features. Enrichment plots were constructed by comparing the read density (number of reads divided by the length of the peak region) in each of the experimental conditions for each set of peak regions. Read densities were found in both siC#1and siKMT2D conditions for all peak regions in the siKMT2D condition; enrichment values were calculated as the scaled difference between the densities. The increase in H3K4me3 read density (comparing siKMT2D to siC#1) was tested with a one-sided Wilcoxon signed-rank test (*P*<.001). Similarly, enrichment values were calculated in both conditions for the peak regions found in siC#1 condition (*P*<0.001).

Luciferase Assay

MIA PaCa-2 cells were transfected with the untreated or CpG MSssI-treated *KMT2D*/*hRluc* constructs and the pGL4.51 [luc2/CMV/Neo] (E1320, Promega) containing synthetic firefly luciferase *luc2* gene. 48 h later luciferase activity was measured using the Dual Luciferase Reporter Assay System (E1960, Promega). Data were expressed ± SE of the mean of 3 independent experiments.

In order to assess whether *STK11* represents a direct transcriptional KMT2D target, MIA PaCa-2 cells were transfected with the LightSwitch RenSP reporter vector carrying

human STK11 promoter (S714439, SwitchGear Genomics) and the pLenti CMV Puro LUC (w168-1) (17477, Addgene) containing Luc reporter gene. At 24 h, the cells were transfected with siC#1 or siKMT2D#2 and 48 h later luciferase activity was measured using the Dual Luciferase Reporter Assay System (Promega). Data were expressed ± SE of the mean of 3 independent experiments.

Metabolic Profiling

Cellular metabolic rates were measured using a XF24-3 Analyzer (Seahorse Biosciences) by the Cellular Bioenergetics Core, UCLA. Cells were plated as a confluent monolayer in the Seahorse plate and left undisturbed for 24 h. Bioenergetic parameters were obtained in basal and after sequential injection of an ATPase inhibitor oligomycin (oligo), a mitochondrial uncoupler (FCCP) and mitochondrial inhibitors rotenone and myxothiazol (RM) in pancreatic cancer cells. Bars represent means ± SD; experiments were performed in quadruplicates for each condition.

Lipids extraction from a) human cancer cells b) tumor tissues from mice bearing human pancreatic cancer xenografts and c) human biopsies, reconstitution in the solvent system suitable for analysis and quantitative evaluation of altered lipid profiles by LC-MS analysis were performed by the Lipidomics Core Facility, Wayne State University. Lipid classes currently analyzed: FAs and total cholesterol. Bars represent means ± SD; experiments were performed in triplicates for each condition.

NADP/NADPH-Glo™ Assay

The bioluminescent homogeneous NADP/NADPH-Glo™ Assay (G9081, Promega) was used for detecting total reduced nicotinamide adenine dinucleotides phosphates (NADPH) in cells pretreated with siC#1, siKMT2D#1 or siKMT2D#2, following the manufacturer's protocol. Bars represent means±SD; experiments were performed in triplicates for each condition.

Lactate Assay

The Lactate Assay Kit (MAK064, Sigma) was used to determine the lactate production in cells pretreated with siC#1, siKMT2D#1 or siKMT2D#2 based on an enzymatic assay, which results in a colorimetric (570 nm) product, proportional to the lactate present, according to manufacturer's instructions. Bars represent means±SD; experiments were performed in triplicates for each condition.

Glucose Uptake Assay

The Glucose Uptake Assay Kit (MAK083, Sigma) was used to determine the glucose uptake in cells pretreated with siC#1, siKMT2D#1 or siKMT2D#, according to manufacturer's instructions. The glucose analogue, 2-deoxyglucose (2-DG) used, is taken up by cells and phosphorylated by hexokinase to 2-DG6P. 2-DG6P cannot be further metabolized and accumulates in cells, directly proportional to the glucose uptake by cells. Briefly, 2-DG uptake is determined by a coupled enzymatic assay in which the 2-DG6P is oxidized, resulting in the generation of NADPH, which is then determined by a recycling amplification reaction in which the NADPH is utilized by glutathione

reductase in a coupled enzymatic reaction that produces glutathione. Glutathione reacts with DTNB to colorimetric product TNB, which is detected at 412 nm. Bars represent means ± SD; experiments were performed in triplicates for each condition.

Cholesterol Uptake Cell-based Assay

Cholesterol Uptake Cell-based Assay Kit (Cayman Chemical) was used to study cellular cholesterol trafficking, following the manufacturer's protocol. Cells were treated with siC#1 or siKMT2D#2 in culture medium containing 20 μg/ml NBD Cholesterol and incubated for 72 h. Detection of cholesterol uptake was assessed by fluorescence microscopy using Axio Observer.D1 inverted microscope (Carl-Zeiss).

Patient Samples

RNA and DNA were extracted from 'normal' (adjacent non-tumoral) and PDAC tissues using TRIZOL (Life Technologies) and (QIAamp DNA Mini Kit, Qiagen), respectively. Samples originating from Cohort I were used for Gene expression profiling that was conducted at the UCLA Clinical Microarray Core, while DNA methylation analysis using Infinium HumanMethylation450 BeadChIP assay has been performed at the Translational Genomics Core, Cambridge, MA. For validation of the Gene expression array data, tissues originating from Cohorts II and III were subjected to RT-qPCR analysis., while FFPE tissues (Cohort IV) were subjected to immunohistochemical analysis. For correlation of *KMT2D* expression with overall patient survival, human pancreatic tumors (Cohort V) were approved by the institutional review boards of Mayo

School of Medicine and informed consent was obtained from all patients prior to tissue procurement and subsequent analysis.

Statistical Analyses

Quantitative data were expressed as means ± SD or SE of the mean, as indicated, or as boxes and whiskers (minimum-to-maximum), using Origin 9.1 Software. Statistical analyses were performed using one-way ANOVA or Pearson correlation. P values of <.05 were considered statistically significant.

Clinical correlations were examined using the SAS software. The Kaplan-Meier test was used for univariate survival analysis. The Cox proportional hazard model was used for multivariate analysis and for determining the 95% confidence interval.

SUPPLEMENTARY REFERENCES

1. Badea L, Herlea V, Dima SO, Dumitrascu T, Popescu I. Combined gene expression analysis of whole-tissue and microdissected pancreatic ductal adenocarcinoma identifies genes specifically overexpressed in tumor epithelia. Hepato-gastroenterology 2008;**55**(88):2016-27
2. Segara D, Biankin AV, Kench JG, et al. Expression of HOXB2, a retinoic acid signaling target in pancreatic cancer and pancreatic intraepithelial neoplasia. Clinical cancer research : an official journal of the American Association for Cancer Research 2005;**11**(9):3587-96 doi: 10.1158/1078-0432.ccr-04-1813[published Online First: Epub Date]|.
3. Vorvis C, Hatziapostolou M, Mahurkar-Joshi S, et al. Transcriptomic and CRISPR/Cas9 technologies reveal FOXA2 as a tumor suppressor gene in pancreatic cancer. American journal of physiology. Gastrointestinal and liver physiology 2016;**310**(11):G1124-37 doi: 10.1152/ajpgi.00035.2016[published Online First: Epub Date]|.
4. Kim BW, Cho H, Chung JY, et al. Prognostic assessment of hypoxia and metabolic markers in cervical cancer using automated digital image analysis of immunohistochemistry. Journal of translational medicine 2013;**11**:185 doi: 10.1186/1479-5876-11-185[published Online First: Epub Date]|.
5. Noushmehr H, Weisenberger DJ, Diefes K, et al. Identification of a CpG island methylator phenotype that defines a distinct subgroup of glioma. Cancer cell 2010;**17**(5):510-22 doi: 10.1016/j.ccr.2010.03.017[published Online First: Epub Date]|.